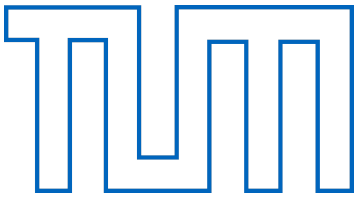

Technischen Universität München
Fakultät für Physik

Applications of Light-Cone Sum Rules in Flavour Physics

Nico Gubernari

Vollständiger Abdruck der von der Fakultät für Physik der Technischen Universität München zur Erlangung des akademischen Grades eines

Doktors der Naturwissenschaften

genehmigten Dissertation.

Vorsitzender:		Prof. Dr. Bastian Märkisch
Prüfer der Dissertation:	1.	TUM Junior Fellow Dr. Danny van Dyk
	2.	apl. Prof. Dr. Norbert Kaiser

Die Dissertation wurde am 29.07.2020 bei der Technischen Universität München eingereicht und durch die Fakultät für Physik am 10.09.2020 angenommen.

All work presented in this thesis is the author's own work, unless stated otherwise. This includes results that have been previously published (or will be published) in the following articles:

- N. Gubernari, A. Kokulu and D. van Dyk, *$B \to P$ and $B \to V$ Form Factors from B-Meson Light-Cone Sum Rules beyond Leading Twist*, *JHEP* **01** (2019) 150 [1811.00983]
- M. Bordone, N. Gubernari, D. van Dyk and M. Jung, *Heavy-Quark expansion for $\bar{B}_s \to D_s^{(*)}$ form factors and unitarity bounds beyond the $SU(3)_F$ limit*, *Eur. Phys. J. C* **80** (2020) 347 [1912.09335]
- N. Gubernari, D. van Dyk and J. Virto, *Non-local matrix elements in $B \to K^{(*)}\ell^+\ell^-$ from light-cone sum rules and dispersive bounds, In preparation*

To Sorano, my hometown,
and to all its inhabitants,
the only system that has both strangeness and beauty
which is not listed among the $s\bar{b}$ bound states.

Abstract

Semileptonic and rare B-meson decays are powerful probes to test electroweak interactions, which are successfully described by the Standard Model (SM) of particle physics, at very high energy scales. In fact, recent measurements of several observables in both $b \to c\ell\nu$ and $b \to s\ell\ell$ transitions have shown tensions with the SM predictions. These tensions are collectively called the B anomalies. In order to determine whether the B anomalies are genuine signs of physics beyond the SM, accurate theoretical predictions of the corresponding hadronic matrix elements (HMEs) are essential. The major theoretical uncertainties in the $B \to D^{(*)}\ell\nu$ and $B_s \to D_s^{(*)}\ell\nu$ semileptonic decays come from the local HMEs, which are parametrized by the meson form factors. We calculate these form factors in the framework of QCD Light-Cone Sum Rules (LCSRs) with B-meson distribution amplitudes. To further improve the precision of our predictions and to extrapolate the form factors to the whole physically allowed region, we combine our LCSRs results with with lattice QCD results and impose dispersive bounds. In rare B decays, besides the local HMEs, also non-local HMEs presently limit the theoretical precision in most of the observables constituting the B anomalies. We calculate these HMEs for $B \to K^{(*)}\ell\ell$ decays using LCSRs as well. To obtain additional constraints for the non-local $B \to K^{(*)}\ell\ell$ HMEs, we extend the dispersive bounds method to make it suitable for this type of objects. Finally, we discuss selected phenomenological implications of our results, giving SM predictions for the Lepton-Flavour Universality ratios $R_{D^{(*)}}$ and other important observables in B decays.

Zusammenfassung

Semileptonische und seltene B-Mesonen-Zerfälle liefern eine ausgezeichnete Möglichkeit, um die elektroschwachen Wechselwirkungen, welche erfolgreich vom Standardmodell (SM) der Elementarteilchenphysik beschrieben werden, bei sehr hohen Energieskalen zu untersuchen. Tatsächlich haben jüngste Messungen mehrerer Observablen von $b \to c\ell\nu$- sowie $b \to s\ell\ell$-Übergängen Abweichungen von SM-Vorhersagen aufgezeigt. Diese Abweichungen werden kollektiv als B-Anomalien bezeichnet. Um festzustellen, ob die B-Anomalien ein tatsächlicher Nachweis von Physik jenseits des SM sind, sind genaue theoretische Vorhersagen der entsprechenden hadronischen Matrixelemente (HME) unerlässlich. Die größten theoretischen Unsicherheiten in den semileptonischen Zerfällen $B \to D^{(*)}\ell\nu$ und $B_s \to D_s^{(*)}\ell\nu$ kommen von den lokalen HME, die durch die Meson-Formfaktoren parametrisiert werden. Wir berechnen diese Formfaktoren im Rahmen der QCD Lichtkegelsummenregeln (LCSR) mit B-Meson-Verteilungsamplituden. Um die Genauigkeit unserer Vorhersagen weiter zu verbessern und die Formfaktoren auf den gesamten physikalischen Bereich zu extrapolieren, kombinieren wir unsere LCSR-Ergebnisse mit den Gitter-QCD-Ergebnissen und legen dispersive Schranken fest. In seltenen B-Zerfällen, abgesehen von den lokalen HME, beschränken gegenwärtig auch nicht-lokale HME die theoretische Genauigkeit in einem Großteil der Observablen, die die B-Anomalien ausmachen. Wir berechnen diese HME für $B \to K^{(*)}\ell\ell$-Zerfällen ebenfalls unter Verwendung von LCSRs. Um zusätzliche Bedingungen für die nicht-lokalen $B \to K^{(*)}\ell\ell$ HME zu erhalten, erweitern wir die Methode der dispersiven Schranken, um sie für diese Art von Objekten geeignet zu machen. Abschließend erörtern wir ausgewählte phänomenologische Implikationen unserer Ergebnisse und treffen dabei SM-Vorhersagen für die Lepton-Flavour-Universalitätsverhältnisse $R_{D^{(*)}}$ und andere wichtige Observablen in B-Zerfällen.

Contents

Introduction

The Standard Model (SM) of particle physics successfully describes three of the four known fundamental interactions (electromagnetic, weak, and strong) through a spontaneously broken gauge theory. So far, direct searches for new particles in high-energy collider experiments have so not found any evidence for physics beyond the SM (BSM). An alternative to the direct searches is to look for BSM effects indirectly, through quantum fluctuations at low energies. In this way, potential effects of BSM physics can be probed at energy scales beyond the reach of earth-bound collider experiments [4].

Flavour physics, which is the branch of particle physics that investigates the transitions and the spectrum of the different quark and lepton flavours, provides complementary means to test the SM up to very high energy scales in indirect searches. Recent results in flavour physics obtained by the B-factory experiments (Belle and BaBar) and by LHC experiments (LHCb, CMS and ATLAS) have shown discrepancies with respect to the SM predictions in several observables in $B \to D^{(*)}\tau\nu$ and $B \to K^{(*)}\ell\ell$ decays. This set of tensions is commonly called the B *anomalies* [5–7].

In view of the present and any forthcoming experimental results, it is crucial to increase the accuracy of theoretical predictions for mainly two reasons. First, to understand whether the B anomalies are a mere statistical fluctuation, an underestimation of systematic uncertainties or signs of BSM physics. Second, even if the B anomalies will not be confirmed as signs of BSM effects, higher precision in theoretical predictions will be beneficial to further constrain new physics and to determine the SM parameters.

Hadronic matrix elements (HMEs) are necessary inputs for theoretical predictions of all the observables in hadron decays (and in particular in B-meson decays). Being genuinely non-perturbative objects, HMEs are hard to determine and hence represent the major uncertainties in these predictions. This is due to the fact that the quarks inside hadrons interact at energies of the order of the hadronic binding energy, for which QCD perturbation theory does not hold.

There are two QCD based methods to compute HMEs: lattice gauge simulations (LQCD) and QCD sum rules. While LQCD will, in the long run, dominate the predictions due to reducible systematic and statistical uncertainties, QCD sum rules can presently elucidate such matrix elements for which there are no or only limited LQCD results available.

It is also possible to combine the results of these two methods, for instance in meson-to-meson transitions. In this case, the local HMEs can be expressed in terms of functions of the momentum transfer q^2, the so-called *form factors*. While LQCD is more effective for large q^2 values, even though recent studies provide excellent results also at $q^2 = 0$ [8], QCD sum rules can only be applied for low q^2 values. This is due to the operator product expansion that is performed to calculate a QCD sum rule (see chapter 3). It is then beneficial to combine LQCD and QCD sum rules predictions to extract the form factors values in the entire physically allowed region. Applications of this method are discussed in subsection 4.3.2.

In this work we use the QCD light-cone sum rules (LCSRs) to compute form factors and other HMEs relevant for semileptonic B decays. The starting point to compute a sum rule is a correlation function, which is calculated in two different ways. The first consists in performing an operator product expansion of the correlator, in order to factorise short- and long-distance contributions. The second corresponds to expressing the same correlator in the form of a hadronic dispersion relation. The two results are then matched using semi-local quark-hadron duality giving a relation between the HMEs and other hadronic quantities, which is called the sum rule. A thorough review of the method is provided in chapter 3.

Employing the LCSRs with B-meson distribution amplitudes, we updated the calculation of the $B \to \pi, \rho, K^{(*)}, D^{(*)}$ form factors including corrections of sub-leading twists [1]. These corrections have a significant impact that amounts to a $\sim 20 - 30\%$ shift of the final results. The corresponding phenomenological implications are discussed in the chapter 4 as well. We also calculated the $B_s \to D_s^{(*)}$ form factors using LCSRs at twist four accuracy [2]. The importance of these results lies in the fact that they represent the first theoretical calculation of the $B_s \to D_s^*$ form factors, except for one lattice data point at maximum momentum transfer (see [9] for the most recent calculation). We used these form factors to predict the lepton flavour universality ratio $R(D_s^*)$ and to critically revisit the dispersive bounds [10] in $B_q \to D_q^{(*)}$ processes (with $q = u, d, s$) beyond the $SU(3)$ flavour symmetry limit. This project acquired even more importance from a phenomenological point of view due to the recent [11, 12] and forthcoming experimental results for $B_s \to D_s^{(*)}$ decays from the LHCb collaboration.

In rare B decays (e.g. $B \to K^{(*)}\ell\ell$ and $B_s \to \phi\ell\ell$) there are also important contributions that come from non-local HMEs, besides the leading contributions proportional to local HMEs, which are parametrized in terms of form factors. While the calculation of non-local HMEs using LQCD is at a conceptual stage, LCSRs allow to estimate their important impact on the theoretical predictions.

We focus on the evaluation of non-local HMEs that contribute to the so-called *charm-loop effects* in $B \to K^{(*)}\ell\ell$ decays. These non-local HMEs are an indispensable hadronic inputs for the understanding of these decays and especially the P_5' anomaly [13]. In fact, they constitute the single-largest systematic uncertainty in $B \to K^{(*)}\ell\ell$ transitions. We have recalculated the soft-gluon contribution to the charm-loop effect, which was originally discussed in ref. [14]. While we reproduce the analytical results given in the original paper (for $B \to K$) and provided by the authors (for $B \to K^*$), we find that crucial contributions are missing. These contributions cancel partially the terms discussed in the literature and reduce the final numerical result by one order of magnitude. This project also includes further improvements on the non-local HMEs, which are work in progress. Hence, this thesis only contains a subset of the work that is going to be published elsewhere [3].

This thesis is organised as follows. In chapter 1 we review the Standard Model and introduce flavour physics, focusing on B-meson decays. The various effective field theories used in this work are presented in chapter 2, while the methods to calculate and/or constrain hadronic matrix elements are discussed in chapter 3. We finally discuss our analytical and numerical results and their phenomenological applications in chapter 4, before we summarise them in the conclusion.

Chapter 1

Flavour Physics and B-meson Decays — a Short Review

In this first chapter we briefly review the Standard Model of particle physics and classify all the states that occur in our studies for the reader's convenience. Next, we give a short introduction to flavour physics, with focus on B-meson decays. We also present the current status of the theoretical predictions and the experimental measurements in flavour physics with special emphasis on the B anomalies.

1.1 The Standard Model Lagrangian

The Standard Model (SM) of particle physics is the theory that successfully describes three of the four fundamental interactions known in Nature: the electromagnetic, the weak and the strong interactions. Even though it is evident that the SM cannot be the ultimate theory of Nature[1], there has not been any experimental measurement in particle physics that contradicts the SM predictions so far.

In the following, we introduce the main features of the SM and the notation that is used throughout this work, without any intent to give a complete and self-contained introduction of the subject. For a more detailed introduction to the SM, we refer the interested reader to standard textbooks (e.g. [16, 17]).

The SM is a gauge theory with symmetry group

$$\mathcal{G}_{SM} = SU(3)_C \times SU(2)_L \times U(1)_Y \,, \tag{1.1}$$

which is spontaneously broken by the Higgs potential to

$$SU(3)_C \times U(1)_Q \,. \tag{1.2}$$

Here, $SU(3)_C$ is the colour symmetry group of strong interactions, $SU(2)_L$ is the weak isospin group, and $U(1)_Y$ and $U(1)_Q$ are the groups of the weak hypercharge and the electric charge transformations, respectively. The weak hypercharge is related to the electric charge Q and the third component of the weak isospin T_3 through the formula

$$Y = 2(Q - T_3).$$

[1] For instance, the SM is not able accommodate gravity, dark matter, dark energy etc. [15].

field	Q_L^i	u_R^i	d_R^i	E_L^i	e_R^i	γ	g	$W^\pm, Z^0$	H
repr.	$(\mathbf{3},\mathbf{2})_{\frac{1}{3}}$	$(\mathbf{3},\mathbf{1})_{\frac{4}{3}}$	$(\mathbf{3},\mathbf{1})_{-\frac{2}{3}}$	$(\mathbf{1},\mathbf{2})_{-1}$	$(\mathbf{1},\mathbf{1})_{-2}$	$(\mathbf{1},\mathbf{1})_0$	$(\mathbf{8},\mathbf{1})_0$	$(\mathbf{1},\mathbf{3})_0$	$(\mathbf{1},\mathbf{2})_1$

Table 1.1: Representation of the SM fields under the gauge group $\mathcal{G}_{SM}$. The notation used is $(\mathbf{C},\mathbf{L})_Y$, where $\mathbf{C}$ is the representation under the $SU(3)_C$ group, $\mathbf{L}$ is the representation under the $SU(2)_L$ group, and Y is the weak hypercharge.

An important feature of the SM is that it distinguishes left- and right-chiral fields[2] by their charges under $\mathcal{G}_{SM}$.

In the SM there are six types (or *flavours*) of quarks: up (u), down (d), strange (s), charm (c), bottom (or beauty) (b) and top (or truth) (t); and six types of leptons: electron (e), muon (μ), tauon (τ), and three neutrinos species (ν_e, ν_μ, ν_τ). Even though the term flavour is also used to refer to different types of leptons, in this work it is only used for quarks. Quarks and leptons are organised in three generations (or families), where the left-chiral fields

$$Q_L^i \equiv \begin{pmatrix} u_L^i \\ d_L^i \end{pmatrix} \equiv \left(\begin{pmatrix} u_L \\ d_L \end{pmatrix} \quad \begin{pmatrix} c_L \\ s_L \end{pmatrix} \quad \begin{pmatrix} t_L \\ b_L \end{pmatrix} \right),$$
$$E_L^i \equiv \begin{pmatrix} \nu_L^i \\ e_L^i \end{pmatrix} \equiv \left(\begin{pmatrix} \nu_{e,L} \\ e_L \end{pmatrix} \quad \begin{pmatrix} \nu_{\mu,L} \\ \mu_L \end{pmatrix} \quad \begin{pmatrix} \nu_{\tau,L} \\ \tau_L \end{pmatrix} \right)$$

are $SU(2)_L$ doublets and the right-chiral fields

$$u_L^i \equiv \begin{pmatrix} u_R & c_R & t_R \end{pmatrix}, \qquad d_L^i \equiv \begin{pmatrix} d_R & s_R & b_R \end{pmatrix}, \qquad e_R^i \equiv \begin{pmatrix} e_R & \mu_R & \tau_R \end{pmatrix}$$

are $SU(2)_L$ singlets. Right-chiral neutrinos are commonly not included in the SM, since they are noy charged under the group $\mathcal{G}_{SM}$. Quarks also carry a colour charge, since they are $SU(3)_C$ triplets, while leptons $SU(3)_C$ are singlets. In addition to these twelve fermions, there are four vector bosons that mediate the interactions, namely the photon (γ), the gluon (g), the $W^\pm$ and the Z^0. The last piece of the SM is the Higgs scalar field (H), which is an $SU(2)$ doublet and, contrary to all the other fields, has a non-zero vacuum expectation value (VEV)

$$\langle H \rangle = \frac{1}{\sqrt{2}} \begin{pmatrix} 0 \\ v \end{pmatrix}. \tag{1.3}$$

The representations of these fields under the SM group $\mathcal{G}_{SM}$ are listed in table 1.1. Besides their representation under the gauge groups and their spin, elementary particles are also characterised by their mass. The particles mass are free parameters in the SM, i.e. they cannot be predicted and hence they have to be measured. As one can see from figure 1.1, the fermion and boson masses differ from each other by several orders of magnitude. Although there is no a priori explanation for this fact in the SM, it is possible to exploit these different energy scales introduced by the particles masses to obtain simpler *effective* field theories, which we review in chapter 2.

Given the above field content, the gauge group $\mathcal{G}_{SM}$, and assuming renormalizability, the SM Lagrangian is the most general Lagrangian, in the sense that it contains all the possible

[2]The definition of left- and right-chiral fields is given in appendix A.

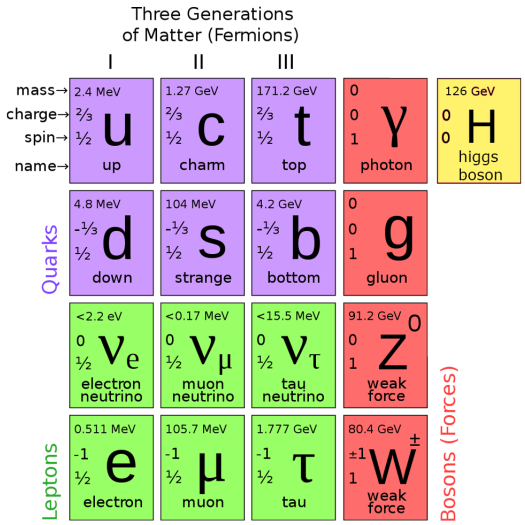

Figure 1.1: Elementary particles of the SM with their respective mass, charge and spin. Image from ref. [18].

terms that fulfil these conditions[3]. Schematically, it reads

$$\mathcal{L}_{SM} = \mathcal{L}_{kin} + \mathcal{L}_{int} + \mathcal{L}_{Yk} + \mathcal{L}_{Higgs}. \tag{1.4}$$

The kinetic and interaction terms of the fermions and gauge bosons read

$$\mathcal{L}_{kin} + \mathcal{L}_{int} = i \sum_{\psi} \bar{\psi} \not{D} \psi - \frac{1}{4} B_{\mu\nu} B^{\mu\nu} - \frac{1}{2} \mathrm{Tr}\{\mathbf{W}_{\mu\nu} \mathbf{W}^{\mu\nu}\} - \frac{1}{2} \mathrm{Tr}\{\mathbf{G}_{\mu\nu} \mathbf{G}^{\mu\nu}\}\,, \tag{1.5}$$

with the field strength tensors

$$\begin{aligned} B_{\mu\nu} &= \partial_\mu B_\nu - \partial_\nu B_\mu\,, \\ \mathbf{W}_{\mu\nu} &= \partial_\mu \mathbf{W}_\nu - \partial_\nu \mathbf{W}_\mu + i g_2 \left[\mathbf{W}_\mu, \mathbf{W}_\nu\right]\,, \\ \mathbf{G}_{\mu\nu} &= \partial_\mu \mathbf{G}_\nu - \partial_\nu \mathbf{G}_\mu + i g_s \left[\mathbf{G}_\mu, \mathbf{G}_\nu\right]\,. \end{aligned}$$

We abbreviate

$$\mathbf{W}_{\mu(\nu)} = W^a_{\mu(\nu)} \frac{\sigma_a}{2}\,, \qquad\qquad \mathbf{G}_{\mu(\nu)} = G^a_{\mu(\nu)} \frac{\lambda_a}{2}\,.$$

Here σ_a are the Pauli matrices and λ_a are the Gell-Mann matrices, each of which are traceless generators of their respective gauge group. The sum in eq. (1.5) runs over all the fermion fields and $\mathbf{W}_{\mu\nu}$, $\mathbf{G}_{\mu\nu}$, and $B_{\mu\nu}$ are the field strength tensors of $SU(3)_C$, $SU(2)_L$, and $U(1)_Y$, respectively. The covariant derivative that act on the left-chiral quark fields reads

$$D_\mu Q_L = \left(\partial_\mu - i Y g_1 B_\mu - i g_2 \mathbf{W}_\mu - i g_s \mathbf{G}_\mu\right) Q_L\,, \tag{1.6}$$

[3]Dropping the renormalizability one obtains a more general Lagrangian, called the Standard Model Effective Field Theory (SMEFT) Lagrangian [19, 20], which is useful to investigate potential NP effects in a model independent way.

where g_1, g_2, and g_s are the coupling constants of $SU(3)_C$, $SU(2)_L$, and $U(1)_Y$, respectively. The electroweak couplings g_1 and g_2 are related to the electron charge e by

$$e = \frac{g_1 g_2}{\sqrt{g_1^2 + g_2^2}} \,.$$

It also useful to define the parameters

$$\alpha_e \equiv \frac{e^2}{4\pi} \,, \qquad\qquad \alpha_s \equiv \frac{g_s^2}{4\pi} \,, \tag{1.7}$$

where $\alpha_e \simeq 1/137$ is the fine-structure constant. The covariant derivatives of the other fermion fields have an analogous form to eq. (1.6).

The Yukawa interaction terms are

$$\mathcal{L}_{Yk} = -Y_e \bar{E}_L H e_R - Y_d \bar{Q}_L H d_R - Y_u \bar{Q}_L i\sigma_2 H^\dagger u_R + h.c. \,, \tag{1.8}$$

while the Higgs potential and kinetic term is

$$\mathcal{L}_{Higgs} = \left(D_\mu H\right)^\dagger \left(D_\mu H\right) - \frac{m_H^2}{2v^2}\left(H^\dagger H - v^2\right)^2 \,. \tag{1.9}$$

The Lagrangian given above is expressed in the flavour basis, where the gauge bosons do not mix quarks of different generations. For numerous applications, it is more convenient to work in the basis where the Yukawa couplings, and hence the fermion mass matrices, are diagonal, which is called the mass basis. To diagonalize the Yukawa couplings, one has to perform a bi-unitary rotation of the quark fields of the form

$$u_L = U_u u_L \,, \qquad\qquad d_L = U_d d_L \,.$$

The only effect of this flavour rotation is on the $W^\pm$ couplings, which become

$$W_\mu^+ \bar{u}_L \gamma^\mu d_L + W_\mu^- \bar{d}_L \gamma^\mu u_L \longrightarrow W_\mu^+ \bar{u}_L^i \gamma^\mu \left(V_{CKM}\right)^{ij} d_L^j + W_\mu^- \bar{d}_L^i \gamma^\mu \left(V_{CKM}^\dagger\right)^{ij} u_L^j \,, \tag{1.10}$$

where

$$U_u^\dagger U_d \equiv V_{CKM} = \begin{pmatrix} V_{ud} & V_{us} & V_{ub} \\ V_{cd} & V_{cs} & V_{cb} \\ V_{td} & V_{ts} & V_{tb} \end{pmatrix} \tag{1.11}$$

is the Cabibbo-Kobayashi-Maskawa (CKM) matrix, a complex unitary matrix with a priori nine real degrees of freedom. Performing a $U(1)^6$ transformation on the fields, one can show that there are only three independent angles and one complex phase out of the original nine degrees of freedom of a generic complex unitary matrix. This complex phase implies that CP is not a symmetry of the SM Lagrangian, and hence CP is not a conserved quantum number. As we will discuss in detail in section 1.3, the current (1.10) is the only one in the SM that does not conserve the flavour quantum numbers.

To have an idea of the relative size of the elements of the CKM matrix, it is convenient to express it using the Wolfenstein parameterization

$$V_{CKM} = \begin{pmatrix} 1 - \frac{\lambda^2}{2} & \lambda & A\lambda^3(K^* - i\eta) \\ -\lambda & 1 - \frac{\lambda^2}{2} & A\lambda^2 \\ A\lambda^3(1 - \rho - i\eta) & -A\lambda^2 & 1 \end{pmatrix} + \mathcal{O}\left(\lambda^4\right) \,, \tag{1.12}$$

where, experimentally, the values of the Wolfenstein parameters are found to be

$$\lambda \simeq 0.23, \qquad A \simeq 0.8, \qquad \rho \simeq 0.1, \qquad \eta \simeq 0.3. \tag{1.13}$$

Notice that the CKM matrix is almost diagonal, thus transitions between different generations are suppressed in the SM. The unitarity of the CKM matrix implies that its matrix elements are related through the identities

$$\sum_i V_{ij} V_{ik}^* = \delta_{jk}\,, \qquad\qquad \sum_l V_{kl} V_{ml}^* = \delta_{km}\,, \tag{1.14}$$

for any j, k and any k, m. Among the equations (1.14), the relation

$$V_{ud} V_{ub}^* + V_{cd} V_{cb}^* + V_{td} V_{tb}^* = 0 \tag{1.15}$$

is particularly famous because it contains V_{ub}, V_{cb} and V_{tb}, which are interesting CKM matrix elements from a phenomenological point of view. Notice also that all the terms in eq. (1.15) are of the same order $\mathcal{O}\left(\lambda^3\right)$. It is helpful to use a graphical representation of eq. (1.15), called the *unitarity triangle*, which is illustrated in figure 1.2. The unitarity triangle is usually represented on the complex plane $(\bar{\rho}, \bar{\eta})$, where

$$\bar{\rho} = \rho\left(1 - \frac{\lambda^2}{2}\right), \qquad\qquad \bar{\eta} = \eta\left(1 - \frac{\lambda^2}{2}\right). \tag{1.16}$$

Normalising eq. (1.15) by $V_{cd} V_{cb}^*$, one obtains

$$\frac{V_{ud} V_{ub}^*}{V_{cd} V_{cb}^*} + 1 + \frac{V_{td} V_{tb}^*}{V_{cd} V_{cb}^*} = 0\,, \tag{1.17}$$

with

$$\frac{V_{ud} V_{ub}^*}{V_{cd} V_{cb}^*} = -(\bar{\rho} + i\bar{\eta}) + \mathcal{O}\left(\lambda^4\right), \qquad \frac{V_{td} V_{tb}^*}{V_{cd} V_{cb}^*} = (\bar{\rho} + i\bar{\eta}) - 1 + \mathcal{O}\left(\lambda^4\right). \tag{1.18}$$

Thus, the sides of the unitarity triangle are given by

$$\left|\frac{V_{ud} V_{ub}^*}{V_{cd} V_{cb}^*}\right| = \sqrt{\bar{\rho}^2 + \bar{\eta}^2}\,, \qquad\qquad \left|\frac{V_{td} V_{tb}^*}{V_{cd} V_{cb}^*}\right| = \sqrt{(1-\bar{\rho})^2 + \bar{\eta}^2}\,, \tag{1.19}$$

while the angles read

$$\alpha \equiv \left[-\frac{V_{td} V_{tb}^*}{V_{ud} V_{ub}^*}\right], \qquad \beta \equiv \left[-\frac{V_{cd} V_{cb}^*}{V_{td} V_{tb}^*}\right], \qquad \gamma \equiv \left[-\frac{V_{ud} V_{ub}^*}{V_{cd} V_{cb}^*}\right]. \tag{1.20}$$

If the CKM matrix were real, the triangle would be degenerate. It follows that its area is related to the magnitude CP violation in the SM. This area can be expressed in terms of the Jarlskog invariant J as

$$\text{Area} = \frac{J}{2}\,, \tag{1.21}$$

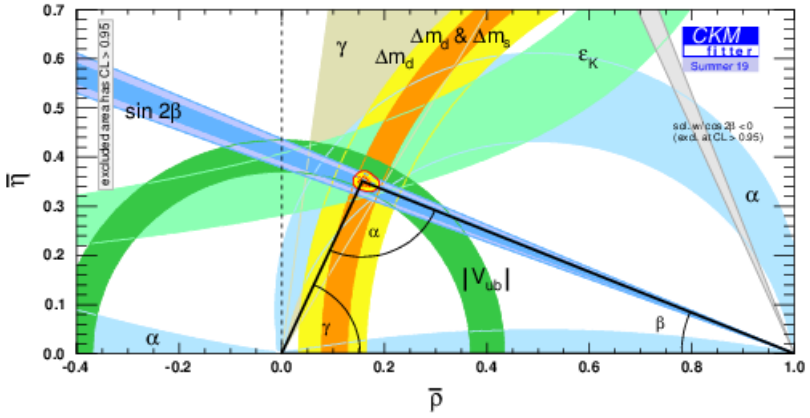

Figure 1.2: The unitarity triangle represented together with various experimental constraints. The small red hashed region around the top vertex of the triangle corresponds to 68% confidence level of the global combination of the experimental measurements done by the CKMfitter group [21].

where J is given by

$$J = \sum_{m,n=1}^{3} \epsilon_{ikm}\epsilon_{jln}\,\mathrm{Im}\left[V_{ij}V_{kl}V_{il}^{*}V_{kj}^{*}\right] \ . \tag{1.22}$$

There would not be no CP violation if and only if $J = 0$. In the SM $J \neq 0$, as one can see from figure 1.2.

After this brief introduction of the SM, we can now list all its nineteen free parameters, which are:

- three lepton masses (neutrinos are massless in the SM),
- six quark masses,
- three coupling constants g_1, g_2 and g_s,
- three angles and one phase of the CKM matrix,
- the Higgs boson mass and its VEV,
- the QCD vacuum angle (see e.g. ref. [17]).

All these parameters have to be determined experimentally since the SM is not able to predict them, which means that they could in principle assume any real (in some case strictly positive) value. There are attempts to solve this conceptual problem by embedding the SM in a more general theory that can relate the values of its free parameters. The interested reader may consult e.g. refs. [22–24]. However, our analysis is mostly focus on the SM and some of the ways to probe its predictions. As a first step, we introduce some nomenclature of the QCD bound states that will be useful in the following chapters.

1.2 QCD Bound States

Free quarks are not observed in Nature. Rather they are confined into hadrons. This phenom is known as *colour confinement* and it is due to the fact that QCD is asymptotically free [25, 26]. Thus, to study quark transitions, in practice one has to study hadron transitions, since only hadrons are accessible by experiments. However, processes involving hadrons are extremely more complicated to study theoretically than processes involving highly energetic quarks. This is because the quarks inside the hadrons interact at energies of the order of the hadronic binding energy, for which QCD perturbation theory is not applicable. We will discuss in detail in chapter 3 two methods to perform non-perturbative calculations, namely lattice QCD and QCD sum rules. In this section, we introduce the names of the hadrons used throughout this work.

There are two kinds of hadrons: baryons, which are bound states of three quarks, and mesons, which are bound states of two quarks (neglecting exotic hadrons such as tetraquarks and pentaquarks). Since we mostly focus on mesons decays, there is no need here to introduce the nomenclature of baryons, for which the reader can consult the Particle Data Group (PDG) review [27]. Furthermore, the list of mesons given below is far from being complete and we restrict ourselves to the states that appear in our analysis.

In order to classify mesons, it is useful to introduce the strangeness (S), the charm (C), the bottomness (or beauty) (B) and the topness (or truth) (T) quantum numbers defined as

$$\begin{aligned} \mathrm{S} &= -\left(n_s - n_{\bar{s}}\right) , \\ \mathrm{C} &= +n_c - n_{\bar{c}} , \\ \mathrm{B} &= -\left(n_b - n_{\bar{b}}\right) , \\ \mathrm{T} &= +n_b - n_{\bar{b}} , \end{aligned}$$

where n_q ans $n_{\bar{q}}$ are the number of q quarks and $\bar{q}$ antiquarks in a meson, respectively. Mesons with $\mathrm{T} \neq 0$ are not observed in nature, since top quarks do not hadronise due to their very short lifetime.

Flavourless mesons are those with $\mathrm{S} = \mathrm{C} = \mathrm{B} = 0$:

our notation	antiparticle	PDG name	valence quark content	mass GeV	J^P
π^+	π^-	$\pi^\pm$	$u\bar{d}$	0.140	0^-
π^0	—	π^0	$\frac{u\bar{u}-d\bar{d}}{\sqrt{2}}$	0.135	0^-
η	—	η	$\frac{u\bar{u}+d\bar{d}-2s\bar{s}}{\sqrt{2}}$	0.548	0^-
η'	—	$\eta'(958)$	$\frac{u\bar{u}+d\bar{d}+s\bar{s}}{\sqrt{2}}$	0.958	0^-
ρ^+	ρ^-	$\rho(770)^\pm$	$u\bar{d}$	0.775	1^-
ρ^0	—	$\rho(770)^0$	$\frac{u\bar{u}-d\bar{d}}{\sqrt{2}}$	0.775	1^-
ω	—	$\omega(782)$	$\frac{u\bar{u}+d\bar{d}}{\sqrt{2}}$	0.783	1^-
ϕ	—	$\phi(1020)$	$s\bar{s}$	1.019	1^-
J/ψ	—	$J/\psi(1S)$	$c\bar{c}$	3.097	1^-
$\Upsilon(4S)$	—	$\Upsilon(4S)$	$b\bar{b}$	10.579	1^-

where J is the spin and P is the parity of the meson considered.
Mesons with S $= \pm 1$ and C $=$ B $= 0$ are called kaons:

K^+	K^-	$K^\pm$	$u\bar{s}$	0.494	0^-
K^0	$\bar{K}^0$	K^0	$d\bar{s}$	0.498	0^-
K^{*+}	K^{*-}	$K^*(892)^\pm$	$u\bar{s}$	0.892	1^-
K^{*0}	$\bar{K}^{*0}$	$K^*(892)^0$	$d\bar{s}$	0.896	1^-

Mesons with C $= \pm 1$, S $= 0, \pm 1$ and B $= 0$ are called D mesons:

D^+	D^-	$D^\pm$	$c\bar{d}$	1.870	0^-
D^0	$\bar{D}^0$	D^0	$c\bar{u}$	1.865	0^-
D_s^+	D_s^-	$D_s^\pm$	$c\bar{s}$	1.968	0^-
D^{*+}	D^{*-}	$D^*(2010)^\pm$	$c\bar{d}$	2.010	1^-
D^{*0}	$\bar{D}^{*0}$	$D^*(2007)^0$	$c\bar{u}$	2.007	1^-
D_s^{*+}	D_s^{*-}	$D_s^{*\pm}$	$c\bar{s}$	2.112	1^-

Mesons with B $= \pm 1$, S $= 0, \pm 1$ and C $= 0, \pm 1$ are called B mesons:

B^+	B^-	$B^\pm$	$u\bar{b}$	5.279	0^-
B^0	$\bar{B}^0$	B^0	$d\bar{b}$	5.280	0^-
B_s	$\bar{B}_s$	B_s^0	$s\bar{b}$	5.366	0^-
B_c^+	B_c^-	$B_c^\pm$	$c\bar{b}$	6.275	0^-
B^{*+}	B^{*-}	$B^{*\pm}$	$u\bar{b}$	5.325	1^-
B^{*0}	$\bar{B}^{*0}$	B^{*0}	$d\bar{b}$	5.325	1^-
B_s^*	$\bar{B}_s^*$	B_s^*	$s\bar{b}$	5.413	1^-
B_c^{*+}	B_c^{*-}	$B_c^{*\pm}$	$c\bar{b}$	6.329	1^-

The superscript "*" is added to flavoured mesons with spin-parity quantum numbers that follow the natural series $J^P = 0^+, 1^-, 2^+, \ldots$. This is useful in practice to distinguish pseudoscalar and vector mesons. Throughout this work, when the flavour of the spectator quark is not relevant, the simplified notation B (B^*) is used to indicate all the pseudoscalar (vector) B mesons, excluding the B_c mesons (i.e. all the mesons with B $=$ C $= \pm 1$). An analogous notation is used for the kaons and the D mesons.

1.3 Flavour Physics

Flavour physics is the branch of particle physics that investigates the different quark and lepton flavours, their transitions, and their spectrum. An interesting aspect of flavour physics is that it provides the means to test the SM up to very high energy scales through the so-called *indirect searches*. In this way, potential effects of beyond the SM (BSM) physics can be probed at energy scales beyond the reach of earth-bound collider experiments [4]. In fact, direct searches for new particles in high-energy colliders have not found any evidence for physics BSM so far, and the only hints at present stem from flavour physics.

The main ingredients of flavour physics are the flavour changing currents, the CKM matrix, and the couplings strength. There are two kinds of flavour changing currents: the ones

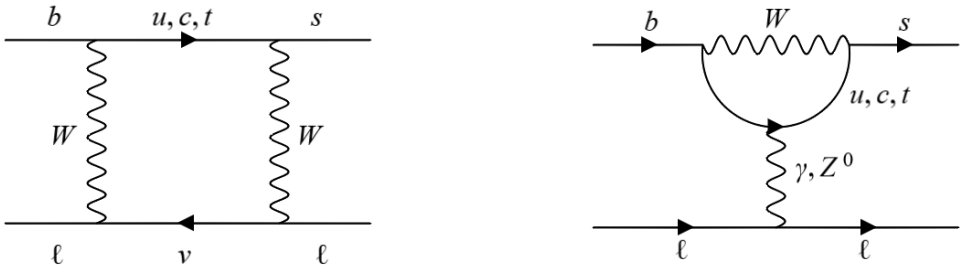

(a) (b)

Figure 1.3: Examples of a box diagram (a) and a penguin diagram (b) for the FCNC process $b \to s\ell\ell$.

mediated by charged currents (flavour changing charged currents (FCCCs)) and the ones mediated by neutral currents (flavour changing neutral currents (FCNCs)). As discussed in section 1.1, the only particle that couples to quarks with different flavours is the W boson, which is a charged particle. This means that FCCCs can already occur at tree level, while FCNCs can only occur at loop level in the SM.

In figure 1.3 there are two examples of diagrams that mediate FCNC processes, which are commonly called box and penguin diagrams. FCNC transitions are extremely suppressed in the SM for the following reasons:

1. They are $(g_2/4\pi)^2$ suppressed, since they arise at one-loop level.

2. In all processes where there are transitions between quarks of different generations, the amplitude is proportional to non-diagonal elements of the CKM matrix, which are much smaller than one (see eq. (1.12)).

3. FCNC transitions between two up type quarks (i.e. $u_i = u, c, t$) are further suppressed by the GIM mechanism [28]. For example, the amplitude of the diagram shown in figure 1.3(a) is of the form

$$\mathcal{M} \propto \sum_{i,j=d,s,b} V_{ic}^* V_{iu} V_{jc}^* V_{ju} F(x_i, x_j)\,, \tag{1.23}$$

   where $F(x_i, x_j)$ is a function that can be computed perturbatively (see e.g. ref. [29]) and expressed in temrs of $x_i = m_{q_i}^2/m_W^2$. In the limit $x_d = x_s = x_b$ the amplitude (1.23) vanishes due to the unitarity of the CKM matrix. Since in nature we have x_d, x_s, $x_b \ll 1$, the amplitude (1.23) is not identically zero but GIM suppressed. For down type quark FCNC transitions the situation is quite different, because the top quark mass is bigger than the W boson mass and $x_u = x_s = x_t$ is no longer a good approximation. Hence, the amplitudes in this case are dominated by the top quark contribution and there is only an incomplete GIM suppression.

4. In some cases, FCNC processes can also be chirality suppressed, since FCNCs couple only to left-chiral fermions in the SM.

As an example, let us consider two different semi-leptonic B-meson decays to illustrate the suppression of FCNCs compared to FCCCs. The $B^0 \to D^{*-}\tau^+\nu_\tau$ decay, which is a $b \to c$

transition, has a relatively large branching fraction [27]

$$\mathrm{Br}\left(B^0 \to D^{*-}\tau^+\nu_\tau\right) = (1.57 \pm 0.10)\%\,, \tag{1.24}$$

while the $B^0 \to K^{*0}\mu^+\mu^-$ decay, which is a $b \to s$ transition, is a *rare process*

$$\mathrm{Br}\left(B^0 \to K^{*0}\mu^+\mu^-\right) = (9.4 \pm 0.5) \times 10^{-7}\,. \tag{1.25}$$

The fact that FCNC decays are strongly suppressed and do not occur at tree level in the SM makes them interesting and suitable to test the SM itself. Indeed, some BSM theories allow FCNCs at tree level, which would generate enhanced contributions with respect to the SM ones and hence easier to detect. Examples of such BSM mediators are the leptoquarks (see ref. [30] for a review), hypothetical particles that couple quarks to leptons and vice versa, and the Z' boson, a heavier version of the Z boson with non-zero couplings to quarks of different generations. Although one may naively think that the $B^0 \to K^{*0}\mu^+\mu^-$ decay is much harder to detect than the $B^0 \to D^{*-}\tau^+\nu_\tau$, since the former is much rarer than the latter, the relative uncertainties of their branching fractions (1.24)-(1.25) are similar. This is one of the reasons why the $B^0 \to K^{*0}\mu^+\mu^-$ decay is a good candidate to study the FCNCs.

The results given in eqs. (1.24)-(1.25), as well as most of the results relevant for flavour physics and in particular for the B-meson physics, are averages done by the PDG collaboration. These averages rely mostly on the measurements carried out by the LHCb, Belle and BaBar collaborations using the data collected by the homonym detectors[4] that are located at the CERN (Geneva, Switzerland), KEK (Tsukuba, Japan) and SLAC (Menlo Park, California) laboratories, respectively. The main purpose of these experiments is (or was, since BaBar ceased its activity in April 2008) to study CP violation and the flavoured hadrons, especially those that contain b quarks. These three detectors have different designs, since they are located at different colliders. The LHC is a proton-proton synchrotron with collision energy of the order of $\sim 10\,\mathrm{TeV}$, built primarily to "hunt" the Higgs boson, whose discovery was announced 4 July 2012 [31], and the particles predicted by supersymmetric theories, which have not been detected yet. SuperKEKB, a major upgrade of KEKB, and PEP-II, which hosted the BaBar experiment, are two electron-positron colliders with center-of-mass energy close to the $\Upsilon(4S)$ resonance. The $\Upsilon(4S)$ decays mostly in a $B - \bar{B}$ pair, indeed

$$\mathrm{Br}\left(\Upsilon(4S) \to B\bar{B}\right) > 96\%\,.$$

This explains why SuperKEKB and PEP-II are known as B-factories.

Since B-meson decays are the main topic of this work, we will introduce in the next section the basic theoretical tools to analyse them and explain the reasons why they are so relevant in particle physics phenomenology.

1.4 B-meson Decays

The decays of the B meson are among the most studied processes in flavour physics. There are several reasons why B mesons are interesting particles to study. As we have seen, the b quark is the heaviest fermion that forms bound states. Being lighter than the top quark, it must decay in quarks of another generation and its decay is necessarily CKM suppressed.

[4] Belle was operative between 1998 and 2010. Belle II started taking data in early 2018.

Thus, B mesons have a relatively large lifetime, $1.6 \cdot 10^{-6}\, s$, making them easier to detect and identify experimentally.

B-meson decays are usually divided into two categories: *inclusive* decays and *exclusive* decays. In inclusive decays one considers all the possible final states of a B meson and hence the decay width Γ can be schematically as

$$\Gamma\left(B \text{ inclusive}\right) = \sum_X \Gamma\left(B \to X\right) , \tag{1.26}$$

where the sum is over all the allowed final states X. One can also consider semi-inclusive B decays, restricting the sum in eq. (1.26) to the processes that include the specified products, for instance

$$\Gamma\left(B \text{ semi-inclusive}\right) = \sum_{X_c} \Gamma\left(B \to X_c \ell\nu\right) , \tag{1.27}$$

where X_c is a state with $\mathrm{C} = \pm 1$. Conversely, in exclusive decays, one analyses one process at the time, as in eqs. (1.24)-(1.25). We mostly focus on exclusive decays throughout this work.

Exclusive decays are further divided into three categories: leptonic, semi-leptonic, and hadronic decays, depending on the nature of the final states. For simplicity, we restrict ourselves to decays into a lepton pair, two mesons or a lepton pair and a meson, neglecting all the other decays with a higher number of particles in the final state.

Let us start with purely leptonic decays, which are the best-understood decays from a theoretical perspective. They can be decomposed as

$$\langle L |\, J_\ell, J_q \,| B \rangle = \langle L |\, j_\ell \,| 0 \rangle \, \langle 0 |\, J_q \,| B \rangle \ . \tag{1.28}$$

Here L represents either an $\ell\nu$ pair for a FCCC process or an $\ell^+\ell^-$ pair for a FCNC process, with $\ell = e, \mu, \tau$, while J_ℓ and J_q are a lepton and a quark current, respectively. We say that the l.h.s. of eq. (1.28) *factorises* into a leptonic matrix element, which is easily calculable, and a hadronic matrix element (HME), which is a genuine non-perturbative object as explained in section 1.2. The local meson-to-vacuum matrix elements can be expressed in terms of the decay constants f_M, defined as

$$\langle 0 |\, J_q^\mu \,| M(k) \rangle = i k^\mu f_M \tag{1.29}$$

for a pseudoscalar meson. The calculation of HMEs is extremely challenging and in many cases the result has large uncertainties, since non-perturbative techniques such as lattice QCD and QCD sum rules are required. We review non-perturbative calculations in chapter 3.

Semi-leptonic decays that contain at least one neutrino and a meson M in the final state also factorise (see e.g ref. [32])

for FCCCs: $$\langle \ell\nu M |\, J_\ell, J_q \,| B \rangle = \langle \ell\nu |\, j_\ell \,| 0 \rangle \, \langle M |\, J_q \,| B \rangle \tag{1.30}$$

and for FCNCs: $$\langle \ell\nu M |\, J_\ell, J_q \,| B \rangle = \langle \ell\nu |\, j_\ell \,| 0 \rangle \, \langle M |\, J_q \,| B \rangle \ . \tag{1.31}$$

The HMEs in this case are even more complicated to calculate than the ones in eq. (1.28), because they cannot be expressed in terms of constants but in terms of functions of the momentum transfer squared q^2:

$$\langle M(k) |\, J_q^a \,| B(q+k) \rangle = \sum_i S_i^a(q,k) F_i(q^2) \,, \tag{1.32}$$

where the sum runs over all the possible Lorentz structures $S_i^a(q,k)$. The functions $F_i(q^2)$ are called hadronic *form factors*, which are classified in detail in appendix B.

Semi-leptonic decays with an $\ell^+\ell^-$ pair in the final state, besides a factorisable part like in eqs. (1.30)-(1.31), contain a non-factorisable part:

$$\langle \ell\ell M|\, J_\ell, J_q\, |B\rangle = \langle \ell\ell|\, j_\ell\, |0\rangle\, \langle M|\, J_q\, |B\rangle + \text{non-fact. contr.}. \tag{1.33}$$

All the contributions that are not contained in the form factors are understood to be "non-factorisable" [33], which are addressed in chapter 4.

Hadronic decays are certainly the most troublesome B-meson two-body decays. The "naive factorisation" ansatz

$$\langle M_1 M_2|\, O_q\, |B\rangle = \langle M_1|\, j_q^1\, |0\rangle\, \langle M_2|\, J_q^2\, |B\rangle\ , \tag{1.34}$$

where O_q is a local four-quark operator, is not a well justified approximation, since it neglects gluon exchanges between the M_1 and the $\{B, M_2\}$ mesons [34–36]. Hence, one needs to treat these decays with more sophisticated methods, such as QCD factorisation [34, 35].

For completeness, we mention the radiative B decays, i.e. decays with at least one photon in the final state. The simplest B-meson radiative decays are $B \to \gamma\gamma$, $B \to V\gamma$ and $B \to (\gamma)\ell\nu$, where V is a vector meson. The $B \to \gamma\ell\nu$ decay is particularly interesting because it is suitable to investigate the internal properties of the B meson [37, 38], whose understanding is fundamental for the non-perturbative calculations performed in this work.

Notice that in the factorisation formulae above we neglected QED corrections, which would be another source of non-factorizable contributions. However, these non-factorizable effects are neglected in this work, since they are small compared to the uncertainties of our results.

As we have seen, different B decays factorise (or do not factorise) in different ways. Factorisation is a fundamental concept in B physics because it allows to split a complicated problem into several simpler problems.

1.5 Optimised Observables and the B Anomalies

All the theoretical predictions of B decays observables are affected by hadronic uncertainties, which increase with the number of hadrons present in the final state. In order to reduce these uncertainties, it is convenient to define observables such that hadronic effects partially cancel. An important example of this kind of observables are the lepton flavour universality (LFU) ratios. Let us recall that a model is said to be lepton flavour universal if its couplings remain unchanged swapping one lepton flavour with another. In the SM, the LFU is broken only by the Yukawa couplings, while the couplings between the leptons and the gauge bosons are lepton flavour independent.

A way to test this property of the SM is to compare the experimental measurements against the theoretical prediction of the following ratios of branching fractions

for FCCCs:
$$R_{X_c}^{\ell_1\ell_2} \equiv \frac{\text{Br}\,(B \to X_c\ell_1\nu)}{\text{Br}\,(B \to X_c\ell_2\nu)} = \frac{\int_{m_{\ell_1}^2}^{q^2_{\text{max}}} \text{d}q^2\, \frac{\text{d}\Gamma(B\to X_c\ell_1\nu)}{\text{d}q^2}}{\int_{m_{\ell_2}^2}^{q^2_{\text{max}}} \text{d}q^2\, \frac{\text{d}\Gamma(B\to X_c\ell_2\nu)}{\text{d}q^2}} \tag{1.35}$$

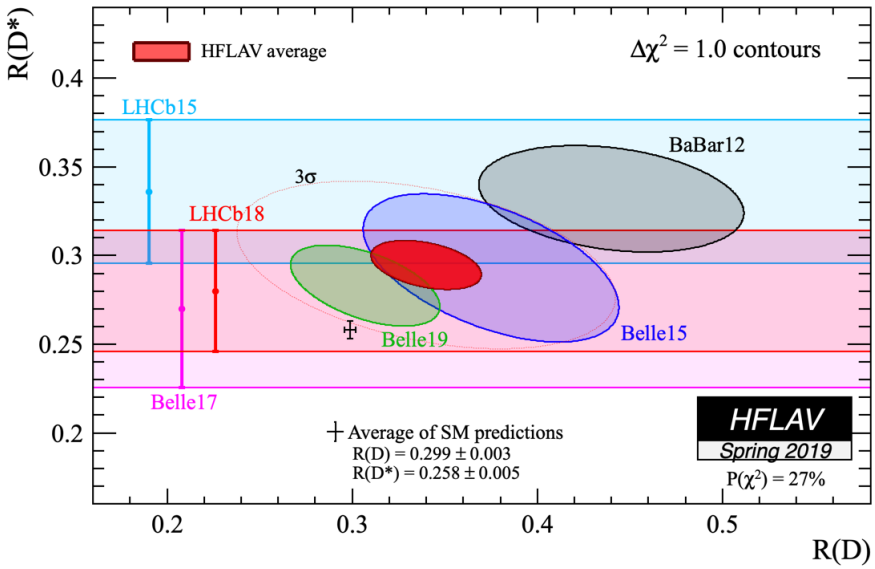

Figure 1.4: The various experimental measurements of R_D and R_{D^*}. The average of the experimental measurements (red area) and of the SM predictions are done by HFLAV [59].

and for FCNCs:
$$R_{X_s}^{\ell_1\ell_2} \equiv \frac{\mathrm{Br}\,(B \to X_s \ell_1 \ell_1)}{\mathrm{Br}\,(B \to X_s \ell_2 \ell_2)} = \frac{\int_{q_a^2}^{q_b^2} \mathrm{d}q^2 \frac{\mathrm{d}\Gamma(B \to X_s \ell_1 \ell_1)}{\mathrm{d}q^2}}{\int_{q_a^2}^{q_b^2} \mathrm{d}q^2 \frac{\mathrm{d}\Gamma(B \to X_s \ell_2 \ell_2)}{\mathrm{d}q^2}} \,. \tag{1.36}$$

Here, $\ell_{1,2}$ are two different leptons and X_c, X_s are hadrons with C $= \pm 1$ and S $= \pm 1$, respectively. While $R_{X_c}^{\ell_1\ell_2}$ is integrated over the whole phase space of the momentum transfer squared q^2, with
$$q^2_{\mathrm{max}} = (m_B - m_{X_c})^2 \,,$$
the LFU ratio $R_{X_s}^{\ell_1\ell_2}$ is usually integrated over smaller regions of the phase space to exclude the narrow $c\bar{c}$ resonances that arise for $7\,\mathrm{GeV}^2 \lesssim q^2 \lesssim 15\,\mathrm{GeV}^2$.

Interestingly, the experimental measurements of the LFU ratios $R_{D^{(*)}}^{\tau\ell}$ [39–45], with $\ell = e, \mu$, and $R_{K^{(*)}}^{\mu e}$ [46–50], are in tension with the SM predictions (see e.g. refs. [2, 51–53] for $R_{D^{(*)}}^{\tau\ell}$ and [5, 54–58] for $R_{K^{(*)}}^{\mu e}$). In the literature, $R_{D^{(*)}}^{\tau\ell}$ and $R_{K^{(*)}}^{\mu e}$ are commonly known as $R_{D^{(*)}}$ and $R_{K^{(*)}}$, which is also the notation that we use in this work.

The experimental results of R_D and R_{D^*} from the Belle, BaBar and LHCb collaborations are shown in figure 1.4. The HFLAV group averages these results and the theoretical predictions, which yields [59]
$$\begin{aligned} R_D^{\mathrm{exp}} &= 0.340 \pm 0.027 \pm 0.013 \,, & R_{D^*}^{\mathrm{exp}} &= 0.295 \pm 0.011 \pm 0.008 \,, \\ R_D^{\mathrm{SM}} &= 0.299 \pm 0.003 \,, & R_{D^*}^{\mathrm{SM}} &= 0.258 \pm 0.005 \,. \end{aligned} \tag{1.37}$$

Here the first uncertainty of the experimental averages is statistical and the second is systematic. The experimental averages of R_D and R_{D^*} exceed the SM predictions by 1.4 and 2.5

standard deviations σ, respectively. The combination of these averages results in a tension of $\sim 3\sigma$ with the SM. As we will see in subsection 4.3.2, this tension increases with the theoretical predictions presented in this work. It is worth emphasising that these discrepancies have been observed by three different experiments that use different approaches and instrumentation. This makes the $R_{D^{(*)}}$ puzzle even more significant and interesting as a potential sign of BSM physics.

There is also the possibility to consider different LFU ratios that involve $b \to c$ transitions to check a potential consistency with the discrepancies in $R_{D^{(*)}}$. In this regard, the LHCb collaboration measured the $R^{\tau\mu}_{J/\psi}$ ratio, which is again 2σ above the SM prediction [60]. This measurement cannot be performed in B-factories because they do not produce any B_c meson. Measurements of further LFU ratios of transitions mediated by FCCCs are in progress [6] and needed for a better understanding of the current situation.

The experimental measurements and the SM predictions of $R_{K^{(*)}}$ are shown in figure 1.5. In this case, the latest and most precise measurements of these LFU ratios were performed by the LHCb collaboration [49, 50], which found

$$\begin{aligned} R_K^{\text{LHCb}} &= 0.846^{+0.060+0.016}_{-0.054-0.014} \quad \text{for } 1.1\,\text{GeV}^2 < q^2 < 6.0\,\text{GeV}^2\,, \\ R_{K^*}^{\text{LHCb}} &= 0.66^{+0.11}_{-0.07} \pm 0.03 \quad \text{for } 0.045\,\text{GeV}^2 < q^2 < 1.1\,\text{GeV}^2\,, \\ R_{K^*}^{\text{LHCb}} &= 0.69^{+0.11}_{-0.07} \pm 0.05 \quad \text{for } 1.1\,\text{GeV}^2 < q^2 < 6.0\,\text{GeV}^2\,. \end{aligned} \tag{1.38}$$

As before, the first uncertainty is statistical and the second systematic. The Belle and BaBar results can be found in refs. [47, 48]. The SM prediction is very precise due to a large cancellation of the hadronic uncertainties. For instance, in ref. [54] the authors found

$$\begin{aligned} R_K^{\text{SM}} &= 1.00 \pm 0.01 \quad \text{for } 1.1\,\text{GeV}^2 < q^2 < 6.0\,\text{GeV}^2\,, \\ R_{K^*}^{\text{SM}} &= 0.906 \pm 0.028 \quad \text{for } 0.045\,\text{GeV}^2 < q^2 < 1.1\,\text{GeV}^2\,, \\ R_{K^*}^{\text{SM}} &= 1.00 \pm 0.01 \quad \text{for } 1.1\,\text{GeV}^2 < q^2 < 6.0\,\text{GeV}^2\,, \end{aligned} \tag{1.39}$$

where the leading uncertainties are due to hard-to-quantify QED corrections. The results given in eqs. (1.38) are $\sim 2.5\sigma$, 2.1σ, 2.4σ below the SM predictions, respectively.

So far, we have only discussed ratios of branching fractions in B decays. However, in these decays there are further observables that are worth studying. For instance, the angular distribution of the four-body decay $B \to K^*(\to K\pi)\ell\ell$ is rich of useful information to test the SM and constrain new physics (NP) contributions. In particular, the angular distribution of $\bar{B}^0 \to \bar{K}^{*0}\ell^+\ell^-$ [5] can be written as (following the notation of refs. [13, 61])

$$\frac{\mathrm{d}^4\Gamma\left(\bar{B}^0 \to \bar{K}^{*0}\ell^+\ell^-\right)}{\mathrm{d}q^2 \mathrm{d}\cos\theta_\ell \mathrm{d}\cos\theta_{K^*}\mathrm{d}\phi} = \frac{9}{32\pi}\sum_i I_i(q^2) f_i(\theta_\ell, \theta_{K^*}, \phi) \tag{1.40}$$

and similarly, for the CP conjugated decay $B^0 \to K^{*0}\ell^+\ell^-$ we have

$$\frac{\mathrm{d}^4\bar{\Gamma}\left(B^0 \to K^{*0}\ell^+\ell^-\right)}{\mathrm{d}q^2 \mathrm{d}\cos\theta_\ell \mathrm{d}\cos\theta_{K^*}\mathrm{d}\phi} = \frac{9}{32\pi}\sum_i \bar{I}_i(q^2) f_i(\theta_\ell, \theta_{K^*}, \phi) \tag{1.41}$$

[5] Here, we distinguish the $\bar{B}^0 \to \bar{K}^{*0}\ell^+\ell^-$ decay from the $B^0 \to K^{*0}\ell^+\ell^-$ decay, since we also discuss the CP observables of these processes.

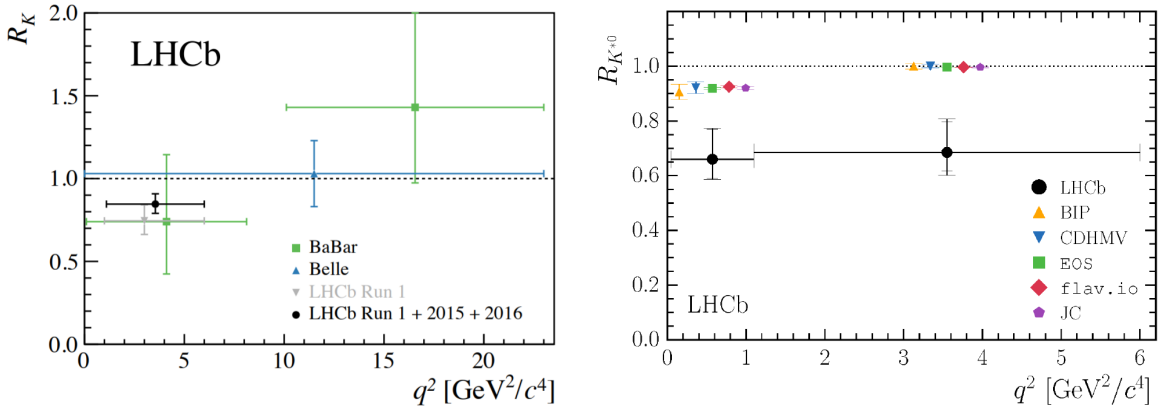

Figure 1.5: Various experimental results and SM predictions of R_K (on the left) and R_{K^*} (on the right). The Belle and BaBar measurements of R_{K^*} are not shown.

with $i = 1s,\, 1c,\, 2s,\, 2c,\, 3,\, 4,\, 5,\, 6s,\, 6c,\, 7,\, 8,\, 9$. The f_i's are simple functions of the angles $\theta_\ell, \theta_{K^*}, \phi$ (see ref. [61] for their definition) and the angular coefficients I_i are functions of the momentum transfer squared q^2. The explicit functional form of the I_i's is given in ref. [62]. Here, we just need to know that they depend on the form factors and the masses of the particles involved plus other constants.

Starting from eqs. (1.40)-(1.41) one can also define the CP averages S_i and the CP asymmetries A_i of the angular coefficients as

$$S_i \equiv \left(I_i + \bar{I}_i\right) \Big/ \frac{\mathrm{d}\left(\Gamma + \bar{\Gamma}\right)}{\mathrm{d}q^2} \tag{1.42}$$

and

$$A_i \equiv \left(I_i + \bar{I}_i\right) \Big/ \frac{\mathrm{d}\left(\Gamma - \bar{\Gamma}\right)}{\mathrm{d}q^2}\,. \tag{1.43}$$

In the limit of massless leptons, which is a good approximation for $\ell = e, \mu$, the twelve S_i's and the twelve A_i's are not all independent, given that the relations $S_{1s} = 3S_{2s}$, $S_{1c} = -S_{2c}$, $A_{1s} = 3A_{2s}$, $A_{1c} = -A_{2c}$ hold. Moreover, in the SM we have $S_{6c} = A_{6c} = 0$. From now on, we focus on the case $\ell = \mu$, since most of the experimental measurements were performed on this channel.

Using the definitions (1.42)-(1.43) and the conventions of ref. [13], we introduce the following optimised observables

$$\begin{aligned} P_1 &\equiv \frac{2S_3}{1 - F_\mathrm{L}}\,, \\ P_2 &\equiv \frac{2}{3}\frac{A_\mathrm{FB}}{(1 - F_\mathrm{L})}\,, \\ P_3 &\equiv -\frac{S_9}{1 - F_\mathrm{L}}\,, \\ P'_{4,5,8} &\equiv \frac{S_{4,5,8}}{\sqrt{F_\mathrm{L}(1 - F_\mathrm{L})}}\,, \end{aligned}$$

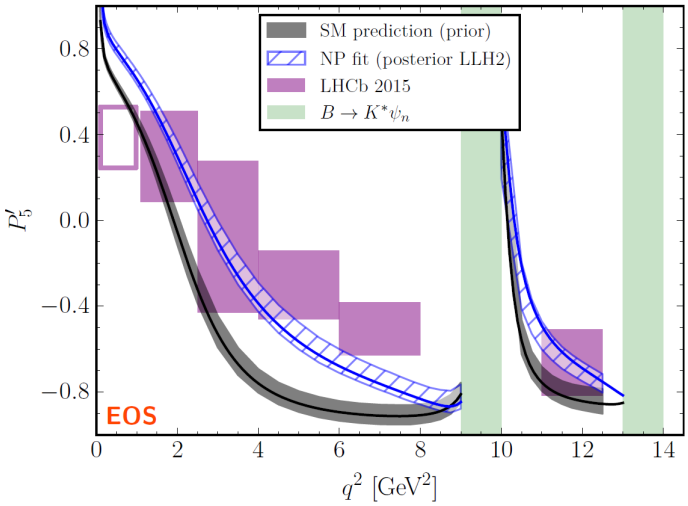

Figure 1.6: The 2015 LHCb measurement compared to the SM fit and a NP fit performed in ref. [68].

$$P_6' \equiv \frac{S_7}{\sqrt{F_{\rm L}(1-F_{\rm L})}}\,.$$

In the SM and for $m_\mu = 0$, the longitudinal polarisation $F_{\rm L}$ and the forward-backward CP asymmetry $A_{\rm FB}$ are given by

$$F_{\rm L} = S_{1c}\,, \qquad\qquad A_{\rm FB} = \frac{3}{4} S_{6s}\,. \tag{1.44}$$

As for the LFU ratios, the P_i's observables are useful because the hadronic uncertainties partially cancel, so one can obtain cleaner theoretical predictions.

The LHCb collaboration performed two angular analyses of the $B^0 \to K^{*0}\ell^+\ell^-$ decay in 2013 [61] and in 2015 [13], measuring the angular observables defined in this section. Both the first [63] and the second analysis reported a tension with the SM bigger than 3σ in the P_5' observable. Also, the Belle [64] and ATLAS [65] results for P_5' are above the SM prediction (see e.g. refs. [63, 66]), while the CMS measurement [67], due to its large uncertainties, is compatible both with the SM prediction and the other experimental results.

In figure 1.6, taken from ref. [68], the LHCb 2015 results for P_5' are shown with the SM fit and a NP fit. One can easily see that the NP fit is in better agreement with the LHCb measurement. It is worth mentioning that in the case of P_5' the SM prediction is not as solid as for the LFU ratios. In fact, the relative uncertainties in P_5' are significant due to a greater dependence on the form factors and on the non-factorizable corrections (see eq. (1.33)), some of which are rather poorly known.

The discrepancies listed in the above are commonly called the *B anomalies*. The term "anomalies" can be misleading, since in quantum field theory one usually calls anomalous those symmetries of the classical Lagrangian broken by quantum effects. However, in this case it merely indicates a set of tensions between the SM predictions and the experimental measurements.

The fact that the B anomalies occur in both $b \to c\ell\bar{\nu}$ and $b \to s\ell\ell$ transitions and in different observables makes them very intriguing, since they could be a genuine sign of NP. There is already an intense research endeavour in formulating NP models that can explain these anomalies (see e.g. refs. [69–73]). Here, we limit ourselves to mentioning some of the general features of the NP that could arise from the B anomalies, without discussing the models in detail.

Values of $R_{K^{(*)}}$ and $R_{D^{(*)}}$ different from the SM ones clearly indicate a NP contribution that is not lepton flavour universal. Moreover, given that these type of discrepancies have only been observed in B decays, and especially in $B \to D^{(*)}\tau\nu$, one could argue that NP mainly couples to the third generation of quarks and leptons.

Starting with these assumptions, one can construct an effective NP Lagrangian (see chapter 2) with four-fermion operators and couplings that obeys the given requirements. To further constrain this effective Lagrangian, one could also add other assumptions, imposing for example zero couplings to right-chiral fermions etc. . Finally, to check whether the Lagrangian proposed is able to explain the anomalies, one has to perform a fit using the experimental measurements as constraints and leaving the coupling as free parameters. If a good fit has been obtained, the next nontrivial step is to investigate what kind of new physics model can generate such an effective Lagrangian. For example, the W' and Z' bosons, which couple either to two quarks or two leptons in analogy to the SM particles W and Z, offer a viable extension of the SM as well as leptoquarks, which have non-vanishing couplings between quarks and leptons. These particles are expected to have masses of the order of few TeV.

The most difficult part in this procedure is to introduce new particles that are consistent with all the theoretical and experimental constraints. One of the strongest and most problematic of these constraints is the experimental measurement of the $B - \bar{B}$ mixing. Nevertheless, as shown for instance in refs. [69–73], it is possible to give a combined explanation to both the $b \to c\ell\bar{\nu}$ and the $b \to s\ell\ell$ anomalies. This makes the B anomalies even more interesting, since they seem to give rise to a very coherent picture.

It is also worth mentioning the so-called V_{cb} puzzle, which is the discrepancy between the determination of the CKM element V_{cb} using semi-inclusive and exclusive semileptonic B-decays (see ref. [74] for a recent update). Contrary to the B anomalies case, it is more difficult to explain this tension through NP contributions, and the discrepancy is probably due to underestimated theoretical and/or experimental uncertainties [75].

One should not forget that to claim a new discovery in particle physics, it is required a 5σ statistical significance in a single measurement. So far, the significance of P_5' has reached the value of 3.7σ in single measurement, while for the averages (not the single measurements!) of $R_{K^{(*)}}$ and $R_{D^{(*)}}$ it is $\sim 3\sigma$ or below. Thus, we cannot ignore the possibility that the B anomalies might be a mere statistical fluctuation or an underestimation of the systematic uncertainties.

In view of these present and any forthcoming experimental results, it is essential to increase the accuracy in theoretical predictions for mainly two reasons. First, to understand whether the B anomalies are due to an underestimation of the uncertainties or are signs of BSM physics. Second, even if B anomalies will not be confirmed, higher precision in theoretical predictions will be beneficial to further constrain new physics and to determine the SM parameters. In fact, the goal of this work is to improve the theoretical predictions of the hadronic matrix elements relevant for B-meson decays.

Chapter 2

Effective Field Theories for Semileptonic B-meson Decays

In chapter 1 we introduced the SM Lagrangian, which describes the electromagnetic, the weak and the strong interactions. However, in many practical applications it is not necessary to use the full SM Lagrangian and it is much more convenient to consider theories that perform specific approximations to simplify the problem considered. These theories are called *effective field theories* (EFTs), which are the main argument of this chapter.

A common feature of all the EFTs is the presence of distinct energy scales that are separated in the effective Lagrangian. This separation is carried out through an operator product expansion (OPE):

$$O_A(x;\mu)O_B(y;\mu) = \sum_i C_i(x-y;\mu)O_i(x;\mu) \qquad \text{for } x \to y\,. \tag{2.1}$$

Here O_A and O_B are two operators of the "full theory", i.e. some field theory from which the EFT is constructed, and μ is some arbitrary scale, whose meaning is discussed below. Equation (2.1), which was originally proposed by K. Wilson [76], implies that one can express the product of two operators at different space-time points as a linear combination of the local effective operators O_i. In general, the series in eq. (2.1) involves an infinite number of terms, but only a finite number of operators O_i contribute to a certain order of $(x-y)$, meaning that it is possible to truncate the series neglecting higher orders in $(x-y)$.

Using an OPE, it is possible to write an effective Lagrangian

$$\mathcal{L}_{eff}(x) = \sum_i C_i(\mu)O_i(x;\mu)\,, \tag{2.2}$$

where some of the degrees of freedom of the SM Lagrangian are "integrated out", in the sense that they are removed from the effective theory. In other words, one can perform certain approximations to focus on the degrees of freedom that are relevant for the process under consideration. In the next sections, we discuss some examples of the procedures to integrate out a field.

The advantage of using an OPE is that it allows to disentangle the short-distance contributions of the full theory, encoded in the Wilson coefficients C_i, and the long-distance contributions, encoded in matrix elements of the operators $\langle f|\, O_i\, |i\rangle$. The scale μ is the separator of these two contributions, and it can be chosen with a certain freedom.

Since the Wilson coefficients are independent of the initial state $|i\rangle$ and the final state $|f\rangle$ considered, they can be interpreted as the couplings of the effective theory. To compute them, one has to use a procedure called *matching*, which consists in imposing that the amplitudes calculated in the effective theory must be equal to the ones calculated in the full theory.

Furthermore, given that physical observables are μ independent, the dependence on μ of the C_i's and the $\langle f|\, O_i\, |i\rangle$'s must cancel in the r.h.s. of eq. (2.2). Unfortunately, this does not always happen in practice due to the fact that in many cases the matrix elements $\langle f|\, O_i\, |i\rangle$ are poorly known. Indeed, as discussed in chapter 1, when long-distance QCD effects are present, perturbation theory cannot be applied to compute matrix elements.

In the next sections, we present the effective field theories for the $b \to s\ell\ell$ and $b \to c\ell\nu$ transitions and the heavy quark effective theory.

2.1 A Simple Example of an Effective Lagrangian

To introduce the idea of effective field theories and show how to integrate out certain degrees of freedom of the full theory, we present an example taken from ref. [29].

Let us consider the $b \to s\bar{c}c$ process at tree level, illustrated in figure 2.1. Its amplitude reads[1]

$$\mathcal{M} = -i\frac{G_F}{\sqrt{2}} V_{cb}V_{cs}^* \frac{m_W^2}{m_W^2 - q^2} \left(\bar{u}_c \gamma^\mu P_L u_b\right) \left(\bar{u}_s \gamma_\mu P_L v_c\right) , \tag{2.3}$$

where the subscripts of the Dirac spinors u, v indicate the quark flavors, while the Fermi constant is given by

$$\frac{4G_F}{\sqrt{2}} \equiv \frac{g_2^2}{8m_W^2} .$$

At low energy, i.e. for $k^2 \ll m_W^2$, the amplitude of eq. (2.3) can be written as

$$\mathcal{M} = -i\frac{4G_F}{\sqrt{2}} V_{cb}V_{cs}^* \left[\left(\bar{u}_c \gamma^\mu P_L u_b\right) \left(\bar{u}_s \gamma_\mu P_L v_c\right) + \mathcal{O}\left(\frac{q^2}{m_W^2}\right)\right] , \tag{2.4}$$

since for $\sqrt{q^2} = 3\,\text{GeV}$ one gets $q^2/m_W^2 \sim 10^{-3}$. Notice that the W-boson propagator does not appear explicitly in eq. (2.4), thus we say that the W boson has been integrated out[2]. In this case, as illustrated in figure 2.1, the $b \to s\bar{c}c$ transition is well described by the four-quark operator

$$O_2^c = \left(\bar{s}\gamma^\mu P_L c\right) \left(\bar{c}\gamma_\mu P_L b\right) , \tag{2.5}$$

where the subscript "2" in O_2^c is due to historical reasons.

The effective interaction Lagrangian at tree level is then given by

$$\mathcal{L}_{eff} = \frac{4G_F}{\sqrt{2}} V_{cb}V_{cs}^* \left[C_2 O_2^c + \mathcal{O}\left(\frac{q^2}{m_W^2}\right)\right] , \tag{2.6}$$

[1] The notations and conventions used in this work are summarised in appendix A.

[2] This terminology comes from the path integral formalism (see e.g. refs. [17, 29]).

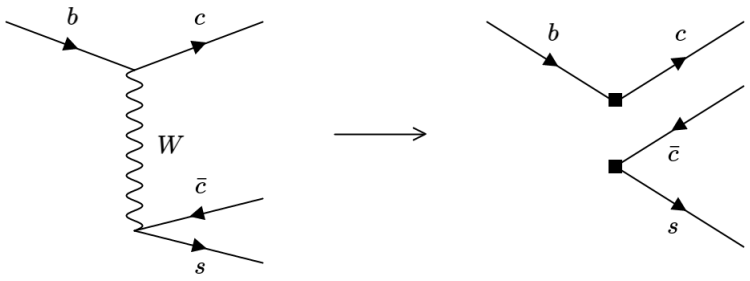

Figure 2.1: The $b \to s\bar{c}c$ transition at tree level in the SM (on the left) and in the corresponding effective theory with the W boson integrated out (on the right).

where $C_2 = 1 + \mathcal{O}(\alpha_s)$ is obtained from the requirement that $\mathcal{L}_{eff}$ reproduces the result of eq. (2.3) up to $\mathcal{O}\left(q^2/m_W^2\right)$ corrections, that is, performing the matching of eq. (2.6) onto eq. (2.4). In eq. (2.6) we have only kept the first term of an OPE, which contains a tower of higher dimensional local operators. In B physics, it is sufficient to consider operators with mass dimension equal to six as O_2^c, since $q^2 \leqslant m_B^2$, implying that $\mathcal{O}\left(q^2/m_W^2\right)$ corrections can be safely neglected.

We will show in the next section that if one goes beyond the tree-level approximation other dimension-six operators appear. Clearly, including all the dimension-six operators plus the infinite tower of higher dimensional operators, one would restore the full theory.

The example considered in this section is completely analogous to the Fermi theory, where beta decays at low energy are described in terms of four-fermion operators. When E. Fermi first proposed this theory the W and Z bosons were not known yet, which have been then included in the Glashow-Weinberg-Salam theory of weak interactions.

This shows an intriguing aspect of effective field theories. While in our example we obtained the effective theory starting from the SM, it is also possible to formulate an effective theory without knowing the respective full theory. Eventually, an effective theory has also the potential to give us some hint about the nature of the full theory itself.

Notice that in general EFTs are non-renormalizable, but they are still predictive and extremely useful in the energy regime where they are valid.

2.2 Effective Lagrangian for $b \to s\ell\ell$ Transitions

In the previous section, we have derived the effective Lagrangian (2.6) for $b \to s\bar{c}c$ tree-level transitions in the SM, which contains only one four-quark operator. Including QCD and higher order electroweak corrections, one obtains additional dimension-six operators. In this section, we present the EFT for $b \to s\ell^+\ell^-$ transitions, which is commonly called weak effective theory (WET), and discuss all the relevant operators that contribute to it. The same EFT can also be applied to $b \to s\gamma$ and $b \to s\bar{\nu}\nu$ transitions.

The interaction Lagrangian of this EFT reads

$$\mathcal{L}_{eff}^{b\to s\ell\ell} = \mathcal{L}_{\text{QED}} + \mathcal{L}_{\text{QCD}} + \mathcal{L}_{D=6}^{b\to s\ell\ell}\,, \tag{2.7}$$

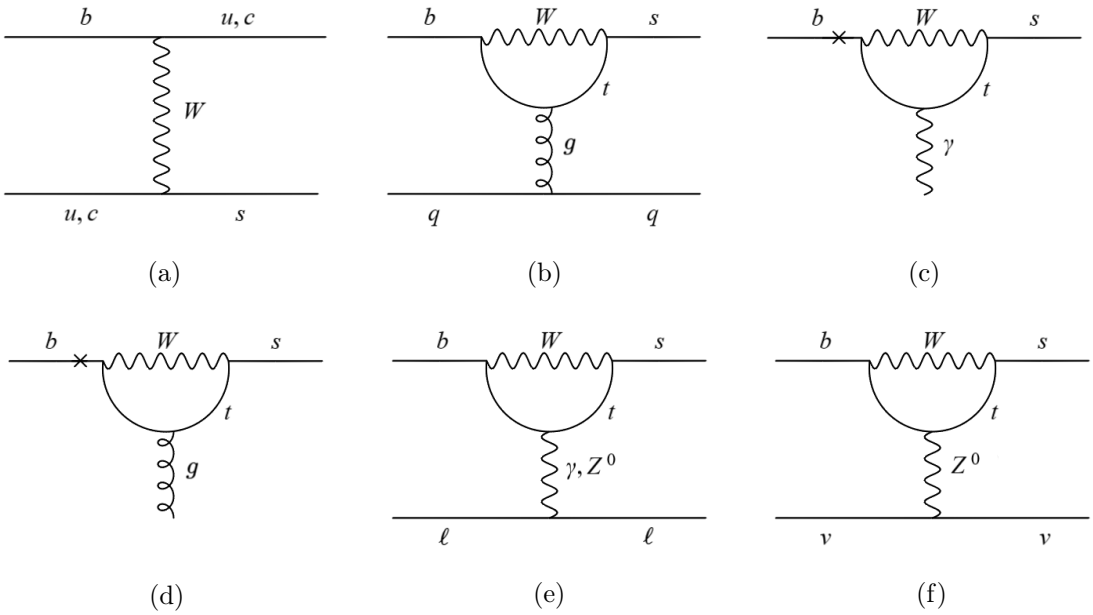

Figure 2.2: Some of the topologies of the diagrams contributing to $b \to s\ell^+\ell^-$, $b \to s\gamma$ and $b \to s\bar{\nu}\nu$ transitions in the SM. See text for details.

where $\mathcal{L}_{\rm QED}$ and $\mathcal{L}_{\rm QCD}$ contain the QED and the QCD interaction terms, excluding the vertices that contain top quarks, since all the degrees of freedom heavier than the bottom quark have been integrated out. The $\mathcal{L}_{D=6}^{b\to s\ell\ell}$ part of the effective Lagrangian Lagrangian includes all the dimension six operators contributing to the transitions listed above up to $\mathcal{O}\left(G_F^2\right)$ corrections:

$$\mathcal{L}_{D=6}^{b\to s\ell\ell} \;=\; -\frac{4G_F}{\sqrt{2}}\left(\lambda_u\left(C_1O_1^u + C_2O_2^u\right) + \lambda_c\left(C_1O_1^c + C_2O_2^c\right) + \left(\lambda_u+\lambda_c\right)\sum_i C_iO_i\right)\,, \quad (2.8)$$

with $\lambda_i = V_{ib}V_{is}^*$. Using the unitarity relation

$$\lambda_u + \lambda_c + \lambda_t = 0\,,$$

it is possible to rewrite eq. (2.8) as

$$\begin{aligned}\mathcal{L}_{D=6}^{b\to s\ell\ell} = {}& \frac{4G_F}{\sqrt{2}}\lambda_t\left(C_1O_1^c + C_2O_2^c + \sum_i C_iO_i\right)\\ & + \frac{4G_F}{\sqrt{2}}\lambda_u\left(C_1\left(O_1^c - O_1^u\right) + C_2\left(O_2^c - O_2^u\right)\right).\end{aligned} \quad (2.9)$$

The second line of this last equation is CKM suppressed with respect to the first one (see eq. (1.12)), so it can be neglected in most of the applications.

The dimension-six operators O_i with non-vanishing Wilson coefficients C_i in the SM are listed below.

- There are two current-current operators, which are distinguished by a different colour structure:

$$O_1^q = \left(\bar{s}^j\gamma^\mu P_L q^i\right)\left(\bar{q}^i\gamma_\mu P_L b^j\right)\,, \qquad O_2^q = \left(\bar{s}\gamma^\mu P_L q\right)\left(\bar{q}\gamma_\mu P_L b\right)\,, \quad (2.10)$$

where the colour indices i and j are shown explicitly in the O_1^q operator, with $q = u, c$, while the O_2^q operator has colour diagonal quark bilinears. These operators, which are the leading contributions in $b \to s\bar{c}c$ transitions, enter in semileptonic decays only when combined with electromagnetic currents. We study in detail these effects in chapter 4, because of their importance in the phenomenology of $B \to K^{(*)}\ell\ell$ decays. In figure 2.2(a) is shown the topology of the diagrams in the full theory from which the O_2 operator originates.

- The QCD penguin operators (figure 2.2(b)) are

$$\begin{aligned} O_3 &= (\bar{s}\gamma^\mu P_L b) \sum_p (\bar{p}\gamma_\mu P_L\, p) \;, \qquad O_4 = \left(\bar{s}^j \gamma^\mu P_L q^i\right) \sum_p \left(\bar{p}^i \gamma_\mu P_L\, p^j\right) \;, \\ O_5 &= (\bar{s}\gamma^\mu P_L b) \sum_p (\bar{p}\gamma_\mu P_R\, p) \;, \qquad O_6 = \left(\bar{s}^j \gamma^\mu P_L q^i\right) \sum_p \left(\bar{p}^i \gamma_\mu P_R\, p^j\right) \;, \end{aligned} \tag{2.11}$$

  where the sum run over all the quarks except the top quark. These operators give subleading α_e contributions in $b \to s\ell^+\ell^-$, $b \to s\gamma$, $b \to s\bar{\nu}\nu$ transitions and their corresponding Wilson coefficients are relatively small compared to the others. Indeed, the QCD penguin operators are often neglected in leptonic, semileptonic and radiative B-decays.

- The electromagnetic and chromomagnetic dipole operators (figures 2.2(c,d)) are

$$O_7 = \frac{e}{16\pi^2} m_b\, (\bar{s}\sigma^{\mu\nu} P_R\, q)\, F_{\mu\nu} \;, \qquad O_8 = \frac{g_s}{16\pi^2} m_b\, (\bar{s}\sigma^{\mu\nu} T_a P_R\, q)\, G^a_{\mu\nu} \;, \tag{2.12}$$

  where $T_a = \lambda_a/2$ and the λ_a's are the Gell-Mann matrices. The T_a's matrices satisfy the equation

$$T^a_{ij} T^a_{kl} = -\frac{1}{6}\delta_{ij}\delta_{lk} + \frac{1}{2}\delta_{ik}\delta_{lj} \;, \tag{2.13}$$

  since the eight Gell-Mann matrices plus the identity matrix form a complete set of 3×3 matrices. The cross in figures 2.2(c,d) indicates a chirality-flip of the b quark field, caused by its mass term in the SM Lagrangian. The analogous contributions with a chirality-flip of the s quark field are suppressed due to the smallness of the strange quark mass.

- The semileptonic operators (figures 2.2(e,f)) are

$$\begin{aligned} O_9 &= \frac{e^2}{16\pi^2} (\bar{s}\gamma^\mu P_L q) \sum_\ell \left(\bar{\ell}\gamma_\mu \ell\right) \;, \qquad O_{10} = \frac{e^2}{16\pi^2} (\bar{s}\gamma^\mu P_L q) \sum_\ell \left(\bar{\ell}\gamma_\mu\gamma_5 \ell\right) \;, \\ O_\nu &= \frac{e^2}{8\pi^2} (\bar{s}\gamma^\mu P_L q) \sum_\ell (\bar{\nu}_\ell \gamma_\mu P_L \nu_\ell) \;. \end{aligned} \tag{2.14}$$

  The electroweak penguin operators with four quarks are usually neglected because they are α_e suppressed in $b \to s\ell^+\ell^-$, $b \to s\gamma$ and $b \to s\bar{\nu}\nu$ transitions.

The operator basis presented in the above coincides with the one given in ref. [77]. Obviously, this basis is not unique and another common convention is the one of ref. [78], where, for example, the first two operators are

$$\tilde{O}_1^q = (\bar{s}\gamma^\mu T^a P_L q)\, (\bar{q}\gamma_\mu T_a P_L b) \;, \qquad \tilde{O}_2^q = (\bar{s}\gamma^\mu P_L q)\, (\bar{q}\gamma_\mu P_L b) \;. \tag{2.15}$$

Using eq. (2.13), it is easy to relate the operators in eq. (2.10) to the ones in eq. (2.15) and the relative Wilson coefficients:

$$\begin{aligned} O_1^q &= 2\tilde{O}_1^q + \frac{1}{2}\tilde{O}_2^q\,, & O_2^q &= \tilde{O}_2^q\,, \\ C_1^q &= \frac{1}{2}\tilde{C}_1^q\,, & C_2^q &= -\frac{1}{6}\tilde{C}_1^q + \tilde{C}_2^q\,. \end{aligned} \tag{2.16}$$

The operators for $b \to d\ell^+\ell^-$, $b \to d\gamma$ and $b \to d\bar{\nu}\nu$ transitions can be obtained by simply replacing the strange quark with a down quark in eqs. (2.10)-(2.14), while the Wilson coefficients are exactly the same for $b \to s$ and $b \to d$ transitions.

If one includes NP effects also other operators become important, for example the same operators that contribute in the SM but with opposite chirality. NP effects can also affect the Wilson coefficients of the operators in eqs. (2.10)-(2.14).

2.3 Effective Lagrangian for $b \to c\ell\nu$ Transitions

The weak interaction effective Lagrangian for $b \to c\ell\nu$ transitions is much simpler than the one for $b \to s\ell^+\ell^-$ transitions, since the coupling term between b and c quarks appears in the SM, and it reads

$$\mathcal{L}_{D=6}^{b\to c\ell\nu} = -\frac{4G_F}{\sqrt{2}} V_{cb} \big(\bar{c}\gamma^\mu P_L b\big)\big(\bar{\ell}\gamma_\mu P_L \nu_\ell\big)\,. \tag{2.17}$$

Also in this case, NP effects introduce operators that in the SM have vanishing Wilson coefficients. Disregarding right-chiral neutrinos, the Lagrangian for $b \to c\ell\nu$ transitions that can accommodate NP contributions reads[3] [80]

$$\mathcal{L}_{D=6}^{b\to c\ell\nu} = -\frac{4G_F}{\sqrt{2}} V_{cb} \left(O_{V_L}^{\ell\ell} + \sum_i C_i^{\ell\ell'} O_i^{\ell\ell'} + \text{h.c.} \right)\,. \tag{2.18}$$

Here, the operators $O_i^{\ell\ell'}$ are

$$\begin{aligned} O_{V_L}^{\ell\ell'} &= \big(\bar{c}\gamma^\mu P_L b\big)\big(\bar{\ell}\gamma_\mu P_L \nu_{\ell'}\big)\,, & O_{V_R}^{\ell\ell'} &= \big(\bar{c}\gamma^\mu P_R b\big)\big(\bar{\ell}\gamma_\mu P_L \nu_{\ell'}\big)\,, \\ O_{S_L}^{\ell\ell'} &= \big(\bar{c} P_L b\big)\big(\bar{\ell} P_L \nu_{\ell'}\big)\,, & O_{S_R}^{\ell\ell'} &= \big(\bar{c} P_R b\big)\big(\bar{\ell} P_R \nu_{\ell'}\big)\,, \\ O_T^{\ell\ell'} &= \big(\bar{c}\,\sigma^{\mu\nu} P_L b\big)\big(\bar{\ell}\,\sigma_{\mu\nu} P_L \nu_\ell\big)\,. \end{aligned} \tag{2.19}$$

Even though we mostly focus on the SM physics, we also consider the hadronic matrix elements of the tensor operators O_T, since they arise in several NP scenarios.

Similar considerations hold for $b \to u\ell\nu$ transitions and in particular eq. (2.17) becomes

$$\mathcal{L}_{D=6}^{b\to u\ell\nu} = -\frac{4G_F}{\sqrt{2}} V_{ub} \big(\bar{u}\gamma^\mu P_L b\big)\big(\bar{\ell}\gamma_\mu P_L \nu_\ell\big)\,. \tag{2.20}$$

[3] For the most general form of this Lagrangian see ref. [79].

2.4 Heavy Quark Effective Theory

The coupling constants of the electroweak and strong interactions are not truly constants, since they are functions of the energy scale, and hence they are called running coupling constants. While the α_e coupling becomes large for large distances, the opposite is true at the α_s coupling, which becomes large at short distances. More precisely, the Landau pole of QCD is located[4] at $\Lambda_{\rm QCD} \sim 0.2\,\text{GeV}$, thus QCD perturbation theory can only be applied for energies $|\mu| \gg \Lambda_{\rm QCD}$.

Considering the numerical value of $\Lambda_{\rm QCD}$, one can split the six quark flavours into two categories: the *heavy quarks*, namely the charm, the bottom and the top quarks, which have masses much larger than $\Lambda_{\rm QCD}$, and the *light quarks*, namely the up, the down and the strange quarks, which have masses smaller than $\Lambda_{\rm QCD}$. Notice that it is not very accurate to assume $m_c \gg \Lambda_{\rm QCD}$, since one could get

$$\frac{\Lambda_{\rm QCD}}{m_c} \sim 0.3\,,$$

depending on the value chosen for the QCD scale and the renormalisation scheme. Thus, $\Lambda_{\rm QCD}/m_c$ is not an optimal expansion parameter and one should to take into account the large power corrections.

A useful tool to study the physics of B and D mesons[5] is the *heavy-quarks effective theory* (HQET), which exploits the fact that at leading order in $\Lambda_{\rm QCD}/m_Q$, with $m_Q = m_c, m_b$, the properties of the mesons are independent of the quark masses and spins. In fact, in the limit $m_Q \to \infty$, there is an $SU(4)$ heavy quark spin-flavor symmetry that leaves observables unchanged by swapping one heavy quark for another or flipping its spin up to higher order corrections.

In this picture, B and D mesons are analogous to a hydrogen atom, with binding due to strong interactions instead of the electromagnetic ones. The heavy quark is surrounded by a light quark "cloud" of gluons, virtual quarks and the light valence quarks, ironically named *brown muck* by N. Isgur [82]. The typical energy scale of the interactions between the brown muck and the heavy quark is $\Lambda_{\rm QCD}$ and hence they cannot be treated is perturbative QCD.

It is then convenient to decompose the momentum of such mesons as

$$p_Q^\mu = m_Q v^\mu + k^\mu\,, \tag{2.21}$$

where v^μ is the meson velocity and k_μ is its residual momentum. Since $v^2 = 1$ and $m_M = m_Q + \bar{\Lambda}$, where m_M is the meson mass and $\bar{\Lambda} \sim \Lambda_{\rm QCD}$, it follows that $k^\mu \sim \bar{\Lambda}$. In other words, the heavy quark, which carries most of the meson momentum, is almost on-shell and the brown muck cannot affect its velocity and/or its spin in a major way. Interactions between the light and heavy degrees of freedom can only change the residual momentum by quantities of the order of $\Lambda_{\rm QCD}$.

In HQET the velocity of the meson v^μ is a conserved quantity, which allows to eliminate the explicit dependence on the momentum p_Q^μ. Integrating out the degrees of freedom of the heavy quark field Q that are responsible for the creation and annihilation of heavy antiquarks, it is possible to expand the full QCD Lagrangian in powers of $1/m_Q$:

[4] The exact value $\Lambda_{\rm QCD}$ depends on the number of active quark flavours (see e.g. ref. [81]).

[5] Clearly, the considerations of this section do not apply to B_c mesons.

$$\mathcal{L}_{eff}^{\rm HQET} = -\frac{1}{2}\,{\rm Tr}\{\mathbf{G}_{\mu\nu}\mathbf{G}^{\mu\nu}\} + \sum_{q=u,d,s} \bar{q}\left(i\not{D} - m_q\right) q + i\bar{h}_v (v\cdot D) h_v \\ - \frac{1}{2m_Q}\sum_{n=0}^{\infty} \bar{h}_v \not{D}_\perp \left(-\frac{iv\cdot D}{2m_Q}\right)^n \not{D}_\perp h_v\,, \quad (2.22)$$

which, cutting the series after the first term, becomes

$$\mathcal{L}_{eff}^{\rm HQET} = -\frac{1}{2}\,{\rm Tr}\{\mathbf{G}_{\mu\nu}\mathbf{G}^{\mu\nu}\} + \sum_{q=u,d,s} \bar{q}\left(i\not{D} - m_q\right) q + i\bar{h}_v (v\cdot D) h_v \\ - \bar{h}_v \frac{D_\perp^2}{2m_Q} h_v - \frac{g_s}{4m_Q}\bar{h}_v \left(\sigma_{\mu\nu}\mathbf{G}^{\mu\nu}\right) h_v + \mathcal{O}\left(\frac{1}{m_Q^2}\right)\,. \quad (2.23)$$

Here D^μ is the covariant derivative introduced in chapter 1 and

$$D_\perp^\mu = D^\mu - v^\mu (v\cdot D)\,.$$

The effective fields h_v and H_v are different projections of the heavy quark field Q, which are defined as

$$\begin{aligned} h_v(x) &= e^{im_Q v\cdot x}\frac{1+\not{v}}{2} Q(x)\,, \\ H_v(x) &= e^{im_Q v\cdot x}\frac{1-\not{v}}{2} Q(x)\,. \end{aligned} \quad (2.24)$$

These effective fields automatically satisfy the equations of motion

$$\begin{aligned} \not{v} h_v &= h_v\,, \\ \not{v} H_v &= -H_v\,, \end{aligned} \quad (2.25)$$

and hence the field Q can be written as

$$Q(x) = e^{-im_Q v\cdot x}\left(h_v(x) + H_v(x)\right). \quad (2.26)$$

From eqs. (2.24)-(2.26), it follows that the effective field H_v would be identically zero if the heavy quark was on-shell. Since the heavy quark is "almost" on shell, H_v and h_v have small and large components, respectively. This is the reason why the effective field H_v can be integrated out and it does not appear explicitly in the effective Lagrangian (2.22).

It is also important to mention that the field h_v annihilates a heavy quark but it does not create the corresponding antiquark, while the opposite is true for H_v. This implies that heavy quark-antiquark pairs cannot be created or annihilated in the limit $m_Q \to \infty$, and that these effects only appear at subleading orders in the $1/m_Q$ expansion of the effective Lagrangian.

In this section, we have given a brief introduction to the main features of HQET. For more details and formal proofs of the results presented above, we refer the reader to, e.g., refs. [83, 84].

Chapter 3

Hadronic Matrix Elements from Dispersion Relations

Hadronic matrix elements (HMEs) cannot be calculated in QCD perturbation theory due to the soft-gluon exchanges between the hadrons constituents, and hence non-perturbative techniques are required to perform such calculations. Currently, the only QCD based methods to compute HMEs are lattice simulations and QCD sum rules.

The central idea of lattice QCD (LQCD) is to use the path integral formulation of quantum field theory, where correlators are replaced by integrals over all possible classical field configurations, and to compute numerically these integrals in the approximation of a finite discretized Euclidean space-time.

In the last few years, several improvements of supercomputers and of algorithms allowed numerous computations of HMEs employing LQCD. One of the remarkable aspects of LQCD is that it is systematically improvable, i.e. its uncertainties can be arbitrarily reduced over time. However, the numerical procedures presently adopted are still highly demanding in terms of time and resources, so that certain computations may require several years. In addition, LQCD is not usually able to provide results over the whole kinematical spectrum, as in the case of $B \to K^{(*)}$ and $B \to D^{(*)}$ form factors [85–90], and the evaluation of non-local HMEs is still at a conceptual stage.

On the other hand, QCD sum rules (QCDSRs) provide an alternative method to calculate HMEs. As we will show in this and in the following chapter, QCDSRs are suitable to compute both local (e.g. the form factors of pseudoscalar and vector mesons) and non-local HMEs (e.g. the soft-gluon contribution to the charm loop in $B \to K^* \ell\ell$).

One advantage of this technique is the fact that sum rules are relations between different hadronic parameters which can be calculated analytically, so that lengthy numerical evaluation are not required. Another advantage is that the functional form of a certain sum rule does not depend on the quark flavours of the transition considered. This means that if, for instance, one calculates the sum rule for $B \to \rho$ form factors, it is straightforward to obtain the sum rule for $B \to K^*$ form factors, since both are B-to-vector meson decays. The only thing that one has to change are the input parameters. Thus, it is relatively easy and fast to obtain theoretical predictions of different HMEs using QCDSRs compared to LQCD.

The main drawback of QCDSRs is the large uncertainties of their predictions, which cannot be reduced below a certain limit. Indeed, all the sum rules depend on an unphysical parameter, called the Borel parameter (see subsection 3.1.2), which produce a non-trivially reducible

systematic uncertainty. Furthermore, QCDSRs rely on the additional assumption of *quark-hadron duality* and on universal non-perturbative inputs, such as vacuum condensates or distribution amplitudes.

Interestingly, QCDSRs can only be used in the calculation of form factors when the momentum transfer[1] q^2 is low enough, while LQCD are usually more effective at high q^2. Hence, one can combine QCDSRs and LQCD results to extract the hadronic form factors in the whole q^2 range.

In addition to these methods, for certain HMEs one can obtain an upper bound on their values. This can be done by using a dispersion relation combined with a unitarity relation. The bounds obtained in this way are called *dispersive bounds* and their derivation is similar to the one of a sum rule, with the advantage that the (semi-global) quark-hadron duality approximation is not needed. The dispersive bounds are very strong constraints on the HMEs and they are extremely useful when one tries to parametrize the HMEs themselves.

Before reviewing the QCDSRs and the dispersive bounds, we introduce the fundamental tools needed to employ these techniques in the next section.

3.1 Foundations

In order to calculate a dispersive bound, one has to construct a dispersion relation where the integral imaginary part of the correlator considered is related to the value of correlator itself in a specific point of the phase space. This point has to be chosen such that the correlator can be expanded in a local OPE, whose Wilson coefficients can be computed in perturbative QCD. The calculation of a sum rule requires in addition the quark-hadron duality approximation. To reduce the error introduced by this approximation, one usually performs Borel transform. All these theoretical means are discussed in the following subsections.

3.1.1 The Dispersion Relation

In this subsection we study the analytic structure of the following vacuum-to-vacuum correlator:

$$\Pi^{\mu\nu}(q) = i \int \mathrm{d}^4x \, e^{iq\cdot x} \langle 0| \, T\{J^\mu(x), J^{\nu,\dagger}(0)\} \, |0\rangle \ , \tag{3.1}$$

which can always be decomposed in terms of scalar functions as

$$\Pi^{\mu\nu}(q) = (q^\mu q^\nu - q^2 g^{\mu\nu})\Pi_{1^-}(q^2) + q^\mu q^\nu \Pi_{0^+}(q^2) \, . \tag{3.2}$$

Here $J^\mu \equiv \bar{q}_1 \gamma^\mu q_2$ is a quark current and the subscript on the functions $\Pi_{J_P}(q^2)$ indicate the spin J and the parity P of the states that can be created or annihilated by J^μ. For an axial vector current $J^\mu_A \equiv \bar{q}_1 \gamma^\mu \gamma_5 q_2$ eq. (3.2) becomes

$$\Pi^{\mu\nu}(q) = (q^\mu q^\nu - q^2 g^{\mu\nu})\Pi_{1^+}(q^2) + q^\mu q^\nu \Pi_{0^-}(q^2) \, . \tag{3.3}$$

The results of this subsection also apply to more general correlators, in particular to those with a hadron in the initial state instead of the vacuum. The main difference in such a case

[1] See section 1.4 for the definition of the momentum transfer.

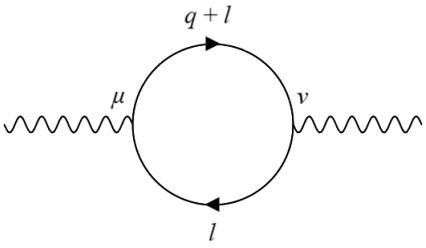

Figure 3.1: The Feynman diagram that corresponds to the correlator $\Pi^{\mu\nu}(q)$ defined in eq. (3.1).

would be the decomposition in independent Lorentz structures (3.2), which would be more complicated due to the additional external momentum carried by the hadron.

We can also ignore the distinction between the functions $\Pi_{0^\pm}(q^2)$ and $\Pi_{1^\pm}(q^2)$, since the only thing that matters here is the analytic structure of these functions, which is analogous in this four cases. Hence, we simply write $\Pi(q^2)$ to indicate one of the four $\Pi_{J^P}(q^2)$ functions.

The two-point correlator $\Pi^{\mu\nu}(q)$ can be thought of as one of the contributions to the self-energy of a gauge boson, whose diagram is shown in figure 3.1. For a virtual gauge boson, the domain of the function $\Pi(q^2)$ is the whole real axis. However, in order to study the properties $\Pi(q^2)$, it is useful to enlarge the domain to the whole complex plane, even though imaginary values of q^2 have no straightforward physical meaning. Thus, $\Pi(q^2)$ will be considered as a complex function $\mathbb{C} \to \mathbb{C}$ in what follows.

In the left half of the complex q^2 plane, i.e. for $\mathrm{Re}(q^2) < 0$, the function $\Pi(q^2)$ is analytic: it has no poles or singularities of any other kind. Moreover, it can be shown that (see e.g. ref. [91]) for

$$-q^2 \gg \Lambda^2_{\mathrm{QCD}} \tag{3.4}$$

the dominant contribution to $\Pi(q^2)$ comes from the quarks that propagate at short distances. If at least one of the quarks in the loop of figure 3.1 is heavy (i.e. has mass $m_Q^2 \gg \Lambda^2_{\mathrm{QCD}}$), the condition (3.4) becomes

$$m_Q^2 - q^2 \gg \Lambda^2_{\mathrm{QCD}}\,, \tag{3.5}$$

which is even easier to satisfy. If the conditions (3.4) or (3.5) are fulfilled, $\Pi(q^2)$ can be expanded in a local OPE, as we will show in subsection 3.2.1.

On the other hand, on the positive real axis the function $\Pi(q^2)$ presents poles generated by bound states and a branch cut which starts at the continuum threshold of the lowest continuum state. As an example, let us consider the current

$$J^\mu = \bar{b}\,\gamma^\mu(\gamma_5)c\,.$$

In this case, there several isolated poles at $q^2 = m^2_{c\bar{b}}$ (see figure 3.2), where $m_{c\bar{b}}$ is the mass of a $c\bar{b}$ bound state. The $c\bar{b}$ bound states with $J^P = 0^+$ appear only in the function Π_{0^+} and so on. The lightest $c\bar{b}$ bound state with $J^P = 0^-$ ($J^P = 1^-$) is the B_c (B_c^*) meson introduced in section 1.2. A more complete list of the known $c\bar{b}$ bound states can be found in refs. [92].

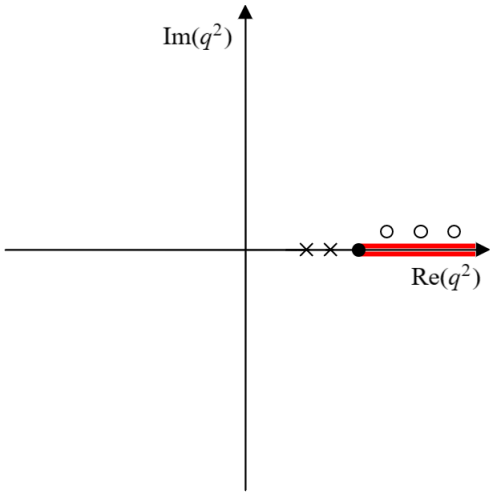

Figure 3.2: Analytic structure of the function $\Pi(q^2)$. The crosses indicate the $c\bar{b}$ bound states, the filled circle represent the branch point at $q^2 = (m_B + m_D)^2$ while the empty circles are the $c\bar{b}$ resonances, which are on the second (unphysical) Riemann sheet technically speaking. The red shaded area illustrate the branch cut.

The point $q^2 = (m_B + m_D)^2$ is a *branch point*, which corresponds to the lightest two-particle state. Branch points are singular points of a complex function, which are radically different from poles and essential singularities. Indeed, while poles and essential singularities are classified as singularities because the function is discontinuous and/or non-differentiable in that point, branch points are associated to the fact that the function is multivalued in its neighbourhood.

To overcome the inconvenience of having a multivalued function, it is possible to use a trick. This trick consists in replacing the q^2 plane with a more complicated manifold, called Riemann surface, and then to define a *branch cut*, i.e. a curve (usually between two branch points) that divide the Riemann surface in different copies of the q^2 plane, called Riemann sheets.

In this way, instead of having a single multivalued function, we have several single-valued functions called *branches*. Crossing the branch cut one can move from one Riemann sheet to another[2]. The number of Riemann sheets depends on the function considered, for example $z^{1/n}$, with $z \in \mathbb{C}$ and $n \in \mathbb{N}$, has n Riemann sheets while $\log(z)$ has infinitely many Riemann sheets.

The branch cut of $\Pi(q^2)$ is a line segment between the first branch point[3] $q^2 = (m_B+m_D)^2$ and $q^2 = +\infty$, which is illustrated in figure 3.2. Even if in this case there are infinite Riemann sheets, for most applications is sufficient to consider only two Riemann sheets: the physical one, where the bound states are located, and the unphysical one, where the resonances are located (see ref. [27], section "Resonances").

Knowing the analytic structure of $\Pi(q^2)$, it is easy to derive the *dispersion relation*. The

[2]A more detailed discussion of these topics of complex analysis can be found in refs. [93, 94].

[3]The branch point at $q^2 = (m_{B_c} + m_\pi)^2$ can be neglected, because it is isospin suppressed.

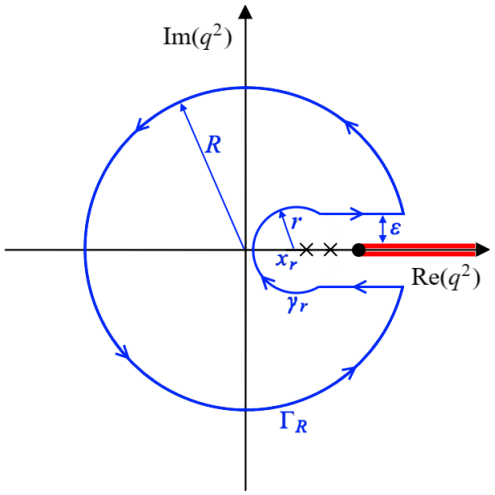

Figure 3.3: The closed curve where the integral in eq. (3.6) is performed.

starting point is to represent $\Pi(q^2)$ through the Cauchy's integral formula

$$\Pi(q^2) = \frac{1}{2\pi i} \oint_\gamma \mathrm{d}s \, \frac{\Pi(s)}{s - q^2} \,, \tag{3.6}$$

where q^2 is a point inside the closed curve γ shown in figure 3.3. To simplify the integral in eq. (3.6), we can take the limit $R \to \infty$ and $r \to 0$. Assuming that

$$\frac{1}{2\pi i} \oint_{\Gamma_R} \mathrm{d}s \, \frac{\Pi(s)}{s - q^2} \to 0 \qquad \text{for } R \to \infty \tag{3.7}$$

and

$$\frac{1}{2\pi i} \oint_{\gamma_r} \mathrm{d}s \, \frac{\Pi(s)}{s - q^2} \to 0 \qquad \text{for } r \to 0 \,, \tag{3.8}$$

eq. (3.6) becomes

$$\Pi(q^2) = \frac{1}{2\pi i} \int_{x_r}^{\infty} \mathrm{d}s \, \frac{\Pi(s + i\varepsilon) - \Pi(s - i\varepsilon)}{s - q^2} \,, \tag{3.9}$$

where ε is an arbitrary small positive number.

While it is easy to see that the condition (3.8) is trivially fulfilled, since one can always choose the point x_r to be on the real axis below the first singularity (as shown in figure 3.3), it may happen that the integral of eq. (3.7) does not vanish. In that case, one has to perform a certain number of subtractions, i.e. take derivatives with respect to q^2, until the condition (3.7) is satisfied.

Using the Schwarz reflection principle, we can rewrite the numerator of the integrand in eq. (3.9) as

$$\Pi(s + i\varepsilon) - \Pi(s - i\varepsilon) = 2i \, \mathrm{Im} \, \Pi(s) \,, \tag{3.10}$$

thus

$$\Pi(q^2) = \frac{1}{\pi}\int_{x_r}^{\infty} \mathrm{d}s\, \frac{\mathrm{Im}\,\Pi(s)}{s-q^2}\,. \tag{3.11}$$

It can be shown that the imaginary part of loop amplitudes come from intermediate particles going on-shell (see e.g. refs. [16, 17]). Using this observation, we can finally write down the dispersion relation:

$$\Pi(q^2) = \frac{1}{\pi}\int_{s_{th}}^{\infty} \mathrm{d}s\, \frac{\mathrm{Im}\,\Pi(s)}{s-q^2}\,, \tag{3.12}$$

where s_{th} is the mass squared of the lightest $c\bar{b}$ bound state with the same spin and parity quantum numbers of $\Pi(q^2)$. The procedure presented here can be easily extended different to quark currents J^μ.

Equation (3.12) is fundamental for the calculation of a sum rule. It implies that if one knows the imaginary part of $\Pi(q^2)$, then $\Pi(q^2)$ is fixed in the whole q^2 plane. Vice versa, if one knows $\Pi(q^2)$ in one single regular point of the complex plane, it is possible extract information about the imaginary part of $\Pi(q^2)$.

Equation (3.12) is also crucial to extract the dispersive bounds, which are non-trivial constraints on HMEs (see section 3.3).

3.1.2 The Borel Transform

A mathematical transform is an operator that maps a function space into a different function space. Mathematical transforms are commonly used to solve certain problems by mapping them into a different function space, where the solution is known. However, we will use the Borel transform for a different purpose, which is to reduce the error in a sum rule due to the quark hadron duality approximation.

Let us introduce the operator [95]

$$\hat{L}_{M^2} = \lim_{\substack{-q^2\to\infty \\ n\to\infty}} \frac{(-q^2)^{n+1}}{n!}\left(\frac{\mathrm{d}}{\mathrm{d}q^2}\right)^n\,, \tag{3.13}$$

where the limit is taken keeping the so-called *Borel parameter* $M^2 \simeq -q^2/n$ fixed. We can then define the function

$$\Pi(M^2) = \hat{L}_{M^2}\Pi(q^2)\,, \tag{3.14}$$

which is the Borel transform of $q^2(-\mathrm{d}/\mathrm{d}q^2)\Pi(q^2)$. Nevertheless, in the context of QCDSRs, $\Pi(M^2)$ is often simply referred to as the Borel transform of $\Pi(q^2)$. We will also adopt this slight abuse of terminology.

Even though we indicate the two functions $\Pi(q^2)$ and $\Pi(M^2)$ with the same symbol, they have a completely different functional form. We will see in the next section that the functional form of $\Pi(M^2)$ is much more convenient to further suppress the contribution coming from the continuum states and the higher orders in the OPE.

Using eq. (3.13) we can compute the Borel transform of several prototypical functions that will appear later on:

$$\begin{aligned}\hat{L}_{M^2}(q^2)^k &= 0\,,\\ \hat{L}_{M^2}\frac{1}{(s-q^2)^k} &= \frac{1}{(k-1)!}\frac{e^{-\frac{s}{M^2}}}{(M^2)^{k-1}}\,,\\ \hat{L}_{M^2}(-q^2)^k\log\left(\frac{-q^2}{\mu}\right) &= k!(-M^2)^{k+1}\,,\end{aligned} \tag{3.15}$$

for $k>0$. For instance, the dispersion relation (3.22) after the Borel transform becomes

$$\Pi(M^2) = \frac{1}{\pi}\int_{s_{th}}^{\infty} \mathrm{d}s\, e^{\frac{s}{M^2}}\,\mathrm{Im}\,\Pi(s)\,. \tag{3.16}$$

3.1.3 Quark-Hadron Duality

As the name suggests, quark-hadron duality relies on the idea that amplitudes computed in perturbative QCD (in a specific energy regime and under certain assumptions) can be approximated by amplitudes computed treating hadrons as fundamental particles, and vice versa.

Quark-hadron duality was originally proposed almost fifty years ago [96], and since then it was widely investigated and exploited in many calculations. In fact, this approach represents an awfully broad topic in QCD and there is extended literature about it. Here, we just sketch some of the main features, while more details can be found in the classic review [97].

In our calculations, we use quark-hadron duality to relate the imaginary part of the OPE calculation[4] to the *true* imaginary part of a certain correlator $\Pi(q^2)$:

$$\int_{s_0}^{\infty}\mathrm{d}s\,\frac{\mathrm{Im}\,\Pi^{\mathrm{OPE}}(s)}{s-q^2} \simeq \int_{s_{2\mathrm{p}}}^{\infty}\mathrm{d}s\,\frac{\mathrm{Im}\,\Pi^{had}(s)}{s-q^2}\,, \tag{3.17}$$

where $\mathrm{Im}\,\Pi^{had}$ coincides with the spectral density function τ_H, which is experimentally observable. In general, the continuum threshold $s_{2\mathrm{p}}$ and the effective threshold s_0 are different as we will see in the next sections. Equation (3.17), which is known as *semi-global (or global) quark-hadron duality*, is extremely useful due to the fact that, while $\mathrm{Im}\,\Pi^{had}$ is essentially unknown, $\mathrm{Im}\,\Pi^{\mathrm{OPE}}$ is in principle calculable. Thus, eq. (3.17) can be used to get rid of the tail of $\mathrm{Im}\,\Pi^{had}$, which always appears in the calculation of a sum rule.

One can also attempt to relate $\mathrm{Im}\,\Pi^{had}$ and $\mathrm{Im}\,\Pi^{\mathrm{OPE}}$ point-by-point:

$$\mathrm{Im}\,\Pi^{\mathrm{OPE}}(q^2) \simeq \mathrm{Im}\,\Pi^{had}(q^2)\,, \tag{3.18}$$

for sufficiently large values of q^2. This equation is usually called *local quark-hadron duality*.

It is crucial to understand the accuracy of the quark-hadron duality relations (3.17)-(3.18) to have precise and reliable theoretical calculations. Obviously, the relations (3.17)-(3.18) are just approximate identities because we are not able to compute $\Pi^{\mathrm{OPE}}(q^2)$ with infinite

[4] We will discuss in the next section how to compute the imaginary part of the OPE.

precision. In fact, if we could compute $\Pi^{\rm OPE}(q^2)$ exactly in the whole q^2 complex plane, there would be no need for duality and we would simply have [97]

$$\Pi^{\rm OPE}(q^2) \equiv \Pi^{had}(q^2)\,. \tag{3.19}$$

However, in practice one computes $\Pi^{\rm OPE}(q^2)$ approximately truncating both the OPE and α_s expansions at some finite order. Even if one was able to calculate all the terms in both series, it would not be helpful since these series are factorially divergent [97].

Besides these expected sources of uncertainties, there are additional ones known as *quark-hadron duality violations*. Duality violations are mostly due to the fact that even for large positive q^2 values, $\mathrm{Im}\,\Pi^{\rm OPE}(q^2)$ is not able to reproduce exactly the resonant structure of $\mathrm{Im}\,\Pi^{had}$ (see e.g. ref. [98]). Although in most of the applications these effects are supposed to be small, one needs to take them in account and to carefully study them.

3.2 QCD Sum Rules in a Nutshell

QCD sum rules are a way to determine HMEs starting from a correlator, which has to be constructed on a case by case basis. This correlator has to be expanded in an OPE, which separates the short-distance contributions, calculable in QCD perturbation theory, from the long-distance contributions, which are expressed in terms of vacuum condensates or distribution amplitudes.

The next step is to express the imaginary part of the correlator in terms of the intermediate bound states plus a continuum of multiparticle states. Both of these contributions must have quantum numbers compatible with the currents appearing in the correlator.

Finally, the dispersion relation allows to match the OPE calculation onto the imaginary part of the correlator. The semi-global quark hadron duality approximation is then used to get rid of the poorly known continuum contribution. The Borel transform is an additional tool adopted to suppress the tail of the OPE calculation and the continuum contribution, reducing in this way the impact of eventual quark-hadron duality violations. The identity obtained after all these steps is the *sum rule*, which is a relation between one or more HMEs, vacuum condensates (or distribution amplitudes), and the masses of the states involved.

There are mainly two kinds of QCD sum rules: the SVZ sum rules and the light-cone sum rules. The SVZ sum rules were originally proposed by Shifman, Vainshtein, Zakharov in the late 1960s [95] (see refs. [91, 99] for a review). A decade later, this method was reworked [100, 101] using a light-cone OPE instead of a local OPE, from which the name light-cone sum rules (LCSRs) derives.

In our analysis we only employ the LCSRs. Nevertheless, it is also useful to review the SVZ sum rules to develop an understanding of the method.

3.2.1 SVZ Sum Rules

To show how to compute an SVZ sum rule, we present an example taken from the review [91] where the ρ-meson decay constant is extracted.

We define the vacuum-to-vacuum correlator

$$\Pi^{\mu\nu}_{(\rho)}(q) = i\int \mathrm{d}^4x e^{iq\cdot x}\,\langle 0|\,T\{J^{\mu}_{(\rho)}(x), J^{\nu,\dagger}_{(\rho)}(0)\}\,|0\rangle = (q^\mu q^\nu - q^2 g^{\mu\nu})\Pi_{(\rho)}(q^2)\,, \tag{3.20}$$

where

$$J^{\mu}_{(\rho)} = \frac{1}{2}(\bar{u}\gamma^{\mu}u - \bar{d}\gamma^{\mu}d)\,. \tag{3.21}$$

Notice that in eq. (3.20) no term proportional to $q^{\mu}q^{\nu}$ appears, since $J^{\mu}_{(\rho)}$ is a conserved current. The correlator (3.20) can be computed in a certain region of the phase space using an OPE, while its imaginary is obtained using a unitarity relation. These two different calculations are then matched by using a dispersion relation and the quark-hadron duality approximation to obtain the sum rule.

Let us start with the OPE calculation. For large negative q^2, i.e. for $-q^2 \gg \Lambda_{\rm QCD}$, the integral of eq. (3.20) is dominated by short distances $x \simeq 1/\sqrt{-q^2}$, and hence we can perform an OPE of the correlator $\Pi_{(\rho)}(q^2)$:

$$\Pi_{(\rho)}(q^2) = \sum_i C_i(q^2;\mu)\langle O_i(\mu)\rangle\,. \tag{3.22}$$

Here the index i indicates the dimension of the operator O_i and

$$\langle O_i(\mu)\rangle \equiv \langle 0|\, O_i(\mu)\,|0\rangle\ .$$

If the condition $-q^2 \gg \Lambda_{\rm QCD}$ is fulfilled, we can truncate the series above after the first few terms. As we have seen in the previous chapter, the main reason to use an OPE is to separate the short-distance contribution of the Wilson coefficients C_i and the long-distance one of the operators O_i.

The matrix elements $\langle O_i(\mu)\rangle$ are the *QCD vacuum condensates*, i.e. the vacuum expectation values of the normal ordered local product of QCD fields (quarks and gluon fields). The first matrix element in the sum of eq. (3.22) is trivial, since the only operator with mass dimension equal to zero is the identity:

$$\langle O_0\rangle = \langle \mathbb{1}\rangle = 1\,.$$

The next non-vanishing matrix element is the one with the dimension-three operator

$$O_3 = \bar{q}q\,,$$

where, in our case, $q = u,\, d$. Moreover, assuming the isospin symmetry, one has $\langle\bar{q}q\rangle = \langle\bar{u}u\rangle = \langle\bar{d}d\rangle$. The condensates with dimension four and five are generated by the following operators

$$O_4 = \frac{\alpha_s}{\pi}G^a_{\mu\nu}G^{\mu\nu}_a\,,$$

$$O_5 = -g_s\bar{q}\,\sigma_{\mu\nu}\mathbf{G}^{\mu\nu}\,q\,.$$

At dimension six, there two different classes of operators:

$$O_{6,1} = g_s^3 f_{abc}G^a_{\mu\nu}G^{\nu\sigma,b}G_{\sigma}{}^{\mu,c}\,,$$

$$O_{6,2} = \alpha_s(\bar{q}\,\Gamma_{\alpha}q)(\bar{q}\,\Gamma^{\alpha}q)\,,$$

where f_{abc} are the structure constants of $SU(3)$, while the Γ_{α} are combinations of Dirac and Gell-Mann matrices.

The dimension-five condensate can be expressed as

$$-g_s\langle\bar{q}\,\sigma_{\mu\nu}\mathbf{G}^{\mu\nu}\,q\rangle \simeq m_0\langle\bar{q}q\rangle\,,$$

where the parameter m_0 can be determined using a sum rule [102]. It is also possible to approximate the condensate $\langle O_{6,2}\rangle$ as (see e.g. refs. [91, 103])

$$\alpha_s\langle(\bar{q}\,\Gamma_\alpha q)(\bar{q}\,\Gamma^\alpha q)\rangle = \kappa\alpha_s\langle\bar{q}q\rangle\,,$$

where κ is a known constant that depends on the traces of the Γ_α matrices.

Vacuum condensates, being genuine non-perturbative quantities, must be computed using lattice QCD or other non-perturbative methods (see e.g. refs. [95, 99, 104, 105]. while see ref. [103] for a review). Condensates with dimension higher than six are usually neglected in most of the applications. On the other hand, the Wilson coefficients can be computed in perturbative QCD. In particular C_0 is given by the Feynman diagram of figure 3.1 and its α_s corrections.

After performing a Borel transformation, the OPE result that includes $\mathcal{O}(\alpha_s)$ corrections and operators up to dimension six reads

$$\begin{aligned}\Pi^{\rm OPE}_{(\rho)}(M^2) = M^2\Bigg[\frac{1}{4\pi^2}\left(1+\frac{\alpha_s}{\pi}\right)+\frac{m_u+m_d}{M^4}\langle\bar{q}q\rangle \\ + \frac{1}{12M^4}\left\langle\frac{\alpha_s}{\pi}G^a_{\mu\nu}G^{\mu\nu}_a\right\rangle - \frac{112\pi}{81}\frac{\alpha_s}{M^6}\langle\bar{q}q\rangle^2\Bigg]\,.\end{aligned} \tag{3.23}$$

Having the OPE result, we proceed with calculation of the imaginary part of $\Pi_{(\rho)}(q^2)$. To this end, we exploit the unitarity relation

$$(q^\mu q^\nu - q^2 g^{\mu\nu})\,\mathrm{Im}\,\Pi^{had}_{(\rho)}(q^2) = \frac{1}{2}\sum\!\!\!\!\!\!\int_H \mathrm{d}\tau_H\,(2\pi)^4\delta^{(4)}(p_H-q)\,\langle 0|J^\mu_{(\rho)}(0)|H\rangle\,\langle H|J^{\dagger,\nu}_{(\rho)}(0)|0\rangle\ , \tag{3.24}$$

where $H(p_H)$ denotes the ρ meson and all the other states with the same quantum numbers, while τ_H is the spectral density function. From eq. (3.24) one immediately obtains

$$\frac{1}{\pi}\,\mathrm{Im}\,\Pi^{had}_{(\rho)}(q^2) = f_\rho^2\delta(q^2-m_\rho^2)+\tau_H(q^2)\theta(q^2-4m_\pi^2)\,, \tag{3.25}$$

where f_ρ is the ρ-meson decay constant defined as

$$\langle 0|J^\mu_{(\rho)}|\rho(k,\eta)\rangle = \frac{i}{\sqrt{2}}\eta^\nu m_\rho f_\rho \tag{3.26}$$

and η^ν is the polarisation vector.

Notice that, in contrast to the example in subsection 3.1.1 with a heavy quark current, here the first bound state is not below the continuum threshold. The same occurs for all the light quark currents. In order to overcome this potential problem, we have considered the ρ meson in the narrow width, to clearly distinguish it from the continuum of multi-particle states background. In principle, one could also go beyond the narrow width approximation and model the ρ-meson resonance with a different distribution (e.g. a Breit-Wigner distribution) [106].

Now, we can recast eq. (3.25) in a dispersive form

$$\frac{1}{\pi}\int_{4m_\pi^2}^{\infty}\mathrm{d}s\,\frac{\mathrm{Im}\,\Pi_{(\rho)}^{had}(s)}{s-q^2}=\frac{f_\rho^2}{m_\rho^2-q^2}+\int_{4m_\pi^2}^{\infty}\mathrm{d}s\,\frac{\tau_H(q^2)}{s-q^2}\,, \tag{3.27}$$

and Borel transform it

$$\frac{1}{\pi}\int_{4m_\pi^2}^{\infty}\mathrm{d}s\,e^{-\frac{s}{M^2}}\,\mathrm{Im}\,\Pi_{(\rho)}^{had}(s)=e^{-\frac{m_\rho^2}{M^2}}f_\rho^2+\int_{4m_\pi^2}^{\infty}\mathrm{d}s\,e^{-\frac{s}{M^2}}\,\tau_H(q^2)\,. \tag{3.28}$$

Matching this result onto the OPE result (3.23) through the dispersion relation (3.16), one obtains

$$\begin{aligned}e^{-\frac{m_\rho^2}{M^2}}f_\rho^2+\int_{4m_\pi^2}^{\infty}\mathrm{d}s\,e^{-\frac{s}{M^2}}\tau_H(q^2)=\\ M^2\left[\frac{1}{4\pi^2}\left(1+\frac{\alpha_s}{\pi}\right)+\frac{m_u+m_d}{M^4}\langle\bar{q}q\rangle+\frac{1}{12M^4}\left\langle\frac{\alpha_s}{\pi}G^a_{\mu\nu}G_a^{\mu\nu}\right\rangle-\frac{112\pi}{81}\frac{\alpha_s}{M^6}\langle\bar{q}q\rangle^2\right],\end{aligned} \tag{3.29}$$

with $\alpha_s\equiv\alpha_s(M)$. To use the semi-global quark-hadron duality approximation (3.17), it is convenient to rewrite the r.h.s. of eq. (3.29) in a dispersive form using the identity

$$M^2=\int_0^{\infty}\mathrm{d}s\,e^{-\frac{s}{M^2}}\,.$$

The sum rule, which allows to extract the ρ-meson decay constant, reads

$$\begin{aligned}f_\rho^2=\int_{s_0^\rho}^{\infty}\mathrm{d}s\,e^{\frac{m_\rho^2-s}{M^2}}\left[\frac{1}{4\pi^2}\left(1+\frac{\alpha_s}{\pi}\right)+\right.\\ \left.\frac{m_u+m_d}{M^4}\langle\bar{q}q\rangle+\frac{1}{12M^4}\left\langle\frac{\alpha_s}{\pi}G^a_{\mu\nu}G_a^{\mu\nu}\right\rangle-\frac{112\pi}{81}\frac{\alpha_s}{M^6}\langle\bar{q}q\rangle^2\right].\end{aligned} \tag{3.30}$$

A few comments are in order concerning this equation and the SVZ sum rules in general:

- A sum rule is a relation between hadronic matrix elements and other parameters (masses, coupling constants, threshold parameters,...). Using a sum rule one can extract a hadronic matrix element by fixing the value of all the other parameters. In this example we have chosen to extract f_ρ, but the same sum rule could be used to compute one of the vacuum condensates if f_ρ would have been taken from other sources.

- Performing a Borel transform is not necessary, but it reduces the error due to the quark-hadron duality approximation. Indeed, the contribution of the continuum becomes exponentially suppressed, as one can see from eq. (3.28).

- The effective threshold s_0 is in general different from the continuum threshold (in this case $s_{2\mathrm{p}}=4m_\pi^2$). To determine s_0 one can eithe use another sum rule or a *daughter sum rule*, as we will show in subsection 4.1.2.

parameter	value	unit	reference
$\langle\bar{q}q\rangle(2\text{ GeV})$	$-(0.272\pm0.010)^3$	GeV^3	[104, 105, 107]
$\left\langle\frac{\alpha_s}{\pi}G^a_{\mu\nu}G^{\mu\nu}_a\right\rangle$	0.012 ± 0.012	GeV^4	[95, 103, 108–110]
s_0^ρ	1.6	GeV^2	[91, 95]

Table 3.1: List of the inputs used to evaluate the sum rule eq. (3.30).

- To improve the accuracy of the sum rule, one can include higher order terms in the α_s expansion and in the OPE. Nevertheless, the uncertainty due to the quark-hadron duality approximation and the dependence on the Borel parameter M^2 cannot be easily reduced (see the next bullet point). Moreover, to evaluate a sum rule one also needs universal non-perturbative inputs, which in the case of the SVZ sum rules are the vacuum condensates, while in the case of the LCSRs are the distribution amplitudes.

- Since the l.h.s. of eq. (3.30) does not depend on the Borel parameter M^2, one would expect that also the r.h.s. of eq. (3.30) would be M^2 independent. However, all the sum rules depend on M^2, which reflects the fact that we can only compute Π^{OPE} approximately. To overcome this problem one should look for an M^2 range where: 1) the Borel parameter dependence of the sum rule is small, 2) the continuum contribution is sufficiently suppressed, and 3) the higher order contributions in the OPE are small compared to the leading ones. In other words, if M^2 is too big the exponential suppression coming from the factor $e^{-\frac{s}{M^2}}$ is no longer effective, while if M^2 is too small further $1/(M^2)^n$ terms become important.
  For instance, all these three conditions are satisfied in the sum rule (3.30) when [91]

$$0.7\,\text{GeV}^2 \lesssim M^2 \lesssim 1.2\,\text{GeV}^2\,. \tag{3.31}$$

  It is not possible to say a priori whether such a range exists for a given sum rule, and one has to verify this case by case.

Using the inputs given in table 3.1 we can evaluate the sum rule eq. (3.30) to predict ρ-meson decay constant

$$f_\rho \simeq 0.21\,\text{GeV}\,. \tag{3.32}$$

As expected, the main contribution to this sum rule comes from the first term in the OPE at leading order in α_s, which is approximately 90 % of the value obtained.

To complete this example, we need to discuss the uncertainties of the result (3.32):

Uncertainties of the inputs The uncertainties of the input parameters are known and can be easily taken into account. Nevertheless, they can be large due to the non-perturbative nature of the inputs (condensates, threshold parameters, etc.). In addition, one should also include the uncertainty due to the scale dependence of the parameters that enter into the sum rule.

Borel parameter dependence As already discussed, after performing a Borel transform every rule shows a fictitious dependence on the Borel parameter M^2. After finding an appropriate M^2 range, one should vary the sum rule in this range and add a related systematic uncertainty. The result of the sum rule (3.30) is essentially constant in the range (3.31), and hence in this case the uncertainty due to the M^2 dependence is negligible. However, we will see that certain LCSRs have a significant M^2 dependence and the related uncertainty needs to be taken into account.
To reduce this of type uncertainty, one could include higher orders in α_s and in the OPE such that the dependence on M^2 becomes smaller. Even if there is no formal proof of this so far, it can be expected since the difference between Π^{OPE} and Π^{had} should get smaller, and Π^{had} does not depend on M^2.

Quark hadron duality approximation As for the M^2 dependence of the sum rule, there is no trivial way to reduce the error due to this approximation, which is also hard to estimate. A check that one should always perform after computing a sum rule is to verify that the tail of OPE calculation, i.e.

$$\int_{s_0}^{\infty} \mathrm{d}s \, \frac{\operatorname{Im} \Pi^{\text{OPE}}(s)}{s - q^2} \,,$$

is not the dominant contribution to the same integral extended from 0 to ∞, i.e.

$$\int_{0}^{\infty} \mathrm{d}s \, \frac{\operatorname{Im} \Pi^{\text{OPE}}(s)}{s - q^2} \,.$$

In the example discussed in this subsection we find

$$\frac{\int_{s_0^\rho}^{\infty} \mathrm{d}s \, \frac{\operatorname{Im} \Pi^{\text{OPE}}_{(\rho)}(s)}{s-q^2}}{\int_{0}^{\infty} \mathrm{d}s \, \frac{\operatorname{Im} \Pi^{\text{OPE}}_{(\rho)}(s)}{s-q^2}} \simeq 0.4 \,,$$

which is large but usually still accepted in literature.

Higher order corrections The uncertainty due to the neglected higher order contributions both in the OPE and in the α_s expansion should be taken into account. Clearly, if other expansions are performed (such as the heavy quark expansion) and truncated at some finite order, one should include these effect in the total uncertainty as well.

Adding up all these error sources, we obtain for our example

$$f_\rho = (0.21 \pm 0.02)\,\text{GeV} \,.$$

This value of f_ρ is in excellent agreement with one extracted from experimental data [27, 66]

$$f_\rho = (0.213 \pm 0.005)\,\text{GeV} \,.$$

In general, it is unlikely to obtain a sum rule prediction with an uncertainty smaller than $\sim 5 - 10\,\%$, which is relatively big compared to most of the recent lattice QCD results for form factors and decay constants. Nevertheless, QCD sum rules are still extremely useful, since their predictions can be combined with the lattice ones (see chapter 4) and they can provide results for hadronic matrix elements that are currently inaccessible for lattice QCD.

	SVZ sum rules	**light-cone sum rules**
correlator type	vacuum-to-vacuum	meson-to-vacuum
universal non-perturbative inputs	QCD condensates	distribution amplitudes
expansion type	local OPE	light-cone OPE
expansion parameter	dimension of the condensates	twist
used to compute	decay constants threshold parameters condensates ...	form factors non-local effects in $B \to K^{(*)}\ell\ell$ threshold parameters ...

Table 3.2: Comparison between SVZ sum rules and LCSRs. See text for details.

3.2.2 Light-Cone Sum Rules

The light-cone sum rules (LCSRs) were originally proposed in refs. [100, 101], and they are very similar to the SVZ sum rule. However, there are few important differences between these two types of sum rules, which are listed in table 3.2 and are discussed in this subsection.

To illustrate the LCSRs at work we present an example in which we calculate the $B \to K$ form factors. In particular, we use the LCSRs with B-meson light-cone distribution amplitudes (B-LCDAs), which were proposed for the first time in refs. [111, 112]. The difference between LCSRs with B-LCDAs and LCSRs with light-meson light-cone distribution amplitudes are discussed at the end of this subsection. Here and throughout this thesis we call the LCSRs with B-LCDAs simply LCSRs, unless explicitly specified otherwise.

Let us first define the $B \to K$ form factors, i.e. functions of the momentum transfer squared q^2 that parametrize local hadronic matrix elements between B and K mesons[5]:

$$\langle K(k)|\,\bar{s}\gamma^\mu b\,|B(p)\rangle = \left[(p+k)^\mu - \frac{m_B^2 - m_K^2}{q^2}q^\mu\right] f_+^{B\to K} + \frac{m_B^2 - m_K^2}{q^2}q^\mu\, f_0^{B\to K}, \quad (3.33)$$

$$\langle K(k)|\,\bar{s}\sigma^{\mu\nu}\, q_\nu b\,|B(p)\rangle = \frac{i f_T^{B\to K}}{m_B + m_K}\,\left[q^2\,(p+k)^\mu - (m_B^2 - m_K^2)\,q^\mu\right], \quad (3.34)$$

where $p^\mu = q^\mu + k^\mu$. While the number of independent form factors is fixed, they can be defined in different equivalent ways. For instance, another common choice is

$$\langle K(k)|\,\bar{s}\gamma^\mu b\,|B(p)\rangle = (p+k)^\mu\, f_+^{B\to K} + q^\mu\, f_-^{B\to K}, \quad (3.35)$$

which is less convenient in phenomenological applications (see appendix B). Comparing eq. (3.33)

[5] We omit the q^2 dependence of the form factor throughout this work by simply writing $f_+^{B\to K}$ instead of $f_+^{B\to K}(q^2)$.

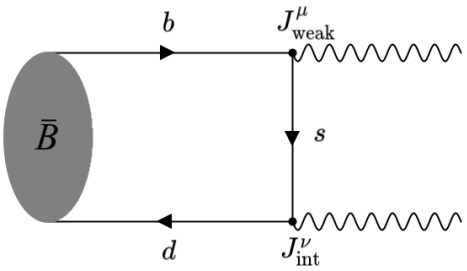

Figure 3.4: Diagram corresponding to the correlator (3.38). Hard- and soft-gluon corrections are not shown explicitly.

and eq. (3.35), one can easily find the relation between these two different definitions:

$$f_0^{B\to K} = f_+^{B\to K} + \frac{q^2}{m_B^2 - m_K^2} f_-^{B\to K} \,. \tag{3.36}$$

This equation implies that

$$f_0^{B\to K}(q^2 = 0) = f_+^{B\to K}(q^2 = 0) \,. \tag{3.37}$$

More details about the meson form factors can be found in appendix B.

The first step to compute a LCSR is to define an appropriate correlator

$$\Pi^{\mu\nu}(q,k) \equiv i \int \mathrm{d}^4x \, e^{ik\cdot x} \, \langle 0| \, T\{J^{\nu}_{\text{int}}(x), J^{\mu}_{\text{weak}}(0)\} \, |\bar{B}(q+k)\rangle \ , \tag{3.38}$$

where the corresponding diagram in shown in figure 3.4. The reason why here one needs to choose a meson-to-vacuum correlator instead of a vacuum-to-vacuum correlator (as in the case of SVZ sum rules) will soon become clear. The currents to compute the $f_+^{B\to K}$ and $f_-^{B\to K}$ form factors are

$$\begin{aligned} J^{\mu}_{\text{weak}} &= \bar{s}\gamma^{\mu} b \,, \\ J^{\nu}_{\text{int}} &= \bar{d}\gamma^{\nu}\gamma_5 s \,. \end{aligned} \tag{3.39}$$

Changing the quark flavours one can compute the form factors for different decays (e.g. $B \to \pi$, $B \to D$, $B_s \to K$, etc.), which are defined analogously to the $B \to K$ ones.

In analogy to the SVZ sum rules, we compute the correlator (3.38) both by using an OPE and employing a unitarity relation to obtain the hadronic representation of the correlator. We then match these two different results by using a dispersion relation and the quark-hadron duality to obtain the sum rule.

Calculating the hadronic representation of the correlator (3.38) is relatively easy. The imaginary part of (3.38) can be extracted inserting a complete set of states with the right quantum numbers between the two currents:

$$\Pi^{\mu\nu}(q,k) = \frac{\langle 0| \, J^{\nu}_{\text{int}}(x) \, |\bar{K}(k)\rangle \, \langle \bar{K}(k)| \, J^{\mu}_{\text{weak}}(0) \, |\bar{B}(q+k)\rangle}{m_{\bar{K}}^2 - k^2} + \frac{1}{\pi}\int_{s_h}^{\infty} \mathrm{d}s \frac{\tau^{\mu\nu}(s)}{s - k^2} \,, \tag{3.40}$$

where $\tau(s)$ is the spectral density function, which encodes the contributions of the excited and continuum states, and s_h is the mass of the lightest or continuum state. We can now use the decay constant definition

$$\langle 0|J^{\nu}_{\text{int}}|\bar{K}(k)\rangle = ik^{\nu} f_K \tag{3.41}$$

and the form factor definition of eq. (3.35) to get the hadronic representation of the correlator (3.38)

$$\Pi^{\mu\nu}(q,k) = k^\nu f_K \frac{(p+k)^\mu\, f_+^{B\to K} + q^\mu\, f_-^{B\to K}}{m_{\bar{K}}^2 - k^2} + \frac{1}{\pi}\int_{s_h}^{\infty} \mathrm{d}s \frac{\tau^{\mu\nu}(s)}{s-k^2}\,. \tag{3.42}$$

In contrast to the derivation of the hadronic representation of the correlator, the OPE calculation can be extremely challenging. First, one has to prove that in a specific region of the phase space it is possible to perform an OPE of the correlator. While for the SVZ sum rules we used a local OPE, where the correlator was expanded around $x \sim 0$, for LCSRs, as the name suggests, we use a light-cone OPE (LCOPE), expanding around $x^2 \sim 0$. Like a local OPE, a LCOPE allows to factorise the long-distance contributions, expressed through a series of distribution amplitudes with increasing twist, and the short-distance contributions, which can be computed in QCD perturbation theory. The definition of twist is given below. After computing the first few terms of the LCOPE, we match this result onto the hadronic representation of the correlator.

Before performing the LCOPE, we expand the correlator (3.38) in HQET

$$\Pi^{\mu\nu}(q,k) \equiv i\int \mathrm{d}^4x\, e^{ik\cdot x}\, \langle 0|\, T\{\bar{d}\gamma^\nu\gamma_5\, s(x), \bar{s}\gamma^\mu h_v(0)\}\, |\bar{B}(v)\rangle + \mathcal{O}\left(\frac{1}{m_b}\right)\,. \tag{3.43}$$

As shown in refs. [91, 112], assuming

$$-k^2,\, -q_{res}^2 \gg \Lambda_{\mathrm{QCD}}\,,$$

the correlator (3.43) can be expanded around $x^2 = 0$ for

$$q^2 < m_b\left(m_b + \frac{k^2}{\bar{\Lambda}}\right)\,, \tag{3.44}$$

where $q^\mu = m_b v^\mu + q_{res}^\mu$ and $\bar{\Lambda} \sim \Lambda_{\mathrm{QCD}}$ (see section 2.4). In this case, the LCOPE is performed expanding the strange-quark propagator near the light-cone. The first two terms of this expansion are [113]

$$\begin{aligned}\langle 0 \mid T\{s(x)\bar{s}(y)\} \mid 0\rangle &= i\int \frac{\mathrm{d}^4k}{(2\pi)^4} e^{-ik\cdot(x-y)}\frac{\not{k}+m_s}{k^2-m_s^2} \\ &- i\int_0^1 \mathrm{d}u\, g_s\mathbf{G}^{\lambda\rho}(ux+(1-u)y)\int\frac{\mathrm{d}^4k}{(2\pi)^4}e^{-ik\cdot(x-y)}\frac{(1-u)(\not{k}+m_s)\sigma_{\lambda\rho}+u\,\sigma_{\lambda\rho}(\not{k}+m_s)}{2(k^2-m_s^2)^2}\,,\end{aligned} \tag{3.45}$$

which are commonly called the two-particle and the three-particle contributions, respectively. Four-particle contributions are not taken into account, because they are expected to be small and the related distribution amplitudes do not mix with the three-particle distribution amplitudes [114]. The two-particle contributions to the correlator are

$$\Pi^{\mu\nu}(q,k)\Big|_{\mathrm{2p}} \equiv \int \mathrm{d}^4x \int \mathrm{d}^4p'\, e^{ix\cdot(k-p')}\, \langle 0|\, \bar{d}^\alpha(x) h_v^\beta(0)\, |\bar{B}(v)\rangle \left[\gamma^\nu\gamma_5\,\frac{\not{p}'+m_s}{m_s^2-p'^2}\gamma^\mu\right]_{\alpha\beta}\,. \tag{3.46}$$

The three-particle ones are

$$\Pi^{\mu\nu}(q,k)\Big|_{3\mathrm{p}} \equiv \int \mathrm{d}^4x \int \mathrm{d}^4p' \int_0^1 \mathrm{d}u\, e^{ix\cdot(k-p')} \times \langle 0|\, \bar{d}^\alpha(x) g_s \mathbf{G}_{\lambda\rho}(ux) h_v^\beta(0)\, |\bar{B}(v)\rangle \left[\gamma^\nu\gamma_5\, S_{3\mathrm{p}}^{\lambda\rho}(u,p')\gamma^\mu\right]_{\alpha\beta}, \quad (3.47)$$

where

$$S_{3\mathrm{p}}^{\lambda\rho}(u,p') \equiv \frac{(1-u)(\not{p}'+m_s)\sigma^{\lambda\rho} + u\sigma^{\lambda\rho}(\not{p}'+m_s)}{2(p'^2-m_s^2)^2}\,. \quad (3.48)$$

The quantities in square brackets in eqs. (3.46)-(3.47) are the hard-scattering kernels, which represent the short-distance contributions to the correlator.

The non-local B-to-vacuum matrix elements that appear in eqs. (3.46)-(3.47) can be parametrized in terms of B-meson light-cone distribution amplitudes (B-LCDAs). The B-LCDAs are ordered by increasing twist, where the twist is defined as the difference between the dimension and the spin of the operator considered. In other words, going beyond the leading order in the LCOPE means both including multi-particle contributions and higher twist B-LCDAs.

In the limit $x^2 = 0$, the two-particle non-local B-to-vacuum matrix element can be parametrized as

$$\langle 0|\, \bar{d}^\alpha(x) h_v^\beta(0)\, |\bar{B}(v)\rangle \;=\; -\frac{i f_B m_B}{4}\int_0^\infty \mathrm{d}\omega\, e^{-i\omega v\cdot x}\left\{(1+\not{v})\left[\phi_+(\omega) + \frac{1}{2}\bar{\phi}(\omega)\gamma^\mu\partial_\mu\right]\gamma_5\right\}^{\beta\alpha}, \quad (3.49)$$

with

$$\bar{\phi}(\omega) \equiv \int_0^\omega \mathrm{d}\eta\, \left(\phi_+(\eta) - \phi_-(\eta)\right), \quad (3.50)$$

where the derivative $\partial_\mu \equiv \partial/\partial(\omega v^\mu)$ acts on the hard-scattering kernel. The leading twist contributions are given by $\phi_+(\omega)$, which has twist two, and $\phi_-(\omega)$, which has twist three. We will explore the correction that arise releasing the assumption $x^2 = 0$ in the next chapter. Models for the B-LCDAs of eq. (3.49) can be found in refs. [37, 114]. In this example, we neglect the three-particle contributions, since they are numerically much smaller than the two-particle ones as shown in ref. [1] (see subsection 4.1.1).

As in the case of SVZ sum rules, we match the hadronic representation (3.42) onto the LCOPE result (3.46). We also use the quark hadron-duality approximation and perform a Borel transform. To extract $f_+^{B\to K}$, we select the part of the correlator proportional to $k^\mu k^\nu$, as one could easily guess looking at (3.42), while the Lorentz structure $q^\mu k^\nu$ gives us $f_+^{B\to K} + f_-^{B\to K}$. The sum rules for these form factors read [1, 112]

$$f_+^{B\to K} = \frac{m_B f_B}{f_K}\int_0^{\sigma(s_0,q^2)} e^{\frac{m_K^2 - s(\sigma,q^2)}{M^2}}\left[\frac{1}{\left(m_B^2\bar{\sigma}^2 + m_s^2 - q^2\right)^2}\Big(2m_B\bar{\sigma}\left(m_s^2-q^2\right)\bar{\phi} + \left(m_B^2\bar{\sigma}^2 + m_s^2 - q^2\right)\left(m_B^2\bar{\sigma}^2\phi_- + \left(m_s^2-q^2\right)\phi_+\right)\Big)\right], \quad (3.51)$$

$$f_+^{B\to K}+f_-^{B\to K}=\frac{m_B f_B}{f_K}\int_0^{\sigma(s_0,q^2)} e^{\frac{m_K^2-s(\sigma,q^2)}{M^2}}\Bigg[-\frac{1}{\bar\sigma\left(m_B^2\bar\sigma^2+m_s^2-q^2\right)^2}$$
$$\times m_B\Bigg(\left(-m_B^2\bar\sigma^2+m_B m_s\bar\sigma+(2\sigma-1)\left(m_s^2-q^2\right)\right)\left(2m_B\bar\sigma\bar\phi\right.$$
$$\left.+\phi_+\left(m_B^2\bar\sigma^2+m_s^2-q^2\right)\right)+m_B\bar\sigma\phi_-\left(m_B^2\bar\sigma^2+m_s^2-q^2\right)(2m_B\sigma\bar\sigma-m_s)\Bigg)\Bigg], \tag{3.52}$$

where the B-LCDAs are functions of $\omega\equiv\sigma m_B$ and

$$s(\sigma,q^2)=\sigma m_B^2+\frac{m_s^2-\sigma q^2}{\bar\sigma}\,,$$

with $\bar\sigma=1-\sigma$.

We can now evaluate numerically the sum rule (3.51) using the inputs listed in appendix C and the B-LCDAs models given in ref. [114]. At $q^2=0$ and obtain

$$f_+^{B\to K}=f_0^{B\to K}=0.35\pm0.08\,. \tag{3.53}$$

We conclude this subsection with a few remarks.

- The uncertainties are estimated in a similar fashion to the SVZ sum rules example of the previous subsection. However, here one also has to consider the errors due to the missing higher order corrections in the HQET expansion.
- The biggest uncertainties come from the parameters λ_B, λ_H^2 and λ_E^2, which appear in the explicit expressions of the B-LCDAs models. We discuss their values and uncertainties in appendix C. It is therefore crucial to have a more precise prediction of these quantities to improve the accuracy of the LCSRs with B-LCDAs.
- The prediction (3.53) differs from the one given in ref. [112], due to the fact that we neglect the three-particle contributions and we use different numerical inputs. Nevertheless, we fully reproduce the analytical results of ref. [112], and we will go beyond them in chapter 4.

***B*-meson LCSRs and Light-meson LCSRs** The sum rules presented above are commonly called B-meson LCSRs, since we started with a B-to-vacuum correlator and then we used the B-meson light-cone distribution amplitudes. Alternatively, one could also start with a correlator

$$\Pi^{\mu\nu}(q,k)\equiv i\int \mathrm{d}^4x\, e^{ik\cdot x}\,\langle M_{light}(q+k)|\,T\{J^\mu_{\rm weak}(x),J^\nu_{\rm int}(0)\}\,|0\rangle\ , \tag{3.54}$$

where M_{light} is a light meson, which is a meson that contains only light quarks (e.g. π, ρ, $K^{(*)}$, etc.). In this case, to compute the $B\to K$ for factors one has to choose

$$\begin{aligned} J^\mu_{\rm weak}&=\bar s\gamma^\mu b\,,\\ J^\nu_{\rm int}&=\bar b\gamma^\nu\gamma_5 s\,. \end{aligned} \tag{3.55}$$

The calculation is analogous to the B-meson LCSRs case, except for the fact that to obtain the hadronic representation, one has to interpolate states with different quantum numbers. Moreover, the non-perturbative inputs are the non-local M_{light}-to-vacuum matrix elements, which are parametrized in terms of light-meson light-cone distribution amplitudes (see e.g. refs. [66, 115, 116]).

Historically, the light-meson LCSRs were the first ones to be applied [100, 101], while the B-meson LCSRs were introduced several years later [111, 112]. In short, the B-meson LCSRs and light-meson LCSRs differ mostly for the inputs used, since these two methods are based on the same ideas. Notice that the $B \to D^{(*)}$ and $B_s \to D_s^{(*)}$ are not accessible with light-meson LCSRs, since both the intial-state meson and the final-state meson are heavy.

3.3 Dispersive Bounds

Dispersive bounds (or unitarity bounds) are upper bounds on the modulus squared of hadronic matrix elements. These bounds are derived using a dispersion relation and unitarity, hence the name. The ispersive bounds method is rather old and was originally applied to kaon decays [117–120], while in the nineties it was also applied to B-meson decays (see e.g. refs. [10, 121–125]). One of the main results of this thesis is the extension of the dispersive bounds method to the more general case where the energy of the first branch point, which we call t_+, does not coincide with the threshold of the matrix element considered, which we call t_H.

In this section, we review the dispersive bounds in the usual case where $t_+ = t_H$, before studying the case where $t_+ \neq t_H$ in section 4.2. In order to do this, we will show an example where we calculate the dispersive bounds for the local $B \to K$ matrix elements, i.e. for the $B \to K$ form factors.

We start with defining the correlator

$$\begin{aligned} \Pi^{\mu\nu}(q) &= i \int \mathrm{d}^4x \, e^{iq\cdot x} \, \langle 0| \, T\{J^\mu(x), J^{\nu,\dagger}(0)\} \, |0\rangle \\ &= (q^\mu q^\nu - q^2 g^{\mu\nu})\Pi_{1^-}(q^2) + q^\mu q^\nu \Pi_{0^+}(q^2) \,, \end{aligned} \tag{3.56}$$

where in this case[6]

$$J^\mu = \bar{s} \, \gamma^\mu b \,. \tag{3.57}$$

In analogy with the QCD sum rules, this correlator can be computed using an OPE for $m_b^2 - q^2 \gg \Lambda^2_{\mathrm{QCD}}$, while its imaginary part, which contributes at positive q^2, is given by unitarity relations.

We can then write down the dispersion relation

$$\Pi(q^2) = \frac{1}{\pi} \int_0^\infty \mathrm{d}s \, \frac{\mathrm{Im}\,\Pi(s)}{s - q^2} \tag{3.58}$$

and perform n subtractions, i.e. take the n-th order derivative with respect to q^2 of this equation, where n is the lowest order of the derivative that renders the l.h.s. finite. One can

[6] Notice that $\langle K(k)| \, \bar{s}\gamma^\mu\gamma_5 b \, |B(p)\rangle = 0$, and hence we do not consider the axial-vector current here.

show that Π_{0^+} needs only one subtraction, while Π_{1^-} needs two subtractions:

$$\begin{aligned}\chi_{0^+}(q^2) &= \frac{\partial}{\partial q^2}\left(q^2\Pi_{0^+}(q^2)\right) = \frac{1}{\pi}\int_0^\infty \mathrm{d}s\,\frac{s\,\operatorname{Im}\Pi_{0^+}(s)}{(s-q^2)^2}\,,\\ \chi_{0^+}(q^2) &= \frac{1}{2}\left(\frac{\partial}{\partial q^2}\right)^2\left(q^2\Pi_{1^-}(q^2)\right) = \frac{1}{\pi}\int_0^\infty \mathrm{d}s\,\frac{s\,\operatorname{Im}\Pi_{1^-}(s)}{(s-q^2)^3}\,.\end{aligned} \tag{3.59}$$

The leading order of the OPE at leading order in α_s is

$$\begin{aligned}\chi_{0^+}^{\mathrm{OPE}}(0) = \frac{1}{8\pi^2\left(m_b^2-m_s^2\right)^3}\Bigg(&12m_b^3m_s^3\log\left(\frac{m_b}{m_s}\right)\\ &+(m_b-m_s)(m_b+m_s)\left(m_b^2-4m_bm_s+m_s^2\right)\left(m_b^2+m_bm_s+m_s^2\right)\Bigg)\,,\end{aligned} \tag{3.60}$$

$$\begin{aligned}\chi_{1^-}^{\mathrm{OPE}}(0) = \frac{1}{32\pi^2\left(m_b^2-m_s^2\right)^5}\Bigg(&3m_b^8+4m_b^7m_s-24m_b^6m_s^2+36m_b^5m_s^3-36m_b^3m_s^5\\ &+24m_b^2m_s^6-24m_b^3m_s^3\left(2m_b^2-3m_bm_s+2m_s^2\right)\log\left(\frac{m_b}{m_s}\right)-4m_bm_s^7-3m_s^8\Bigg)\,.\end{aligned} \tag{3.61}$$

This result can be improved by including higher orders in α_s and in the OPE (see e.g. ref. [126]). The hadronic representation, as usual, can be easily obtained using unitarity relations, that is by inserting a complete set of states between the two currents

$$\begin{aligned}\operatorname{Im}\Pi^{\mu\nu}(q) &= (q^\mu q^\nu - q^2g^{\mu\nu})\operatorname{Im}\Pi_{1^-}(q^2) + q^\mu q^\nu \operatorname{Im}\Pi_{0^+}(q^2)\\ &= \frac{1}{2}\sum\!\!\!\!\!\!\int_H \mathrm{d}\tau_H\,(2\pi)^4\delta^{(4)}(p_H-q)\,\langle 0|J^\mu(0)|H\rangle\,\langle H|J^{\dagger,\nu}(0)|0\rangle\,,\end{aligned} \tag{3.62}$$

where the sum runs over all the states $H(p_H)$ with the allowed quantum numbers, and τ_H is the spectral density function.

The lowest energy states that arise in eq. (3.62) are $s\bar{b}$ bound states and resonances, i.e. the B_s meson and its exited states. Their contribution to the hadronic representation of the correlator can be written as

$$\frac{1}{\pi}\operatorname{Im}\Pi_{J^P}^{1\mathrm{p}}(q^2) = \sum_i f_{s\bar{b}(i,J^P)}^2\delta(q^2-m_{s\bar{b}(i,J^P)}^2)\,, \tag{3.63}$$

where the sum runs over all the $s\bar{b}(i,J^P)$ bound states whose masses and decay constants are known, and hence their contribution can be included in the bounds. In this case there is only one bound state per spin-parity channel: the B_s for $J^P=0^-$ and the B_s^* for $J^P=1^-$.

The first two-particle state that appears in eq. (3.62) is $H=BK$. Using crossing symmetry, it is possible to express the matrix element $\langle 0|J^\mu(0)|BK\rangle$ in terms of the $B\to K$ form factors:

$$\langle 0|\,\bar{s}\gamma^\mu b\,|B(p)\bar{K}(-k)\rangle = \langle K(k)|\,\bar{s}\gamma^\mu b\,|B(p)\rangle\,.$$

Notice that, even though the physical range of the form factors is from $q^2 = 0$ to $q^2 = (m_B - m_K)^2$, they can be analytically continued in the whole complex plane, where they are analytic except for the branch cut on the positive real axis starting at $q^2 = (m_B + m_K)^2$. Using the definition of the $B \to K$ form factors given in eq. (3.33), the imaginary part of $\Pi_{J^P}^{BK}$ reads

$$\begin{aligned}
\frac{1}{\pi}\,\mathrm{Im}\,\Pi_{0^+}^{BK}(q^2) &= \frac{(m_B^2 - m_K^2)^2 \lambda^{\frac{1}{2}}}{16\pi^2 (q^2)^3} |f_0^{B\to K}|^2\, \theta(q^2 - (m_B + m_K)^2)\,, \\
\frac{1}{\pi}\,\mathrm{Im}\,\Pi_{1^-}^{BK}(q^2) &= \frac{\lambda^{\frac{3}{2}}}{48\pi^2 (q^2)^3} |f_+^{B\to K}|^2\, \theta(q^2 - (m_B + m_K)^2)\,,
\end{aligned} \tag{3.64}$$

where $\lambda \equiv \lambda(m_B^2, m_K^2, q^2)$ is the Källén function, defined as

$$\lambda(a,b,c) \equiv a^2 + b^2 + c^2 - 2ab - 2bc - 2ac\,. \tag{3.65}$$

The definition of the $B \to K$ form factors (3.33) is motivated by the fact that the correlator can be written as a sum of form factors squared. Thus, we say that the definition (3.33) "diagonalizes" the hadronic representation of the correlator. This not true in general, since the alternative definition of the $B \to K$ form factor (3.35) does not diagonalize the hadronic representation of the correlator:

$$\begin{aligned}
\frac{1}{\pi}\,\mathrm{Im}\,\Pi_{0^+}^{BK}(q^2) = \theta(q^2 - (m_B + m_K)^2)\, \frac{\lambda^{\frac{1}{2}}}{16\pi^2 (q^2)^3} \\
\left((m_B^2 - m_K^2)^4 |f_+^{B\to K}|^2 + (q^2)^2 |f_-^{B\to K}|^2 + 2q^2 (m_B^2 - m_K^2)^2\, \mathrm{Re}\left\{ f_+^{B\to K} f_-^{B\to K} \right\} \right).
\end{aligned}$$

Plugging the OPE results (3.60)-(3.61) and the hadronic representations (3.64) into the subtracted dispersion relations (3.59), we finally obtain the dispersive bounds

$$\chi_{J^P}^{\mathrm{OPE}}(0) > \sum_i \frac{f^2_{s\bar{b}(i,J^P)}}{(m^2_{s\bar{b}(i,J^P)})^n} + \frac{1}{\pi} \int_{t_{BK}}^{\infty} \mathrm{d}s\, \frac{\mathrm{Im}\,\Pi_{J^P}^{BK}(s)}{s^{n-1}}\,, \tag{3.66}$$

where $t_{BK} \equiv (m_B + m_K)^2$ and n is the number of subtractions required. For simplicity, we have chosen $q^2 = 0$, even though selecting a large negative q^2 value would improve the convergence of the OPE [10]. The dispersive bounds can be made more constraining including further hadronic states in the hadronic representation of the correlator (e.g. $H = BK$, BK^*, B^*K, $\Lambda_b\Lambda$), which would give a positive contribution to the r.h.s. of (3.66). Indeed, the higher the number of states considered, the closer the inequality (3.66) gets to saturation.

Usually the dispersive bounds (3.66) are used to constrain the form factors, after calculating $\chi_{J^P}^{\mathrm{OPE}}$. The decay constants and the masses of the $s\bar{b}$ resonances of eq. (3.63) can be taken from experimental data or lattice QCD calculations.

Dispersive bounds are also particularly useful to constrain the parameters of the so-called z-expansion. Let us first introduce the map

$$z = \frac{\sqrt{t_+ - q^2} - \sqrt{t_+ - t_0}}{\sqrt{t_+ - q^2} + \sqrt{t_+ - t_0}}\,, \tag{3.67}$$

where t^+ is the branch point with the lowest energy and t_0 can be arbitrarily chosen in the open interval $(-\infty, t^+]$. In this case we have $t_+ = t_{BK} = (m_B + m_K)^2$, since the branch cut stating at $q^2 = (m_{B_s} + m_\pi)^2$ can be neglected due to its isospin suppression. We study in detail in section 4.2 the case where t_+ does not coincide with the lower bound of the integral in (3.66). As we will see this has important implications for the formalism that we are going to present. The choice of t_0 determines what q^2 point is mapped onto the origin of the z plane. In practice, t_0 is usually chosen in the interval from 0 to $t_0 = (m_B - m_K)^2$, because it minimises the magnitude of z in the phenomenologically relevant region for the form factors.

After this mapping, eq. (3.66) becomes

$$\tilde{\chi}^{\rm OPE}_{J^P}(0) > \frac{1}{\pi} \oint\limits_{|z|=1} \mathrm{d}z \, \frac{\mathrm{d}s(z)}{\mathrm{d}z} \, \frac{\mathrm{Im}\,\Pi^{BK}_{J^P}(z)}{(s(z))^{n-1}} \,, \tag{3.68}$$

where

$$\tilde{\chi}^{\rm OPE}_{J^P}(0) \equiv \chi^{\rm OPE}_{J^P}(0) - \sum_i \frac{f^2_{s\bar{b}(i,J^P)}}{(m^2_{s\bar{b}(i,J^P)})^n} \,. \tag{3.69}$$

The integral between t_{BK} and ∞ in the q^2 plane is mapped onto the integral over the unit circle in the z plane. As we have already discussed, the function $\Pi^{BK}_{J^P}(q^2)$ has a branch cut on the real positive axis starting at the branch point $q^2 = t_+$. The first Riemann sheet of $\Pi^{BK}_{J^P}(q^2)$ is mapped into the unit disk centred in $z = 0$, while the second Riemann sheet is mapped into the exterior of this unit disk.

Expressing the integral of eq. (3.68) in polar coordinates and employing eqs. (3.64), one obtains

$$\begin{aligned} 1 &> \int_0^{2\pi} \mathrm{d}\alpha \, |\phi_0(s)|^2 \, |f_0^{B\to K}(s)|^2 \Big|_{s\equiv s(z(\alpha))} \,, \\ 1 &> \int_0^{2\pi} \mathrm{d}\alpha \, |\phi_+(s)|^2 \, |f_+^{B\to K}(s)|^2 \Big|_{s\equiv s(z(\alpha))} \,, \end{aligned} \tag{3.70}$$

where

$$\begin{aligned} |\phi_0(s)|^2 &= \frac{1}{2} \frac{1}{\tilde{\chi}^{\rm OPE}_{0^+}(0)} \frac{\mathrm{d}z(\alpha)}{\mathrm{d}\alpha} \frac{\mathrm{d}s}{\mathrm{d}z} \frac{(m_B^2 - m_K^2)^2 \lambda^{\frac{1}{2}}}{16\pi^2 s^4} \Big|_{s\equiv s(z(\alpha))} \,, \\ |\phi_+(s)|^2 &= \frac{1}{2} \frac{1}{\tilde{\chi}^{\rm OPE}_{1^-}(0)} \frac{\mathrm{d}z(\alpha)}{\mathrm{d}\alpha} \frac{\mathrm{d}s}{\mathrm{d}z} \frac{\lambda^{\frac{3}{2}}}{48\pi^2 s^5} \Big|_{s\equiv s(z(\alpha))} \,. \end{aligned} \tag{3.71}$$

The functions ϕ_j are usually called the *outer functions*. It is important to stress that the modulus squared $|\phi_j|^2$ has, in general, kinematical singularities (e.g. the outer functions considered in this example have a pole at $s = 0$), but the outer functions can (and should) be defined such that they are not singular inside the unit disk and on the integration contour, i.e. the unit circle.

Besides these kinematical singularities, one also has to remove the dynamical singularities of the hadronic matrix elements that appear in the dispersion relation. In fact, the form

factors have poles due to $s\bar{b}$ resonances below the branch cut. To remove them, it is sufficient to multiply each form factor $f_j^{B\to K}$ by the so-called Blaschke factors

$$\mathcal{B}_{J^P} \equiv \prod_i \frac{z - z_{i,J^P}}{1 - z z_{i,J^P}}\,, \tag{3.72}$$

which have zeros at the positions of such poles and have the modulus squared equal to one. Here $z_{i,J^P} = z(s = m^2_{s\bar{b}(i,J^P)})$ is the location of the $s\bar{b}$ poles inside the unit disk. We can now define the function

$$\hat{f}_j^{B\to K}(z) \equiv \phi_j(z)\mathcal{B}_{J^P}(z) f_j^{B\to K}(z)\,, \tag{3.73}$$

which is analytic inside the unit disk. Being analytic, $\hat{f}_j^{B\to K}(z)$ can be Taylor expanded around $z = 0$:

$$\hat{f}_j^{B\to K}(z) = \sum_{k=0}^{\infty} a_{j,k} z^k\,. \tag{3.74}$$

Even though this series is convergent (at least inside the unit disk), it is not possible to estimate the error that arises from cutting the series at some finite order. This is where the dispersive bounds in the form (3.70) come into play. Using the fact that the positive powers of z form an orthonormal basis on the unit circle, we can plug eq. (3.74) into (3.70) obtaining

$$\begin{aligned} \sum_{k=0}^{\infty} |a_{+,k}|^2 < 1\,, \\ \sum_{k=0}^{\infty} |a_{0,k}|^2 < 1\,. \end{aligned} \tag{3.75}$$

In the case where more form factors appear in the same spin parity channel, one also has to sum over the different form factors.

In this section, we have shown how the dispersive bounds allow to put an upper bound on the size of higher order terms in the Taylor series (3.74), when one cuts it at some finite order. Considering the first two or three terms of the series is usually sufficient for most of the applications (see e.g. ref. [126]).

The dispersive bounds (3.75) are commonly known as *weak dispersive bounds*, to distinguish them from the *strong dispersive bounds* proposed in ref. [10], where also HQET is exploited to connect the various spin parity channels (see ref. [52]). In this work, we employ both the weak dispersive bounds in the general case where $t_+ \neq t_H$ and the strong dispersive bounds to constrain the $B_{(s)} \to D_{(s)}^{(*)}$ form factors.

Chapter 4

New Results for Hadronic Matrix Elements and Phenomenological Implications

In this last chapter we present our results, both the ones that are already published [1, 2] and those that are not public yet [3]. We begin with our new analytical results for the LCSRs to calculate the meson form factors and the soft-gluon contribution to the charm-loop in $B \to K^{(*)}\ell\ell$. Next, we evaluate numerically our LCSRs, to obtain predictions for the corresponding matrix elements. We then formulate dispersive bounds for the case where non-negligible subthreshold branch cuts appear. Finally, we extrapolate the form factors in the whole physically allowed region and study the phenomenological implications of our results, focusing on the predictions of observables in $B_{(s)} \to D_{(s)}^{(*)}$ decays.

4.1 Light-Cone Sum Rules beyond Leading Twist

The light-cone sum rules (LCSRs) allow to calculate both local and non-local hadronic matrix elements for small values of the momentum transfer q^2. On the other hand, lattice QCD can precisely predict local hadronic matrix elements, especially for large q^2 values, while the computation of non-local hadronic matrix elements is still under study.

In one of our publications [1] and in an ongoing project [3], we revisit the LCSRs to calculate the form factors (local hadronic matrix elements) in B-meson decays and the soft-gluon contribution to the charm loop (non-local hadronic matrix elements) in $B \to K^{(*)}\ell\ell$ decays. These LCSRs were originally presented in refs. [14, 112, 127], however, the new results on the B-meson distribution amplitudes (B-LCDAs) of ref. [114] triggered our interest in recalculating them. The main improvement carried out in ref. [114] regards the three-particle B-LCDAs, since their complete set as well as their models up to twist four are given for the first time. The two-particle B-LCDAs, which were previously known up to twist three, are extended up to twist four as well.

As will show subsection 4.1.3 and in subsection 4.1.4, these improvements have an important impact on the numerical results, reducing of $\sim 20 - 30\%$ the form factors central values and making the soft-gluon contribution to the non-local hadronic matrix one order of magnitude smaller.

process	J^ν_{int}	J^μ_{weak}	form factor
$\bar{B}^0 \to \pi^+$	$\bar{d}\gamma^\nu\gamma_5 u$	$\bar{u}\gamma^\mu h_v$	$f_+^{B\to\pi}$, $f_{+/-}^{B\to\pi}$
		$\bar{u}\sigma^{\mu\{q\}} h_v$	$f_T^{B\to\pi}$
$\bar{B}^0 \to \bar{K}^0$	$\bar{d}\gamma^\nu\gamma_5 s$	$\bar{s}\gamma^\mu h_v$	$f_+^{B\to K}$, $f_{+/-}^{B\to K}$
		$\bar{s}\sigma^{\mu\{q\}} h_v$	$f_T^{B\to K}$
$\bar{B}^0 \to D^+$	$\bar{d}\gamma^\nu\gamma_5 c$	$\bar{c}\gamma^\mu h_v$	$f_+^{B\to D}$, $f_{+/-}^{B\to D}$
		$\bar{c}\sigma^{\mu\{q\}} h_v$	$f_T^{B\to D}$
$\bar{B}_s^0 \to K^+$	$\bar{s}\gamma^\nu\gamma_5 u$	$\bar{u}\gamma^\mu h_v$	$f_+^{B\to K}$, $f_{+/-}^{B\to K}$
		$\bar{u}\sigma^{\mu\{q\}} h_v$	$f_T^{B\to K}$
$\bar{B}_s^0 \to D_s^+$	$\bar{s}\gamma^\nu\gamma_5 c$	$\bar{c}\gamma^\mu h_v$	$f_+^{B\to D_s}$, $f_{+/-}^{B\to D_s}$
		$\bar{c}\sigma^{\mu\{q\}} h_v$	$f_T^{B\to D_s}$
$\bar{B}^0 \to \rho^+$	$\bar{d}\gamma^\nu u$	$\bar{u}\gamma^\mu h_v$	$V^{B\to\rho}$
		$\bar{u}\gamma^\mu\gamma_5 h_v$	$A_0^{B\to\rho}$, $A_1^{B\to\rho}$, $A_2^{B\to\rho}$
		$\bar{u}\sigma^{\mu\{q\}} h_v$	$T_1^{B\to\rho}$
		$\bar{u}\sigma^{\mu\{q\}}\gamma_5 h_v$	$T_2^{B\to\rho}, T_3^{B\to\rho}$
$\bar{B}^0 \to \bar{K}^{*0}$	$\bar{d}\gamma^\nu s$	$\bar{s}\gamma^\mu h_v$	$V^{B\to K^*}$
		$\bar{s}\gamma^\mu\gamma_5 h_v$	$A_0^{B\to K^*}$, $A_1^{B\to K^*}$, $A_2^{B\to K^*}$
		$\bar{s}\sigma^{\mu\{q\}} h_v$	$T_1^{B\to K^*}$
		$\bar{s}\sigma^{\mu\{q\}}\gamma_5 h_v$	$T_2^{B\to K^*}, T_3^{B\to K^*}$
$\bar{B}^0 \to D^{*+}$	$\bar{d}\gamma^\nu c$	$\bar{c}\gamma^\mu h_v$	$V^{B\to D^*}$
		$\bar{c}\gamma^\mu\gamma_5 h_v$	$A_0^{B\to D^*}$, $A_1^{B\to D^*}$, $A_2^{B\to D^*}$
		$\bar{c}\sigma^{\mu\{q\}} h_v$	$T_1^{B\to D^*}$
		$\bar{c}\sigma^{\mu\{q\}}\gamma_5 h_v$	$T_2^{B\to D^*}, T_3^{B\to D^*}$
$\bar{B}_s^0 \to K^+$	$\bar{s}\gamma^\nu u$	$\bar{u}\gamma^\mu h_v$	$V^{B\to K^*}$
		$\bar{u}\gamma^\mu\gamma_5 h_v$	$A_0^{B\to K^*}$, $A_1^{B\to K^*}$, $A_2^{B\to K^*}$
		$\bar{u}\sigma^{\mu\{q\}} h_v$	$T_1^{B\to K^*}$
		$\bar{u}\sigma^{\mu\{q\}}\gamma_5 h_v$	$T_2^{B\to K^*}, T_3^{B\to K^*}$
$\bar{B}_s^0 \to \phi$	$\bar{s}\gamma^\nu s$	$\bar{s}\gamma^\mu h_v$	$V^{B\to\phi}$
		$\bar{s}\gamma^\mu\gamma_5 h_v$	$A_0^{B\to\phi}$, $A_1^{B\to\phi}$, $A_2^{B\to\phi}$
		$\bar{s}\sigma^{\mu\{q\}} h_v$	$T_1^{B\to\phi}$
		$\bar{s}\sigma^{\mu\{q\}}\gamma_5 h_v$	$T_2^{B\to\phi}, T_3^{B\to\phi}$
$\bar{B}_s^0 \to D_s^{*+}$	$\bar{s}\gamma^\nu c$	$\bar{c}\gamma^\mu h_v$	$V^{B\to D_s^*}$
		$\bar{c}\gamma^\mu\gamma_5 h_v$	$A_0^{B\to D_s^*}$, $A_1^{B\to D_s^*}$, $A_2^{B\to D_s^*}$
		$\bar{c}\sigma^{\mu\{q\}} h_v$	$T_1^{B\to D_s^*}$
		$\bar{c}\sigma^{\mu\{q\}}\gamma_5 h_v$	$T_2^{B\to D_s^*}, T_3^{B\to D_s^*}$

Table 4.1: List of the processes for which we determine the form factors. The currents J^ν_{int} and J^μ_{weak} are listed as well. We abbreviate $\sigma^{\mu\{q\}} \equiv \sigma^{\mu\nu}q_\nu$.

4.1.1 Analytical Results for the Form Factor LCSRs

In subsection 3.2.2 we computed the $B \to K$ form factors using a LCSR. In that introductory example we considered only the two-particle contributions up to twist three, while we neglected the three-particle contributions. Here, we both include the twist four two-particle contributions and the full set of three-particle B-LCDAs for the transitions listed in table 4.1.

As usual, the first step to compute a sum rule is to define a correlator so that we can extract the desired matrix elements. In this case, we define

$$\Pi^{\mu\nu}(q,k) \equiv i \int \mathrm{d}^4x\, e^{ik\cdot x}\, \langle 0|\, T\{J^{\nu}_{\text{int}}(x), J^{\mu}_{\text{weak}}(0)\}\, |\bar{B}_{q_2}(q+k)\rangle\ , \tag{4.1}$$

where $J^{\nu}_{\text{int}} \equiv \bar{q}_2\Gamma^{\nu}_2 q_1$ and $J^{\mu}_{\text{weak}} \equiv \bar{q}_1\Gamma^{\mu}_1 h_v$. The explicit form of these quark currents for the considered transitions is given in table 4.1. By inserting a complete set of hadronic states in the correlator (4.1) we obtain the hadronic dispersion relation

$$\Pi^{\mu\nu}(q,k) = \frac{\langle 0|\, J^{\nu}_{\text{int}}(x)\, |M(k)\rangle\, \langle M(k)|\, J^{\mu}_{\text{weak}}(0)\, |\bar{B}_{q_2}(q+k)\rangle}{m_M^2 - k^2} + \frac{1}{\pi}\int_{s_h}^{\infty} \mathrm{d}s \frac{\tau^{\mu\nu}(s)}{s-k^2}\,. \tag{4.2}$$

Here, $\tau^{\mu\nu}(s)$ is the spectral density function, which encodes the information about the continuum as well as the exited states, and s_h is the continuum states threshold. The local hadronic matrix elements in eq. (4.2) can be expressed in terms of decay constants and form factors using the following definitions:

$$\langle 0|\, \bar{q}_2\gamma^{\nu}\gamma_5 q_1\, |P(k)\rangle = ik^{\nu} f_P\,, \tag{4.3}$$

$$\langle 0|\, \bar{q}_2\gamma^{\nu} q_1\, |V(k,\eta)\rangle = i\eta^{\nu} m_V f_V\,, \tag{4.4}$$

$$\begin{aligned}\langle P(k)|\, \bar{q}_1\gamma^{\mu} b\, |B(p)\rangle &= \left[(p+k)^{\mu} - \frac{m_B^2 - m_P^2}{q^2} q^{\mu}\right] f_+^{B\to P} \\ &\quad + \frac{m_B^2 - m_P^2}{q^2} q^{\mu}\, f_0^{B\to P},\end{aligned} \tag{4.5}$$

$$\langle P(k)|\, \bar{q}_1\sigma^{\mu\nu}\, q_{\nu} b\, |B(p)\rangle = \frac{i f_T^{B\to P}}{m_B + m_P}\, \left[q^2\,(p+k)^{\mu} - (m_B^2 - m_P^2)\, q^{\mu}\right]\,, \tag{4.6}$$

$$\langle V(k,\eta)|\, \bar{q}_1\gamma^{\mu} b\, |B(p)\rangle = \epsilon^{\mu\nu\rho\sigma}\eta^*_{\nu} p_{\rho} k_{\sigma} \frac{2V^{B\to V}}{m_B + m_V}\,, \tag{4.7}$$

$$\begin{aligned}\langle V(k,\eta)|\, \bar{q}_1\gamma^{\mu}\gamma_5 b\, |B(p)\rangle &= i\eta^*_{\nu}\, \Bigg[g^{\mu\nu}(m_B + m_V) A_1^{B\to V} - \frac{(p+k)^{\mu} q^{\nu}}{m_B + m_V}\, A_2^{B\to V} \\ &\quad - q^{\mu} q^{\nu} \frac{2m_V}{q^2}\left(A_3^{B\to V} - A_0^{B\to V}\right)\Bigg]\,,\end{aligned} \tag{4.8}$$

$$\langle V(k,\eta)|\, \bar{q}_1 i\sigma^{\mu\nu}\, q_{\nu} b\, |B(p)\rangle = 2\epsilon^{\mu\nu\rho\sigma}\eta^*_{\nu} p_{\rho} k_{\sigma} T_1^{B\to V}\,, \tag{4.9}$$

$$\begin{aligned}\langle V(k,\eta)|\, \bar{q}_1 i\sigma^{\mu\nu}\, q_{\nu}\gamma_5 b\, |B(p)\rangle &= i\eta^*_{\nu}\Bigg[\left(g^{\mu\nu}(m_B^2 - m_V^2) - (p+k)^{\mu} q^{\nu}\right) T_2^{B\to V} \\ &\quad + q^{\nu}\left(q^{\mu} - \frac{q^2}{m_B^2 - m_V^2}(p+k)^{\mu}\right) T_3^{B\to V}\Bigg]\,.\end{aligned} \tag{4.10}$$

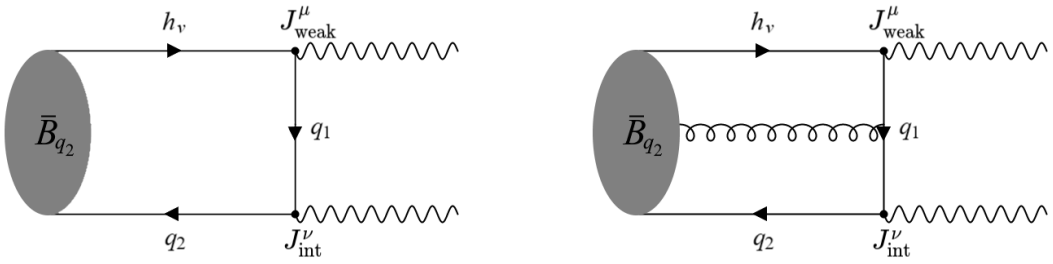

(a) (b)

Figure 4.1: The two- and the three-particle contributions to the correlator.

Here P denotes a pseudoscalar meson and V denotes a vector meson with polarisation vector η_ν. The momentum transfer is defined as $q_\mu \equiv p_\mu - k_\mu$. In eq. (4.9), the form factor $A_3^{B\to V}$ is redundant, since it can be expressed in terms of $A_1^{B\to V}$ and $A_2^{B\to V}$ as[1]

$$A_3^{B\to V} = \frac{m_B + m_V}{2m_V} A_1^{B\to V} - \frac{m_B - m_V}{2m_V} A_2^{B\to V} \,. \tag{4.11}$$

Having obtained the hadronic dispersion relation, we now need to perform a light-cone OPE (LCOPE) of the correlator (4.1). As in subsection 3.2.2, we first expand the correlator in HQET and then for light-cone distances $x^2 \sim 0$. In momentum space, the light-cone expansion can be applied for [91, 112]

$$q^2 < m_b \left(m_b + \frac{k^2}{\bar{\Lambda}} \right) , \tag{4.12}$$

with $-k^2$, $-q_{res}^2 \gg \Lambda_{\text{QCD}}$ and $q^\mu = m_b v^\mu + q_{res}^\mu$. Retaining terms up to next-to-leading order in the LCOPE, we obtain

$$\begin{aligned}\Pi^{\mu\nu}(q,k) = &\int \mathrm{d}^4x \int \mathrm{d}^4p' \, e^{i(k-p')\cdot x} \left[\Gamma_2^\nu \frac{\not{p}' + m_1}{m_1^2 - p'^2} \Gamma_1^\mu \right]_{\alpha\beta} \langle 0| \, \bar{q}_2^\alpha(x) h_v^\beta(0) \, |\bar{B}_{q_2}(v)\rangle \\ &+ \int \mathrm{d}^4x \int \mathrm{d}^4p' \int_0^1 \mathrm{d}u \, e^{i(k-p')\cdot x} \left[\Gamma_2^\nu \frac{(1-u)(\not{p}' + m_1)\sigma^{\lambda\rho} + u\sigma^{\lambda\rho}(\not{p}' + m_1)}{2(p'^2 - m_1^2)^2} \Gamma_1^\mu \right]_{\alpha\beta} \\ &\times \langle 0| \, \bar{q}_2^\alpha(x) g_s \mathbf{G}_{\lambda\rho}(ux) h_v^\beta(0) \, |\bar{B}_{q_2}(v)\rangle \,, \end{aligned} \tag{4.13}$$

which are the two- and the three-particle contributions to the correlator, respectively. These two contributions are illustrated schematically in figure 4.1. In eq. (4.13), α and β are spinor indices, and m_1 is the mass of the virtual quark q_1. We do not include α_s corrections to the hard-scattering kernel, which have only been considered in the framework of SCET LC-SRs [128–131] so far. The calculation of the α_s corrections in our framework is left for a future work.

The non-local B-to-vacuum matrix elements of eq. (4.13) can be expressed in terms of B-LCDAs. In eq. (3.49), we parametrized the two-particle B-to-vacuum matrix element in

[1] See appendix B for a more detailed discussion of the form factors and the derivation of eq. (4.11).

the limit $x^2 = 0$. If x^2 is non-zero but still small (i.e. $|x^2| \ll 1/\Lambda_{\rm QCD}$), off-light-contributions arise in the form

$$\phi(v\cdot x) \to \phi(v\cdot x) + x^2 g(v\cdot x) + \mathcal{O}\left(x^4\right) \tag{4.14}$$

in position space. Including $\mathcal{O}\left(x^2\right)$, eq. (3.49) becomes [114]

$$\begin{aligned}\langle 0|\, \bar{q}_2^\alpha(x) h_v^\beta(0)\, |\bar{B}(v)\rangle =& \\ &-\frac{i f_B m_B}{4}\int_0^\infty \mathrm{d}\omega\, e^{-i\omega v\cdot x}\Big\{(1+\not{v})\Big[\phi_+(\omega) - g_+(\omega)\partial_\sigma\partial^\sigma \\ &\qquad + \left(\frac{\bar{\phi}(\omega)}{2} - \frac{\bar{g}(\omega)}{2}\partial_\sigma\partial^\sigma\right)\gamma^\mu\partial_\mu\Big]\gamma_5\Big\}^{\beta\alpha}\end{aligned} \tag{4.15}$$

in momentum space. Here, we have abbreviated

$$\begin{aligned}\bar{\phi}(\omega) &\equiv \int_0^\omega \mathrm{d}\eta\ (\phi_+(\eta) - \phi_-(\eta))\ , \\ \bar{g}(\omega) &\equiv \int_0^\omega \mathrm{d}\eta\ (g_+(\eta) - g_-(\eta))\ .\end{aligned} \tag{4.16}$$

The derivative $\partial_\mu \equiv \partial/\partial l^\mu$, with $l^\mu = \omega v^\mu$, is understood to act on the hard-scattering kernel. Since $\phi_+(\omega)$ and $\phi_-(\omega)$ are twist two and three, respectively (see subsection 3.2.2), eq. (4.14) implies that $g_+(\omega)$ and $g_-(\omega)$ are twist four and five.

Although models for B-LCDAs are known up to twist four and $g_-(\omega)$ is a genuine twist five contribution, we include it in our results using the Wandzura-Wilcek approximation. This approximation consists in neglecting the three-particle contributions in the equation of motion of $g_-(\omega)$, which is given in ref. [114], and it allows to express $g_-(\omega)$ in terms of $\phi_+(\omega)$ and $\phi_-(\omega)$. It is important to include the contribution of $g_-(\omega)$ because is expected to be of the same order of magnitude of $g_+(\omega)$. In fact, the twist suppression occurs every two units of twist, as one can infer from eq. (4.14), where higher twists are suppressed by additional powers of $\Lambda_{\rm QCD}/m_b$. Moreover, these contributions of $g_+(\omega)$ and $g_-(\omega)$ partially cancel each other, as one can see from eq. (4.16). This reduces the impact of the off-light-cone corrections. We will explicitly observe this cancellation in the next subsection, where we present the numerical results for the individual contributions of the two-particle B-LCDAs in table 4.2.

The complete decomposition of the three-particle non-local B-to-vacuum matrix element in independent Lorentz structures reads [114]

$$\begin{aligned}&\langle 0|\bar{q}_2^\alpha(x) g_s \mathbf{G}_{\mu\nu}(ux) h_v^\beta(0)\, |\bar{B}_{q_2}(v)\rangle = \\ &=\frac{f_B m_B}{4}\int_0^\infty \mathrm{d}\omega_1 \int_0^\infty \mathrm{d}\omega_2\, e^{-i(\omega_1+u\omega_2)\, v\cdot x}\Big\{(1+\not{v})\Big[(v_\mu\gamma_\nu - v_\nu\gamma_\mu)[\psi_A - \psi_V] - i\sigma_{\mu\nu}\psi_V \\ &\quad + (\partial_\mu v_\nu - \partial_\nu v_\mu)\overline{X}_A - (\partial_\mu\gamma_\nu - \partial_\nu\gamma_\mu)[\overline{W} + \overline{Y}_A] + i\epsilon_{\mu\nu\alpha\beta}\partial^\alpha v^\beta\gamma_5\overline{\tilde{X}}_A \\ &\quad - i\epsilon_{\mu\nu\alpha\beta}\partial^\alpha\gamma^\beta\gamma_5\overline{\tilde{Y}}_A - u(\partial_\mu v_\nu - \partial_\nu v_\mu)\not{\partial}\overline{\overline{W}} + u(\partial_\mu\gamma_\nu - \partial_\nu\gamma_\mu)\not{\partial}\overline{\overline{Z}}\Big]\gamma_5\Big\}^{\beta\alpha}(\omega_1,\omega_2)\,.\end{aligned} \tag{4.17}$$

Here, a gauge link is implied between the fields, and the derivatives are abbreviated as $\partial_\mu \equiv \partial/\partial l^\mu$, with $l^\mu = (\omega_1 + u\omega_2)v^\mu$. Throughout, these derivatives are understood to act only on the hard-scattering kernel. In addition, we used the following shorthand notation

$$\begin{aligned}\overline{\psi}_{3\mathrm{p}}(\omega_1,\omega_2) &\equiv \int_0^{\omega_1} \mathrm{d}\eta_1\, \psi_{3\mathrm{p}}(\eta_1,\omega_2)\,,\\ \overline{\overline{\psi}}_{3\mathrm{p}}(\omega_1,\omega_2) &\equiv \int_0^{\omega_1} \mathrm{d}\eta_1 \int_0^{\omega_2} \mathrm{d}\eta_2\, \psi_{3\mathrm{p}}(\eta_1,\eta_2)\,,\end{aligned} \tag{4.18}$$

where $\psi_{3\mathrm{p}}$ represents any of the three-particle B-LCDAs.

The B-LCDAs of eq. (4.17) do not have definite twist. However, in ref. [114] a basis of three-particle B-LCDAs with definite twist was introduced, and they relate to the ones of eq. (4.17) as

$$\begin{aligned}\phi_3(\omega_1,\omega_2) &= [\psi_A - \psi_V](\omega_1,\omega_2)\,,\\ \phi_4(\omega_1,\omega_2) &= [\psi_A + \psi_V](\omega_1,\omega_2)\,,\\ \psi_4(\omega_1,\omega_2) &= [\psi_A + X_A](\omega_1,\omega_2)\,,\\ \chi_4(\omega_1,\omega_2) &= [\psi_V - \tilde{X}_A](\omega_1,\omega_2)\,,\\ \tilde{\phi}_5(\omega_1,\omega_2) &= [\psi_A + \psi_V + 2Y_A - 2\tilde{Y}_A + 2W](\omega_1,\omega_2)\,,\\ \psi_5(\omega_1,\omega_2) &= [-\psi_A + X_A - 2Y_A](\omega_1,\omega_2)\,,\\ \chi_5(\omega_1,\omega_2) &= [-\psi_V - \tilde{X}_A + 2\tilde{Y}_A](\omega_1,\omega_2)\,,\\ \phi_6(\omega_1,\omega_2) &= [\psi_A - \psi_V + 2Y_A + 2\tilde{Y}_A + 2W - 4Z](\omega_1,\omega_2)\,,\end{aligned} \tag{4.19}$$

where the subscripts 3, 4, 5, 6 indicate the twist of the respective B-LCDA. Note that we adopt the same nomenclature for the LCDAs as in ref. [114], except for renaming $\tilde{\psi}_{4,5} \to \chi_{4,5}$. Inverting the relations (4.19), we obtain

$$\begin{aligned}\psi_A &= \frac{1}{2}\,[\phi_3 + \phi_4](\omega_1,\omega_2)\,,\\ \psi_V &= \frac{1}{2}\,[-\phi_3 + \phi_4](\omega_1,\omega_2)\,,\\ X_A &= \frac{1}{2}\,[-\phi_3 - \phi_4 + 2\psi_4](\omega_1,\omega_2)\,,\\ Y_A &= \frac{1}{2}\,[-\phi_3 - \phi_4 + \psi_4 - \psi_5](\omega_1,\omega_2)\,,\\ \tilde{X}_A &= \frac{1}{2}\,[-\phi_3 + \phi_4 - 2\chi_4](\omega_1,\omega_2)\,,\\ \tilde{Y}_A &= \frac{1}{2}\,[-\phi_3 + \phi_4 - \chi_4 + \chi_5](\omega_1,\omega_2)\,,\\ W &= \frac{1}{2}\,[\phi_4 - \psi_4 - \chi_4 + \tilde{\phi}_5 + \psi_5 + \chi_5](\omega_1,\omega_2)\,,\\ Z &= \frac{1}{4}\,[-\phi_3 + \phi_4 - 2\chi_4 + \tilde{\phi}_5 + 2\chi_5 - \phi_6](\omega_1,\omega_2)\,.\end{aligned} \tag{4.20}$$

These equalities can be plugged in eq. (4.17), allowing us to compute the three-particle contributions in a sum rule for each level of twist.

In order to evaluate a LCSR numerically, one needs to model the B-LCDAs. The modelling of the B-LCDAs is a broad topic, which has been extensively discussed in the literature (see e.g. refs. [114, 132–134]). Here, we just want to point out that this model dependence is negligible compared to the parametric uncertainties that presently enter into a LCSR [135]. For our numerical evaluations we use the "Model I: Exponential" for B-LCDAs up to twist four given in ref. [114].

Notice also that the three-particle B-LCDA with the lowest twist is ϕ_3, which has twist three. Hence, we do not need to take into account the off-light-cone three-particle contributions, since they only start at twist five. We emphasise that there are eight independent three-particle B-LCDAs, as pointed out in ref. [114], while in refs. [14, 112, 127] a basis with only four B-LCDAs is used. This is particularly important in the calculation of soft-gluon contribution to the charm loop (see the next subsection), where the leading contribution in the LCOPE comes from the three-particle B-LCDAs, while the two-particle contribution is absent.

We can now match the hadronic representation of the correlator (4.2) onto the LCOPE result (4.13) using a dispersion relation:

$$\begin{aligned}
&\frac{\langle 0|\, J^{\nu}_{\text{int}}(x)\,|M(k)\rangle\,\langle M(k)|\, J^{\mu}_{\text{weak}}(0)\,|\bar{B}_{q_2}(q+k)\rangle}{m_M^2-k^2}+\frac{1}{\pi}\int_{s_h}^{\infty}\mathrm{d}s\frac{\tau^{\mu\nu}(s)}{s-k^2}\\
&\qquad=\int \mathrm{d}^4x\int \mathrm{d}^4p'\,e^{i(k-p')\cdot x}\,\left[\Gamma_2^{\nu}\,\frac{\not{p}'+m_1}{m_1^2-p'^2}\Gamma_1^{\mu}\right]_{\alpha\beta}\langle 0|\,\bar{q}_2^{\alpha}(x)h_v^{\beta}(0)\,|\bar{B}_{q_2}(v)\rangle\\
&\quad+\int \mathrm{d}^4x\int \mathrm{d}^4p'\int_0^1\mathrm{d}u\,e^{i(k-p')\cdot x}\,\left[\Gamma_2^{\nu}\,\frac{(1-u)(\not{p}'+m_1)\sigma^{\lambda\rho}+u\sigma^{\lambda\rho}(\not{p}'+m_1)}{2(p'^2-m_1^2)^2}\Gamma_1^{\mu}\right]_{\alpha\beta}\\
&\qquad\qquad\times\langle 0|\,\bar{q}_2^{\alpha}(x)g_s\mathbf{G}_{\lambda\rho}(ux)h_v^{\beta}(0)\,|\bar{B}_{q_2}(v)\rangle\ . \qquad (4.21)
\end{aligned}$$

The hadronic matrix elements in this equation are defined by eqs. (4.3)-(4.10) and eqs. (4.15)-(4.17).

To isolate the contribution of a single form factor in the dispersion relation (4.21), one has to select a suitable Lorentz structure. For convenience, we define the following combinations of form factors

$$f_{+/-}^{B\to P}\equiv f_+^{B\to P}+f_-^{B\to P}\,, \qquad (4.22)$$

$$A_{30}^{B\to V}\equiv A_3^{B\to V}-A_0^{B\to V}\,, \qquad (4.23)$$

$$T_{23A}^{B\to V}\equiv T_2^{B\to V}+\frac{q^2}{m_B^2-m_V^2}T_3^{B\to V}\,, \qquad (4.24)$$

$$T_{23B}^{B\to V}\equiv \frac{1}{2}T_2^{B\to V}+\frac{1}{2}\left(\frac{q^2}{m_B^2-m_V^2}-1\right)T_3^{B\to V}\,, \qquad (4.25)$$

with

$$f_0^{B\to P}=f_+^{B\to P}+\frac{q^2}{m_B^2-m_P^2}f_-^{B\to P}. \qquad (4.26)$$

Our analytical results are presented in the basis

$$f_+^{B\to P},\, f_{+/-}^{B\to P},\, f_T^{B\to P}, \tag{4.27}$$

for $B \to P$ form factors and

$$V^{B\to V},\, A_1^{B\to V},\, A_2^{B\to V},\, A_{30}^{B\to V},\, T_1^{B\to V},\, T_{23A}^{B\to V},\, T_{23B}^{B\to V}, \tag{4.28}$$

for $B \to V$ form factors.

The form factors $f_+^{B\to P}$ and $f_{+/-}^{B\to P}$ are extracted by selecting the Lorentz structures $k^\mu k^\nu$ and $q^\mu k^\nu$ in the dispersion relation (4.21), respectively. To extract $f_T^{B\to P}$, one can use both $k^\mu k^\nu$ and $q^\mu k^\nu$. We choose $q^\mu k^\nu$ for an easier comparison with the analytical results of ref. [112]. We also verified that the difference between the numerical results obtained using $k^\mu k^\nu$ and $q^\mu k^\nu$ is negligible.
It is straightforward to isolate the contribution of $V^{B\to V}$, $A_1^{B\to V}$, and $A_2^{B\to V}$ by selecting the Lorentz structures $\epsilon^{\mu\nu\{k\}\{q\}}$, $g^{\mu\nu}$, and $k^\mu q^\nu$, respectively. The extraction of $A_{30}^{B\to V}$ requires a simple trick, since there is no Lorentz structure that allows to obtain *only* $A_{30}^{B\to V}$. It consists in performing the change of variables $k^\mu \to (r^\mu - q^\mu)/2$ and then simply taking the terms proportional to $q^\mu q^\nu$. The contribution of $T_1^{B\to V}$, $T_{23A}^{B\to V}$, and $T_{23B}^{B\to V}$ is given by the structures $\epsilon^{\mu\nu\{k\}\{q\}}$, $k^\mu q^\nu$, and $q^\mu q^\nu$, respectively.

In order to get rid of the contributions of the exited and continuum states in eq. (4.21), we exploit the semi-global quark-hadron duality approximation (see subsection 3.1.3). We also perform a Borel transform to further suppress the contribution of these states (see chapter 3). The resulting sum rule can be written as

$$\begin{aligned} F =& \frac{f_B m_B}{K^{(F)}} \sum_{n=1}^{4} \Bigg\{ (-1)^n \int_0^{\sigma_0} \mathrm{d}\sigma\; e^{\frac{m_{P,V}^2 - s(\sigma,q^2)}{M^2}} \frac{1}{(n-1)!(M^2)^{n-1}} I_n^{(F)}(\sigma,q^2) \\ & - \left[\frac{(-1)^{n-1}}{(n-1)!} e^{\frac{m_{P,V}^2 - s(\sigma,q^2)}{M^2}} \sum_{j=1}^{n-1} \frac{1}{(M^2)^{n-j-1}} \frac{1}{s'} \left(\frac{\mathrm{d}}{\mathrm{d}\sigma} \frac{1}{s'} \right)^{j-1} I_n^{(F)}(\sigma,q^2) \right]_{\sigma=\sigma_0} \Bigg\}, \end{aligned} \tag{4.29}$$

where F is one of the form factors listed in eqs. (4.27)-(4.28). In eq. (4.29), we abbreviate

$$\begin{aligned} &\bar\sigma \equiv 1-\sigma\,, && s(\sigma,q^2) \equiv \sigma m_B^2 + \frac{m_1^2 - \sigma q^2}{\bar\sigma}\,, \\ &s'(\sigma,q^2) \equiv \frac{\mathrm{d}s(\sigma,q^2)}{\mathrm{d}\sigma}\,, && \sigma_0 \equiv \sigma(s_0,q^2)\,, \end{aligned}$$

where $\sigma(s,q^2)$ is the inverse function of $s(\sigma,q^2)$. We also use the following notation for the differential operator

$$\left(\frac{\mathrm{d}}{\mathrm{d}\sigma} \frac{1}{s'} \right)^n I_n^{(F)}(\sigma,q^2) \equiv \left(\frac{\mathrm{d}}{\mathrm{d}\sigma} \frac{1}{s'} \left(\frac{\mathrm{d}}{\mathrm{d}\sigma} \frac{1}{s'} \dots I_n^{(F)}(\sigma,q^2) \right) \right).$$

The coefficient functions $I_n^{(F)}$ can be written in the following form

$$I_n^{(F,\,2\mathrm{p})}(\sigma,q^2) = \frac{1}{\bar\sigma^n} \sum_{\psi_{2\mathrm{p}}} C_n^{(F,\psi_{2\mathrm{p}})}(\sigma,q^2)\, \psi_{2\mathrm{p}}(\sigma m_B), \qquad \psi_{2\mathrm{p}} = \phi_+, \bar\phi, g_+, \bar g, \tag{4.30}$$

$$I_n^{(F,\,3\mathrm{p})}(\sigma,q^2)=\frac{1}{\bar{\sigma}^n}\int\limits_0^{\sigma m_B}\mathrm{d}\omega_1\int\limits_{\sigma m_B-\omega_1}^{\infty}\frac{\mathrm{d}\omega_2}{\omega_2}\sum_{\psi_{3\mathrm{p}}}C_n^{(F,\psi_{3\mathrm{p}})}(\sigma,u,q^2)\,\psi_{3\mathrm{p}}(\omega_1,\omega_2)\Bigg|_{u=(\sigma m_B-\omega_1)/\omega_2},$$

$$\psi_{3\mathrm{p}}=\phi_3,\phi_4,\psi_4,\chi_4, \qquad (4.31)$$

with $\sigma=\omega/m_B$ in eq. (4.30) and $\sigma=(\omega_1+u\omega_2)/m_B$ in eq. (4.31). The coefficients $C^{(F,\psi)}$ as well as the normalisation factors $K^{(F)}$ of eq. (4.29) are listed in appendix D.

Oue results are full agreement with the two-particle contributions considered in ref. [112]. We also find agreement with the three-particle contributions of ref. [112], even though these results are incomplete since only four out of eight three-particles B-LCDAs were considered. We then provide for the first time the analytical results for the two-particle contributions up to twist four and of the three-particle contributions using the full set of B-LCDAs correctly expanded in units of twists. The numerical impact of our analytical results is assessed in subsection 4.1.3, while in the next subsection we discuss the effective threshold determination.

4.1.2 Effective Threshold Determination

The effective threshold s_0 is a non-perturbative input parameter that enters in every sum rule. Considering the case of our form factor LCSR, the effective threshold can be computed in two different ways. The first consists in using an SVZ sum rule, which is calculated from the vacuum-to-vacuum correlator of the interpolating current and its Hermitian conjugate:

$$\Pi^{\mu\nu}(q)=i\int\mathrm{d}^4x\,e^{iq\cdot x}\,\langle 0|\,T\{J^{\mu}_{\mathrm{int}}(x),J^{\nu,\dagger}_{\mathrm{int}}(0)\}\,|0\rangle\ .$$

All the parameters of the resulting sum rule are taken as external inputs except for s_0, which can then be extracted.

The second way uses a "daughter" LCSR [136], which is a sum rule derived from the LCSR for the form factors (4.29). This method consists in multiplying eq. (4.29) by $e^{-m^2_{P,V}/M^2}$, obtaining schematically

$$F\,e^{-\frac{m^2_{P,V}}{M^2}}=\int_0^{\sigma_0}\mathrm{d}\sigma\;e^{-\frac{s(\sigma,q^2)}{M^2}}J^{(F)}(\sigma,q^2,M^2)-e^{-\frac{s(\sigma_0,q^2)}{M^2}}G^{(F)}(\sigma_0,q^2,M^2)\,, \qquad (4.32)$$

and then taking the derivative of this equation with respect to $-1/M^2$. The ratio of this derivative to eq. (4.32) yields

$$m^2_{P,V}=\frac{\frac{\mathrm{d}}{\mathrm{d}(-1/M^2)}\left(\int_0^{\sigma_0}\mathrm{d}\sigma\;e^{-\frac{s(\sigma,q^2)}{M^2}}J^{(F)}(\sigma,q^2,M^2)-e^{-\frac{s(\sigma_0,q^2)}{M^2}}G^{(F)}(\sigma_0,q^2,M^2)\right)}{\int_0^{\sigma_0}\mathrm{d}\sigma\;e^{-\frac{s(\sigma,q^2)}{M^2}}J^{(F)}(\sigma,q^2,M^2)-e^{-\frac{s(\sigma_0,q^2)}{M^2}}G^{(F)}(\sigma_0,q^2,M^2)}\,. \qquad (4.33)$$

All the quantities in this equation are known except for s_0, which can now be extracted.

We prefer to use the method of the daughter sum rule to compute the effective thresholds of our LCSRs, since eq. (4.33) is a strong constraint that every LCSR should fulfil. Also, the effective threshold calculated with an SVZ sum rule might be slightly different from the effective threshold of the corresponding LCSR, and these differences require further investigation. For the $B\to\pi$, $B\to\rho$, and $B\to K$ transition we do not employ the daughter sum rule method and we use the same effective thresholds of ref. [112], which are computed with

an SVZ sum rule. This choice is motivated by the fact that the daughter sum rule (4.33) is not able to reproduce the masses of the π, ρ and K mesons for reasonable values of s_0. This might be due to large corrections that are not included in our calculation (α_s corrections, higher twist, $1/m_b$ corrections, etc.), which can substantially change the ratio in eq. (4.33). One could also argue that the π and K mesons are pseudo-Goldstone bosons, whose masses are generated dynamically through the breaking of the chiral symmetry. A deeper study of this issue is left for a future work.

The values of the effective thresholds used in our numerical analysis are listed in appendix C.

4.1.3 Numerical Results for the Form Factor LCSRs

All the inputs used in our analysis are listed in appendix C. Before we present our numerical results, we briefly discuss the Borel parameter M^2. As we have seen in the previous chapter, one has to look for a range of values where the Borel parameter is neither too large, so that the continuum and exited states are sufficiently suppressed, nor too small, so that higher order terms in the LCOPE are not enhanced. In addition, one has to check if the sum rule is sufficiently stable within such a Borel window, i.e. if it is constant with respect to M^2 or it only mildly depends on it. If such a Borel window exists, the parameter M^2 has to be varied within it. We then assign the following systematic uncertainties to take into account this fictitious dependence on M^2 of the form factors:

$$\begin{aligned} &B \to \pi : 15\%\,, \qquad B \to \rho : 12\%\,, \\ &B \to K : 8\%\,, \qquad B \to K^* : 5\%\,, \\ &B \to D^{(*)} : 3\%\,, \quad B_s \to D_s^{(*)} : 9\%\,. \end{aligned} \tag{4.34}$$

The values of the Borel parameter used in this work can be found in appendix C as well.

In order to propagate the parametric uncertainties to the final result, we carry our numerical analysis in the Bayesian framework. We then add in quadrature these uncertainties with the systematic uncertainties of eq. (4.34). All our analytical results are part of the EOS software [137]. We predict the form factors at five different q^2 points, namely for $q^2 = \{-15, -10, -5, 0, +5\}\,\text{GeV}^2$. For the final states D and D^*, we discard the point $q^2 = +5\,\text{GeV}^2$, since we observed that the LCSRs in these cases becomes unstable for positive values of q^2. This could be expected from the condition (4.12), which becomes more constraining for heavier final states. The form factor values at negative q^2, even though they have no physical meaning, are useful additional inputs when fitting to a parametrization, as we will show in subsection 4.3.2. In fact, form factors are analytic functions of q^2, and they are well defined the whole complex q^2 plane, except for the singularities on the real positive axis (see chapter 3).

We show the individual contributions of the various B-LCDAs at $q^2 = 0$ to our form factor results in table 4.2. As expected, the two-particle leading and next-to-leading twist (i.e. ϕ_+ and ϕ_-) contributions are dominant, while the magnitude of the g_+ and g_-^{WW} contributions is $\sim [20, 30]\%$ of the leading ones. Notice also that the sum of the g_+ and g_-^{WW} contributions always decreases the form factors central values. We conclude that the twist expansion seems to converge, although this convergence is slower than for the LCSRs with light-meson light-cone distribution amplitudes (see e.g. ref. [138]).

	2 pt.			
form factor	$\phi_\pm$	g_+	$g_-^{\rm WW}$	3-pt. $[10^{-2}]$
$f_+^{B\to\pi}$	0.28	$+0.00$	-0.06	-0.00
$f_T^{B\to\pi}$	0.25	$+0.01$	-0.07	-0.29
$f_+^{B\to K}$	0.35	$+0.00$	-0.08	-0.01
$f_T^{B\to K}$	0.33	$+0.02$	-0.09	-0.37
$f_+^{B\to D}$	0.84	$+0.02$	-0.21	-0.03
$f_T^{B\to D}$	0.65	$+0.33$	-0.41	-0.52
$A_1^{B\to\rho}$	0.28	-0.08	$+0.01$	-0.19
$A_{12}^{B\to\rho}$	0.31	$+0.01$	-0.07	-0.10
$V^{B\to\rho}$	0.37	-0.11	-0.00	-0.34
$T_1^{B\to\rho}$	0.32	-0.09	$+0.01$	-0.25
$T_{23}^{B\to\rho}$	0.69	$+0.07$	-0.18	-0.96
$A_1^{B\to K^*}$	0.33	-0.08	$+0.01$	-0.21
$A_{12}^{B\to K^*}$	0.26	$+0.01$	-0.05	-0.06
$V^{B\to K^*}$	0.44	-0.12	-0.00	-0.38
$T_1^{B\to K^*}$	0.37	-0.10	$+0.01$	-0.28
$T_{23}^{B\to K^*}$	0.68	$+0.04$	-0.14	-0.84
$A_1^{B\to D^*}$	0.73	-0.17	$+0.04$	-0.10
$A_{12}^{B\to D^*}$	0.21	$+0.01$	-0.03	-0.01
$V^{B\to D^*}$	1.02	-0.29	-0.04	-0.38
$T_1^{B\to D^*}$	0.83	-0.21	$+0.01$	-0.19
$T_{23}^{B\to D^*}$	0.88	$+0.08$	-0.15	-0.37

Table 4.2: Contributions of $\phi_\pm$, g_+, $g_-^{\rm WW}$, and the three-particle B-LCDAs at $q^2 = 0$ to our LCSR results for the form factors.

As shown in table 4.2, the three-particle contributions are extremely small, especially when compared to the results found in refs. [112, 127]. This is due to three reasons:

- The independent three-particle B-LCDAs are eight [114], while in refs. [112, 127] only four of them were considered. Moreover, we find that the contribution of the four B-LCDAs of refs. [112, 127] partially cancel with the four new ones introduced in ref. [114]. This cancellation is independent of choice of the B-LCDA model. Hence, it is crucial to consider the full set of three-particle B-LCDAs.

- In order to consistently truncate the twist expansion, one has to express the three-particle B-LCDAs of eq. (4.17) in terms of B-LCDAs with definite twist, using the

relations (4.20). This step was not carried out in refs. [112, 127].

- The values of the parameters $\lambda^2_{B,H}$ and $\lambda^2_{B,E}$ used in [112, 127] are substantially larger than the predictions of ref. [139], which we use. These parameters enter the normalisation of the B-LCDAs. More details are given in appendix C.

In total, all these differences make our three-particle contributions two orders of magnitude smaller than in refs. [112, 127]. We observe the same effect in the LCSR for the soft-gluon contribution to the charm loop, which we discuss in the next subsection.

Our results including uncertainty for the $B \to \pi, K, D$ and $B \to \rho, K^*, D^*$ form factors at $q^2 = 0$ are shown in table 4.3, where we also compare our results with other LCSR calculations. These calculations were done with both B-meson and light-meson LCSRs[2]. Usually, the light-meson LCSRs have smaller uncertainties than the B-meson LCSRs, since the light-meson light-cone distribution amplitudes and the respective inputs are better known than the B-LCDAs. Nevertheless, the B-meson LCSRs are very useful for mainly two reasons. First, to have additional independent results to compare and combine with light-meson LCSRs results. Second, the calculation of heavy-to-heavy form factors, like the $B_{(s)} \to D^{(*)}_{(s)}$ form factors, are clearly not accessible with light-meson LCSRs.

The calculation of the form factors for B_s decays differs only in the inputs used with respect to the calculation of the form factors for B decays. The most critical input is the first inverse moment $1/\lambda_{B_s,+}$ of the B-LCDA $\phi_+(\omega)$. The procedure to estimate it is described in appendix C.

All our LCSRs results for the $B \to \pi, \rho, K^{(*)}, D^{(*)}$ and $B_s \to D_s^{(*)}$ form factors are published as part the EOS software [137]. The constraints are accessible under the names

```
B->pi::FormFactors[f_+,f_0,f_T]@GKvD2018
B->rho::FormFactors[V,A_0,A_1,A_2,T_1,T_2,T_23]@GKvD2018
B->K::FormFactors[f_+,f_0,f_T]@GKvD2018
B->K^*::FormFactors[V,A_0,A_1,A_2,T_1,T_2,T_23]@GKvD2018
B->D^(*)::FormFactors[f_+,f_0,f_T,V,A_0,A_1,A_2,T_1,T_2,T_23]@GKvD2018
B_s->D_s^(*)::FormFactors[f_+,f_0,f_T,V,A_0,A_1,A_2,T_1,T_2,T_23]@BGJvD2019
```

The numerical results for the $B_s \to \phi$ form factors will be published in ref. [3].

4.1.4 Soft-gluon Contribution to the Charm Loop with LCSRs

The decay amplitude of the $B \to K^{(*)}\ell\ell$ decays can be decomposed as

$$\mathcal{A}(B \to K^{(*)}\ell^+\ell^-) = \frac{G_F\,\alpha_e\,V_{ts}^* V_{tb}}{\sqrt{2}\pi}\left[(C_9\,L_V^\mu + C_{10}\,L_A^\mu)\,\mathcal{F}_\mu - \frac{L_V^\mu}{q^2}\Big\{2im_b C_7\,\mathcal{F}_\mu^T + \mathcal{H}_\mu\Big\}\right], \tag{4.35}$$

where $L^\mu_{V(A)} \equiv \bar{u}_\ell(q_1)\gamma^\mu(\gamma_5)v_\ell(q_2)$. We also defined the local hadronic matrix elements

$$\mathcal{F}_\mu = \langle K^{(*)}(k)|\bar{s}\gamma_\mu P_L\,b|B(q+k)\rangle\,, \qquad \mathcal{F}_\mu^T = \langle K^{(*)}(k)|\bar{s}\sigma_{\mu\nu}q^\nu P_R\,b|B(q+k)\rangle \tag{4.36}$$

[2]The differences between the B-meson and light-meson LCSRs are summarised at the end of subsection 3.2.2.

form factor	our result	literature	reference
$f_+^{B\to\pi}$	0.21 ± 0.07	0.258 ± 0.031	[115]
		0.25 ± 0.05	[112]
		0.28 ± 0.05	[140]
		0.31 ± 0.02	[136]
		0.281 ± 0.038	[130]
		0.301 ± 0.023	[141]
$f_T^{B\to\pi}$	0.19 ± 0.06	0.253 ± 0.028	[115]
		0.21 ± 0.04	[112]
		0.273 ± 0.021	[141]
		0.26 ± 0.06	[142]
$f_+^{B\to K}$	0.27 ± 0.08	0.331 ± 0.041	[115]
		0.31 ± 0.04	[112]
		0.395 ± 0.033	[141]
		0.364 ± 0.05	[142]
$f_T^{B\to K}$	0.25 ± 0.07	0.358 ± 0.037	[115]
		0.27 ± 0.04	[112]
		0.381 ± 0.027	[141]
		0.363 ± 0.08	[142]
$f_+^{B\to D}$	0.65 ± 0.08	0.69 ± 0.2	[127]
		0.673 ± 0.063	[131]
$f_T^{B\to D}$	0.57 ± 0.05	—	—
$A_1^{B\to\rho}$	0.22 ± 0.10	0.24 ± 0.08	[112]
		0.262 ± 0.026	[66]
$A_2^{B\to\rho}$	0.19 ± 0.11	0.21 ± 0.09	[112]
$V^{B\to\rho}$	0.27 ± 0.14	0.32 ± 0.10	[112]
		0.327 ± 0.031	[66]
$T_1^{B\to\rho}$	0.24 ± 0.12	0.28 ± 0.09	[112]
		0.272 ± 0.026	[66]
$T_{23}^{B\to\rho}$	0.56 ± 0.15	0.747 ± 0.076	[66]
$A_1^{B\to K^*}$	0.26 ± 0.08	0.30 ± 0.08	[112]
		0.269 ± 0.029	[66]
$A_2^{B\to K^*}$	0.24 ± 0.09	0.26 ± 0.08	[112]
$V^{B\to K^*}$	0.33 ± 0.11	0.39 ± 0.11	[112]
		0.341 ± 0.036	[66]
$T_1^{B\to K^*}$	0.29 ± 0.10	0.33 ± 0.10	[112]
		0.282 ± 0.031	[66]
$T_{23}^{B\to K^*}$	0.58 ± 0.13	0.668 ± 0.083	[66]
$A_1^{B\to D^*}$	0.60 ± 0.09	0.73 ± 0.19	[127]
$A_2^{B\to D^*}$	0.51 ± 0.09	0.66 ± 0.30	[127]
$V^{B\to D^*}$	0.69 ± 0.13	0.96 ± 0.29	[127]
$T_1^{B\to D^*}$	0.63 ± 0.10	—	—
$T_{23}^{B\to D^*}$	0.81 ± 0.11	—	—

Table 4.3: Our results for the form factors at $q^2 = 0$ compared with other LCSR calculations in the literature. Our results are in good agreement with the previous calculations, also due to the large uncertainties of these results.

and the non-local hadronic matrix elements

$$\mathcal{H}^{\mu}(q,k) = i\int \mathrm{d}^4x\, e^{iq\cdot x}\, \langle K^{(*)}(k)|T\big\{J^{\mu}_{cc}(x), (C_1O^c_1 + C_2O^c_2)\,(0)\big\}|B(q+k)\rangle\,, \tag{4.37}$$

with the electromagnetic current $J^{\mu}_{cc} = \bar{c}\gamma^{\mu}c$. The WET operators O_i and the respective Wilson coefficients C_i were introduced in section 2.2. In writing eq. (4.35), we have neglected several contributions that are strongly numerically suppressed in the SM (see e.g. ref. [143] for more details).

The local matrix elements $\mathcal{F}_{\mu}$ and $\mathcal{F}^T_{\mu}$ are parametrized by the $B \to K^{(*)}$ form factors, which we calculated in subsection 4.1.1. The most important non-local contributions are generated by the current-current operators $O^c_{1,2}$ contacted with the electromagnetic current J^{μ}_{cc}, which are contained in the definition of the non-local matrix elements $\mathcal{H}^{\mu}$. These contributions are commonly called *charm-loop effects*.

To calculate $\mathcal{H}^{\mu}$ it is possible to use both a local OPE and a light-cone OPE (LCOPE). In fact, for $|q^2| \sim m_b^2$ the integral of eq. (4.37) is dominated by short distances $x \sim 1/m_b^2$ and a local OPE for $\mathcal{H}^{\mu}$ can be performed [143, 144]. On the other hand, for $q^2 \ll 4m_c^2$ the integral of eq. (4.37) is dominated by light-like distances $x^2 \sim 1/(4m_c^2 - q^2)$, which allows to perform a LCOPE [14].

The leading order term of the local OPE and of the LCOPE are identical and they read

$$\mathcal{H}^{\mathrm{fact}}_{\mu}(q,k) = \frac{3}{32\pi^2}\,(3C_1 + C_2)\left[\big(q_{\mu}q_{\rho} - q^2 g_{\mu\rho}\big)\, g^{(9)}(q^2)\mathcal{F}^{\rho} + 2im_b\, g^{(7)}(q^2)\mathcal{F}^T_{\mu}\right]. \tag{4.38}$$

These contributions, illustrated in figure 4.2(a), are called *factorisable* in ref. [33], since they can be written as a $B \to K^{(*)}$ form factor multiplied by the Wilson coefficients $g^{(7)}$ and $g^{(9)}$. Like all the Wilson coefficients, $g^{(7)}$ and $g^{(9)}$ can be computed carrying out the perturbative calculation and then performing the matching. At leading order in α_s, one finds (see e.g. refs. [14, 145])

$$g^{(7)}_{\mathrm{LO}}(q^2) = 0\,, \tag{4.39}$$

$$\begin{aligned} g^{(9)}_{\mathrm{LO}}(q^2) = {} & -\frac{8}{9}\ln\left(\frac{m_c}{m_b}\right) + \frac{8}{27} + \frac{4}{9}y(q^2) \\ & - \frac{4}{9}\big(2 + y(q^2)\big)\,\sqrt{y(q^2)-1}\,\arctan\left(\frac{1}{\sqrt{y(q^2)-1}}\right), \end{aligned} \tag{4.40}$$

with $y(q^2) = 4m_c^2/q^2 > 1$. The result (4.40) has been already renormalised, with $\mu = m_b$. The α_s corrections of these Wilson coefficients have been calculated independently in refs. [145, 146].

The next-to-leading order in the LCOPE can be written as

$$\begin{aligned} \mathcal{H}^{\mathrm{soft}}_{\mu}(q,k) = {} & C_2\,\varepsilon^{\sigma\tau\alpha\beta}\int \mathrm{d}\omega_2\, I_{\mu\rho\sigma\tau}(q,\omega_2) \\ & \langle K^{(*)}|\,\bar{s}(0)\gamma^{\rho}P_L\,\delta\Big(\omega_2 - n_+\cdot iD\Big)\, g_s\mathbf{G}_{\alpha\beta}(0)\, b(0)\,|B(q+k)\rangle + \mathcal{O}\left(\alpha_s\right), \end{aligned} \tag{4.41}$$

where the corresponding diagram is shown in figure 4.2(b). The gluon field $\mathbf{G}_{\alpha\beta}(ux)$ arise from the expansion of the charm-quark propagator near the light-cone through eq. (3.45).

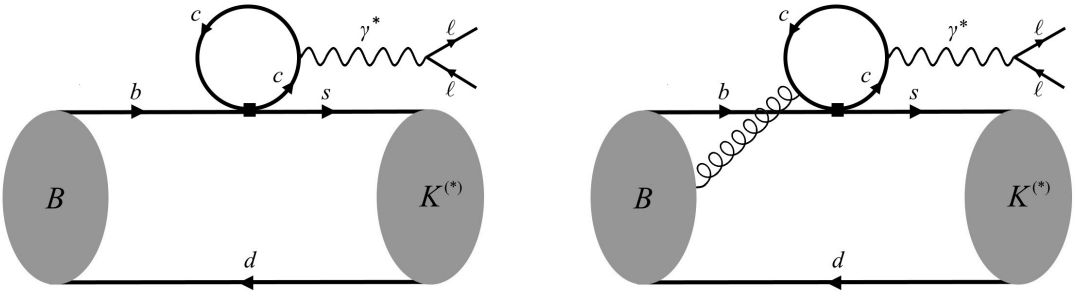

(a) (b)

Figure 4.2: Charm-loop effects in $B \to K^{(*)}\ell\ell$ decays. We show the leading order in the (LC)OPE (a) and one of the two diagrams corresponding to the next-to-leading order in the (LC)OPE (b). We do not consider α_s corrections.

Following ref. [14], we can use the translation operator to rewrite the gluon field as

$$\mathbf{G}_{\alpha\beta}(ux) = e^{-iux\cdot(iD)}\mathbf{G}_{\alpha\beta}(0) \tag{4.42}$$

and then we decompose the covariant derivative in light-cone vectors

$$D^\mu = (n_+ \cdot D)\,\frac{n_-^\mu}{2} + (n_- \cdot D)\,\frac{n_+^\mu}{2} + D_\perp^\mu\,, \tag{4.43}$$

The usual relations for the light-cone vectors

$$\frac{(q+k)^\mu}{m_B} \equiv v^\mu = \frac{1}{2}(n_+^\mu + n_-^\mu)\,, \qquad n_+^2 = n_-^2 = 0\,, \qquad (n_+ \cdot n_-) = 2$$

hold. Choosing the light-cone vectors such that

$$(n_- \cdot q) \sim m_b\,, \qquad (n_- \cdot q) \sim \frac{q^2}{m_b}\,, \qquad q_\perp^\mu = (0,0,0,0)\,, \tag{4.44}$$

it is possible to approximate

$$D^\mu \simeq (n_+ \cdot D)\,\frac{n_-^\mu}{2}\,,$$

as shown in ref. [14]. Finally, we write the gluon field as

$$\mathbf{G}_{\alpha\beta}(ux) = e^{-iu\frac{x\cdot n_-}{2}(n_+\cdot D)}\mathbf{G}_{\alpha\beta}(0) = \int \mathrm{d}\omega_2\, e^{-iu\frac{x\cdot n_-}{2}\omega_2}\,\delta\Big(\omega_2 - n_+\cdot iD\Big)\mathbf{G}_{\alpha\beta}(0)\,, \tag{4.45}$$

which is the form we have used in eq. (4.41). This trick of writing the gluon field in the form of eq. (4.45) is crucial for our sum rule calculation.

The Wilson coefficient $I_{\mu\rho\sigma\tau}$ was also calculated in ref. [14]. We fully agree with its calculation and we write it in the form

$$\tilde{I}_{\mu\rho\alpha\beta} \equiv \varepsilon^{\sigma\tau}{}_{\alpha\beta} I_{\mu\rho\sigma\tau}(q,\omega_2) = \int_0^1 \mathrm{d}u \int_0^1 \mathrm{d}t \frac{1}{128\pi^2(t(1-t)\tilde{q}^2 - m_c^2)}$$

$$\left(4t(1-t)\left(\tilde{q}_\mu\varepsilon_{\rho\alpha\beta\{\tilde{q}\}}-2u\tilde{q}_\beta\varepsilon_{\mu\rho\alpha\{\tilde{q}\}}+2u\tilde{q}^2\varepsilon_{\mu\rho\alpha\beta}\right)+\tilde{q}^2\left(1-2u\right)\varepsilon_{\mu\rho\alpha\beta}\right), \quad (4.46)$$

which is slightly different from the one presented in ref. [14], but analytically equivalent.

In order to evaluate the contribution of $\mathcal{H}_\mu^{\rm soft}$, we need to calculate the non-local matrix element of eq. (4.41). We then define a correlator, which is the starting point of our sum rule calculation:

$$\Pi^{\mu\nu}(q,k)=i\int \mathrm{d}^4y e^{iky}\,\langle 0|\,T\left\{J^\nu_{\rm int}(y),\tilde{O}^\mu(q)\right\}|\bar{B}(q+k)\rangle\ , \quad (4.47)$$

where

$$\tilde{O}^\mu(q)=\int \mathrm{d}\omega_2\,\tilde{I}^{\mu\rho\alpha\beta}\bar{s}(0)\gamma_\rho P_L\,\delta\Big(\omega_2-n_+\cdot iD\Big)\,g_s\mathbf{G}_{\alpha\beta}(0)\,b(0)\,. \quad (4.48)$$

We also define $J^\nu_{\rm int}=\bar{d}\gamma^\nu\gamma_5 s$ for the $B\to K$ transition, while $J^\nu_{\rm int}=\bar{d}\gamma^\nu s$ for the $B\to K^*$ transition.

We can now obtain the hadronic representation of the correlator inserting a complete set of states in eq. (4.47)

$$\Pi^{\mu\nu}(q,k)=\frac{\langle 0|\,J^\nu_{\rm int}(x)\,|K^{(*)}(k)\rangle\,\langle K^{(*)}(k)|\,\tilde{O}^\mu(q,\omega_2)(0)\,|B(q+k)\rangle}{m^2_{K^{(*)}}-k^2}+\frac{1}{\pi}\int_{s_h}^\infty \mathrm{d}s\frac{\tau^{\mu\nu}(s)}{s-k^2}\,. \quad (4.49)$$

The local $K^{(*)}$-to-vacuum matrix elements have already been defined in eqs. (4.3)-(4.4), while the non-local matrix elements can be parametrized as [14]

$$\langle K(k)|\tilde{\mathcal{O}}_\mu(q)|B(q+k)\rangle=((k\cdot q)q_\mu-q^2k_\mu)\tilde{\mathcal{A}}(q^2)\,, \quad (4.50)$$

$$\begin{aligned}\langle K^*(k,\eta)|\tilde{\mathcal{O}}_\mu(q)|B(q+k)\rangle&=\epsilon_{\mu\alpha\beta\gamma}\eta^{*\alpha}q^\beta k^\gamma\tilde{\mathcal{V}}_1(q^2)\\&+i\left((m_B^2-m^2_{K^*})\eta^*_\mu-(\eta^*\cdot q)(2k+q)_\mu\right)\tilde{\mathcal{V}}_2(q^2)\\&+i(\eta^*\cdot q)\left(q_\mu-\frac{q^2}{m_B^2-m^2_{K^*}}(2k+q)_\mu\right)\tilde{\mathcal{V}}_3(q^2)\,.\end{aligned} \quad (4.51)$$

The LCOPE calculation of $\Pi^{\mu\nu}$ becomes straightforward, since we have already computed $\tilde{I}_{\mu\rho\alpha\beta}$:

$$\begin{aligned}\Pi^{\mu\nu}(q,k)=\int \mathrm{d}\omega_2\int \mathrm{d}^4y\int \mathrm{d}^4p'\,e^{i(k-p')\cdot y}\tilde{I}^{\mu\rho\alpha\beta}\left[\Gamma^\nu_{\rm int}\frac{\not{p}'+m_s}{m_s^2-p'^2}\gamma_\rho P_L\right]_{ab}\\ \langle 0|\,\bar{d}^a(y)\delta\Big(\omega_2-n_+\cdot iD\Big)g_s\mathbf{G}_{\alpha\beta}(0)h_v^b(0)\,|B(q+k)\rangle\ .\end{aligned} \quad (4.52)$$

Here, the correlator has been expanded in HQET, as in our form factor calculation. The parametrization of the matrix element

$$\int \mathrm{d}\omega_2\,\langle 0|\,\bar{d}^a(y)\delta\Big(\omega_2-n_+\cdot iD\Big)g_s\mathbf{G}_{\alpha\beta}(0)h_v^b(0)\,|B(q+k)\rangle \quad (4.53)$$

	result of ref. [14]	our results
$\tilde{\mathcal{A}}$	$(-1.3^{+1.0}_{-1.1}) \cdot 10^{-4}$	$(+5.5^{+3.0}_{-2.8}) \cdot 10^{-7}$
$\tilde{\mathcal{V}}_1$	$(-1.5^{+1.3}_{-1.6}) \cdot 10^{-4}$	$(-4.8^{+2.5}_{-2.7}) \cdot 10^{-7}$
$\tilde{\mathcal{V}}_2$	$(+7.3^{+7.4}_{-6.5}) \cdot 10^{-5}$	$(+3.8^{+2.0}_{-1.9}) \cdot 10^{-7}$
$\tilde{\mathcal{V}}_3$	$(+2.4^{+2.5}_{-1.9}) \cdot 10^{-4}$	$(+1.1^{+0.6}_{-0.6}) \cdot 10^{-6}$

Table 4.4: Comparison between the results of ref. [14] and our results at $q^2 = 1\,\text{GeV}^2$.

is given in eq. (4.17). The reason why we have written the gluon field in the form of eq. (4.45) retaining only the n_- component is now clear: the fields of the three-particle B-to-vacuum matrix element must be aligned in the same light-cone direction otherwise eq. (4.17) does not hold. In other words, the gluon is dominantly emitted in the direction of the strange quark, which means that one can use eq. (4.17) to parametrize the three-particle B-to-vacuum matrix element.

Finally, we match the hadronic representation of the correlator (4.49) onto the LCOPE result (4.52). To obtain the sum rule, we perform a Borel transform after using the semi-global quark-hadron duality approximation. This sum rule can be written in the same way as the sum rule for the form factors (4.29), i.e.

$$\tilde{F} = \frac{f_B m_B}{K^{(\tilde{F})}} \sum_{n=1}^{\infty} \left\{ (-1)^n \int_0^{\sigma_0} \mathrm{d}\sigma \; e^{(-s(\sigma,q^2)+m^2_{K^{(*)}})/M^2} \frac{1}{(n-1)!(M^2)^{n-1}} I_n^{(\tilde{F})} \right.$$
$$\left. - \left[\frac{(-1)^{n-1}}{(n-1)!} e^{(-s(\sigma,q^2)+m^2_{K^{(*)}})/M^2} \sum_{j=1}^{n-1} \frac{1}{(M^2)^{n-j-1}} \frac{1}{s'} \left(\frac{\mathrm{d}}{\mathrm{d}\sigma} \frac{1}{s'} \right)^{j-1} I_n^{(\tilde{F})} \right]_{\sigma=\sigma_0} \right\}. \tag{4.54}$$

The only differences with respect to eq. (4.29) are the constants $K^{(\tilde{F})}$ and the coefficient functions $I_n^{(\tilde{F})}$. In this case we have

$$I_n^{(\tilde{F})}(\sigma, q^2) = \frac{1}{(1-\sigma)^n} \int_0^{\infty} \mathrm{d}\omega_2 \int_0^1 \mathrm{d}u \int_0^1 \mathrm{d}t \sum_{\psi_{3\mathrm{p}}} \sum_{r=0}^{2} \left(\frac{\omega_2}{m_B} \right)^r C_{n,r}^{(\tilde{F},\psi_{3\mathrm{p}})}(\sigma, u, t, q^2)\, \psi_{3\mathrm{p}}(\omega_1, \omega_2) \Big|_{\omega_1 = \sigma m_B},$$
$$\psi_{3\mathrm{p}} = \phi_3, \phi_4, \psi_4, \chi_4\,. \tag{4.55}$$

The values of the normalization constants $K^{(\tilde{F})}$ and of the coefficients $C_{n,r}^{(\tilde{F},\psi_{3\mathrm{p}})}$ will be published in [3].

We fully reproduce both the analytical and the numerical results of ref. [14]. However, our numerical results are ~ 200 times smaller with similar relative uncertainties, as shown in table 4.4. The reason for this huge difference in the central values follows the same explanation as the suppression of the three-particle contributions in the form factors (see subsection 4.1.3). The inputs used for our numerical results are collected in appendix C.

4.2 Dispersive Bounds in the Presence of Subthreshold Branch Cuts

In section 3.3 we reviewed the dispersive bounds. Here, we generalise this method to allow for the cases where non-negligible subthreshold branch cuts are present. As an example, let us consider the non-local matrix element

$$\langle 0|\mathcal{K}^{\mu}(x,0)|B(q+k)K^{(*)}(-k)\rangle \tag{4.56}$$

of the Hermitian operator

$$\mathcal{K}^{\mu}(x,0) \equiv T\big\{J^{\mu}_{cc}(x),(C_1O^c_1+C_2O^c_2)\,(0)\big\}\,, \tag{4.57}$$

which is related to the matrix element of eq. (4.37) through crossing symmetry. This matrix element has a series of branch cuts starting at $q^2 = 4m_D^2 \equiv t_+$, while the energy threshold for the production of a $BK^{(*)}$ pair is obviously $q^2 = (m_B + m_{K^{(*)}})^2 \equiv t_H$. Hence, we have to adapt the classical dispersive bounds presented in section 3.3, where one always assumes that $t_+ = t_H$. In some cases, there are subthreshold branch cuts that can be safely neglected if their magnitude is suppressed, as in the example presented in section 3.3. This is not possible in this case, where the subthreshold branch cuts give a relevant contribution.

To construct the dispersive bounds, we define the four-point correlator

$$\begin{aligned}\Pi^{\mu\nu}(q) &= i\int \mathrm{d}^4x\,\mathrm{d}^4y\,\mathrm{d}^4z\,e^{-iq\cdot(x-y)}\,\langle 0|\,T\{\mathcal{K}^{\mu}(x,0),\mathcal{K}^{\nu,\dagger}(y+z,z)\}\,|0\rangle \\ &= (q^{\mu}q^{\nu}-q^2g^{\mu\nu})\Pi(q^2)\end{aligned} \tag{4.58}$$

and write down the corresponding subtracted dispersion relation

$$\chi(q^2) = \frac{1}{n!}\left(\frac{\partial}{\partial q^2}\right)^n\left(q^2\Pi(q^2)\right) = \frac{1}{\pi}\int_0^{\infty}\mathrm{d}s\,\frac{s\,\mathrm{Im}\,\Pi(s)}{(s-q^2)^n}\,, \tag{4.59}$$

where n is the minimum number of subtractions to make χ finite. We now insert a complete set of states in the correlator Π to compute its imaginary part, which reads

$$\begin{aligned}\mathrm{Im}\,\Pi(q^2) = \left(\frac{1}{3q^2}\right)(q^{\mu}q^{\nu}-q^2g^{\mu\nu})\frac{1}{2}\int \mathrm{d}^4x\,\mathrm{d}^4y\,e^{-iq\cdot(x-y)} \\ \times \sum\!\!\!\!\!\!\int_{H_bH_{\bar{s}}} d\rho_{H_bH_{\bar{s}}}\,(2\pi)^4\delta^{(4)}(p_{H_bH_{\bar{s}}}-q) \\ \times\,\langle 0|\mathcal{K}^{\mu}(0,x)|H_bH_{\bar{s}}\rangle\,\langle H_bH_{\bar{s}}|\mathcal{K}^{\nu,\dagger}(0,y)|0\rangle + \dots\,.\end{aligned} \tag{4.60}$$

Here, the sum runs over all the states $H_bH_{\bar{s}}$ with bottomness $\mathrm{B} = -1$ and strangeness $\mathrm{S} = 1$, while the ellipsis stands for the positive contributions[3] to the imaginary part coming from the other branch cuts. Using two-body phase space measure

$$\int d\rho_{X\,Y}(2\pi)^4\delta^{(4)}(p_{X\,Y}-q) = \frac{1}{8\pi}\,\frac{\sqrt{\lambda(m_X^2,m_Y^2,s)}}{q^2}\,\theta(q^2-(m_X+m_Y)^2)\,, \tag{4.61}$$

[3]These contributions must be positive, since the operators appearing in eq. (4.61) are Hermitian.

and parametrizing the $B \to K^{(*)}$ non-local matrix elements as in appendix B, we obtain

$$\begin{aligned}\operatorname{Im}\Pi(q^2) = &\frac{m_B^4\left(\sqrt{\lambda(m_B^2,m_K^2,q^2)}\right)^3}{16\pi\, q^2}\left|\mathcal{H}_{BK,0}(q^2)\right|^2\theta(q^2-(m_B+m_K)^2)\\ &+\frac{m_B^6\sqrt{\lambda(m_B^2,m_{K^*}^2,q^2)}}{16\pi}\left(\left|\mathcal{H}_{BK^*,\perp}(q^2)\right|^2+\left|\mathcal{H}_{BK^*,\parallel}(q^2)\right|^2+\left|\mathcal{H}_{BK^*,0}(q^2)\right|^2\right)\\ &\times\theta(q^2-(m_B+m_K^*)^2)+\text{further positive terms}\,.\end{aligned} \tag{4.62}$$

We can now write down the dispersive bounds

$$\begin{aligned}\chi(q^2) > &\int_{(m_B+m_K)^2}^{\infty}\mathrm{d}s\left(\frac{m_B^4\left(\sqrt{\lambda(m_B^2,m_K^2,s)}\right)^3}{16\pi^2 s(s-q^2)^n}\,|\mathcal{H}_{BK,0}(s)|^2\right)\\ &+\int_{(m_B+m_{K^*})^2}^{\infty}\mathrm{d}s\left(\frac{m_B^6\sqrt{\lambda(m_B^2,m_{K^*}^2,s)}}{16\pi^2(s-q^2)^n}\sum_{\lambda=\perp,\parallel,0}|\mathcal{H}_{BK^*,\lambda}(s)|^2\right),\end{aligned} \tag{4.63}$$

where $\chi(q^2)$ can be computed performing an OPE for $m_Q^2-q^2\gg\Lambda_{\rm QCD}^2$. Following the same procedure explained in section 3.3, we map the first Riemann sheet of the complex q^2 plane onto the unit disk of z plane via the map

$$z=\frac{\sqrt{t_+-q^2}-\sqrt{t_+-t_0}}{\sqrt{t_+-q^2}+\sqrt{t_+-t_0}}\,. \tag{4.64}$$

Here $t_+=4m_D^2$ is the position of the first branch point and $t_0<t_+$ can be arbitrarily chosen. After transforming in polar coordinates, eq. (4.63) becomes

$$\begin{aligned}1 > &\int_{-\alpha_{BK}}^{+\alpha_{BK}}\mathrm{d}\alpha\,|\phi_{BK}(s)|^2\,|\mathcal{H}_{BK,0}(s)|^2\Big|_{s\equiv s(z(\alpha))}\\ &+\int_{-\alpha_{BK^*}}^{+\alpha_{BK^*}}\mathrm{d}\alpha\,|\phi_{BK^*}(s)|^2\sum_{\lambda=\perp,\parallel,0}|\mathcal{H}_{BK^*,\lambda}(s)|^2\Big|_{s\equiv s(z(\alpha))},\end{aligned} \tag{4.65}$$

where the integral limits are

$$\alpha_{BK^{(*)}}\equiv|\arg z((M_B+M_{K^{(*)}})^2)| \tag{4.66}$$

and the modulus squared of the outer functions is

$$\begin{aligned}|\phi_{BK}(s)|^2 &= \frac{1}{2}\frac{1}{\chi(q^2)}\frac{\mathrm{d}z(\alpha)}{\mathrm{d}\alpha}\frac{\mathrm{d}s}{\mathrm{d}z}\frac{m_B^4\left(\sqrt{\lambda(m_B^2,m_K^2,s)}\right)^3}{16\pi^2 s(s-q^2)^n}\Big|_{s\equiv s(z(\alpha))},\\ |\phi_{BK^*}(s)|^2 &= \frac{1}{2}\frac{1}{\chi(q^2)}\frac{\mathrm{d}z(\alpha)}{\mathrm{d}\alpha}\frac{\mathrm{d}s}{\mathrm{d}z}\frac{m_B^6\sqrt{\lambda(m_B^2,m_{K^*}^2,s)}}{16\pi^2(s-q^2)^n}\Big|_{s\equiv s(z(\alpha))},\end{aligned} \tag{4.67}$$

assuming that the value of q^2 is fixed. To remove the poles inside the unit disk due to both $c\bar{c}$ and $b\bar{s}$ bound states, we multiply the integrand of eq. (4.65) by the appropriate Blaschke factors $\mathcal{B}$, which have been defined in section 3.3. Finally, the dispersive bounds assume a very simple form

$$\begin{aligned} 1 > & \int_{-\alpha_{BK}}^{+\alpha_{BK}} \mathrm{d}\alpha \left|\hat{\mathcal{H}}_{BK,0}(s)\right|^2 \Big|_{s\equiv s(z(\alpha))} \\ & + \int_{-\alpha_{BK^*}}^{+\alpha_{BK^*}} \mathrm{d}\alpha \sum_{\lambda=\perp,\parallel,0} \left|\hat{\mathcal{H}}_{BK^*,\lambda}(s)\right|^2 \Big|_{s\equiv s(z(\alpha))} , \end{aligned} \tag{4.68}$$

where we have defined

$$\begin{aligned} \hat{\mathcal{H}}_{BK,0}(z) &\equiv \phi_{BK}(z)\,\mathcal{B}_0(z)\,\mathcal{H}_{BK,0}(z)\,, \\ \hat{\mathcal{H}}_{BK^*,\lambda}(z) &\equiv \phi_{BK^*}(z)\,\mathcal{B}_\lambda(z)\,\mathcal{H}_{BK^*,\lambda}(z) \qquad \text{for } \lambda = 0,\perp,\parallel\ . \end{aligned}$$

Since the integral of eq. (4.68) is not over the whole unit circle, but only over an arc of it, the set

$$\{z^0, z^1, z^2, z^3, \dots\}$$

is not an orthonormal basis for this case. The first three orthonormal polynomials on the arc of the unit circle of eq. (4.68) are

$$\begin{aligned} p_{i,0}(z) &= \frac{1}{\sqrt{2\alpha_i}}\,, \\ p_{i,1}(z) &= \left(z - \frac{\sin(\alpha_i)}{\alpha_i}\right)\sqrt{\frac{\alpha_i}{2\alpha_i^2 + \cos(2\alpha_i) - 1}}\,, \\ p_{i,2}(z) &= \left(z^2 + \frac{\sin(\alpha_i)(\sin(2\alpha_i) - 2\alpha_i)}{2\alpha_i^2 + \cos(2\alpha_i) - 1} z + \frac{2\sin(\alpha_i)(\sin(\alpha_i) - \alpha_i\cos(\alpha_i))}{2\alpha_i^2 + \cos(2\alpha_i) - 1}\right) \\ &\quad \times \sqrt{\frac{2(2\alpha_i^2 + \cos(2\alpha_i) - 1)}{-9\alpha_i + 8\alpha_i^3 + 8\alpha_i\cos(2\alpha_i) + \alpha_i\cos(4\alpha_i) + 4\sin(2\alpha_i) - 2\sin(4\alpha_i)}}\,, \end{aligned}$$

for $\alpha_i = \alpha_{BK}$, α_{BK^*}. Thus, expanding the functions $\hat{\mathcal{H}}_i$ as

$$\hat{\mathcal{H}}_i(z) = \sum_{k=0}^{\infty} a_{i,k}\, p_{i,k}\,, \tag{4.69}$$

the dispersive bounds can be written as

$$\sum_{k=0}^{\infty} |a_{BK,k}|^2 + \sum_{\lambda=\perp,\parallel,0} \sum_{k=0}^{\infty} |a_{\lambda,k}|^2 < 1\,. \tag{4.70}$$

The disadvantage of the polynomials $p_{i,k}$ is that on the real axis around $z = 0$ they grow exponentially in magnitude for $k \to \infty$ [147], while z^k goes to zero for $k \to \infty$ inside the unit disk. However, the series (4.69) is still convergent, since

$$\hat{\mathcal{H}}_i(z) = \sum_{k=0}^{\infty} a_{i,k}\, p_{i,k} = \sum_{k=0}^{\infty} b_{i,k}\, z^k \tag{4.71}$$

and the Taylor series is convergent, being $\hat{\mathcal{H}}_i$ an analytic function of z inside the unit disk.

The idea is to truncate the series (4.69) and to fit its first few coefficients to experimental data and/or theoretical predictions. This fit and the calculation of χ will be presented in ref. [3].

The method presented in this section can be applied to obtain the dispersive bounds for all the matrix elements that have non-negligible subthreshold branch cuts, even though we focused only on the example of $B \to K^{(*)}\ell\ell$ non-local matrix elements. In fact, we are also applying this method to obtain dispersive bounds for the $\Lambda_b \to \Lambda_c$ form factors.

4.3 Form Factor Extrapolation and Phenomenological Applications

Light-cone sum rules (LCSRs) can only be used for low or negative q^2 values, in order to ensure the convergence of the LCOPE. To extrapolate the form factors values in the whole physically allowed region, we parametrize the form factors themselves and fit the coefficients of this parametrization to our LCSRs results. It is also possible to add additional information in these fits, using for instance lattice QCD results and dispersive bounds.

Once we have the form factors, we can predict several interesting observables in B decays. Here, we focus on the lepton flavour universality ratios R_D and R_{D^*}, while the results for all the other observables that we predicted in $B_{(s)} \to D_{(s)}^{(*)}$ decays are given in ref. [2].

4.3.1 Form Factors Parametrization

To obtain the form factors in the interval $0 < q^2 < (m_B - m_{P,V})^2$, i.e. for all the allowed q^2 values in $B \to P$ and $B \to V$ transitions, we use the parametrization suggested in ref. [66], which reads

$$F(q^2) = \frac{1}{1 - q^2/m_{R,F}^2} \sum_{k=0}^{2} \alpha_k^{(F)} \left(z(q^2) - z(0)\right)^k \,. \tag{4.72}$$

The z map is the same one as defined in the previous section, with $t_\pm = (m_B \pm m_{P,V})^2$ and $t_0 \equiv t_+ \left(1 - \sqrt{1 - t_-/t_+}\right)$. The mass of the sub-threshold resonances $m_{R,F}$, which have the same quantum number of the weak current of the corresponding transition, are listed in table 4.5.

For each transition we perform two different fits: the first using only our LCSRs results, the second using both LCSRs and the available lattice QCD data points. In both cases, we find a p value close to one, which is not surprising given the large uncertainties and the small number of degrees of freedom. Our results for the $B \to K^*$ and the $B \to D^*$ transitions are shown in figure 4.3 and figure 4.4, respectively. The plots for the remaining transitions can be found in ref. [1]. The central values, the uncertainties and the correlation matrix of the parameters $\alpha_k^{(F)}$ of eq. (4.72) are attached as ancillary files to the arXiv preprint of refs. [1] and part of the EOS software [137] as constraints named

```
B->pi::FormFactors[parametric,LCSR]@GKvD2018
B->pi::FormFactors[parametric,LCSRLattice]@GKvD2018
B->rho::FormFactors[parametric,LCSR]@GKvD2018
B->K::FormFactors[parametric,LCSR]@GKvD2018
```

J^P	form factors	resonance masses [GeV]		
		$B_{u,d}(J^P)$	$B_s(J^P)$	$B_c(J^P)$
0^-	$A_0^{B\to V}$	5.279	5.336	6.275
0^+	$f_0^{B\to P}$	5.540	5.630	6.420
1^-	$f_+^{B\to P}$, $f_T^{B\to P}$, $V^{B\to V}$, $T_1^{B\to V}$	5.325	5.412	6.330
1^+	$A_1^{B\to V}$, $A_{12}^{B\to V}$, $T_2^{B\to V}$, $T_{23}^{B\to V}$	5.724	5.829	6.767

Table 4.5: List of the masses of the lowest-lying resonances in the individual $b \to \{u, d\}$, $b \to s$ and $b \to c$ transitions, and their association to the respective form factors. The values of these masses, which are necessary inputs for the form factor parametrization (4.72), are taken from refs. [66, 148].

```
B->K::FormFactors[parametric,LCSRLattice]@GKvD2018
B->K^*::FormFactors[parametric,LCSR]@GKvD2018
B->K^*::FormFactors[parametric,LCSRLattice]@GKvD2018
B->D^(*)::FormFactors[parametric,LCSR]@GKvD2018
B->D^(*)::FormFactors[parametric,LCSRLattice]@GKvD2018
```

In order to reduce the form factors uncertainties, it is possible to use the dispersive bounds to constrain the parameters of a form factor parametrization. In addition, one can also use heavy quark effective theory (HQET) to relate the various $B \to D^{(*)}$ (and $B_s \to D_s^{(*)}$) form factors and obtain stronger constraints on such parameters. This method, originally proposed in ref. [10], has been recently applied in refs. [2, 149] including $\overline{\Lambda}/m_c^2$ corrections. It consists in expanding every $B^{(*)} \to D^{(*)}$ form factor in the heavy-quark limit as

$$F(q^2) = \xi(q^2)\left(a + \frac{\alpha_s}{\pi}b + \frac{\overline{\Lambda}}{m_b}\,c_b^{(i)}\left[L_i(q^2)\right] + \frac{\overline{\Lambda}}{m_c}\,c_c^{(i)}\left[L_i(q^2)\right] + \left(\frac{\overline{\Lambda}}{m_c}\right)^2 d^{(i)}\left[\ell_i(q^2)\right]\right). \tag{4.73}$$

Here ξ, L_i, and ℓ_i are the so-called Isgur-Wise (IW) functions (see e.g. ref. [84]). The coefficients a, b, $c_b^{(i)}$, $c_c^{(i)}$, and $d^{(i)}$ in this expansion are linear combinations of Wilson coefficients from the matching of HQET onto QCD and kinematic functions. In eq. (4.73) we use the same power counting of ref. [149], where $\alpha_s/\pi \sim \overline{\Lambda}/m_b \sim (\overline{\Lambda}/m_c)^2 \sim \varepsilon^2$. In fact, while $\overline{\Lambda}/m_b$ and $(\overline{\Lambda}/m_c)^2$ are next-to-leading power and next-to-next-to-leading power in the heavy-quark expansion, respectively, they are numerically similar.

There is one independent leading power IW function ξ and three next-to-leading power IW functions L_i [150]. We consider only six next-to-next-to-leading IW functions ℓ_i, although there are more than six, since we are interested only in the $(\overline{\Lambda}/m_c)^2$ corrections and not in the $(\overline{\Lambda}/m_b)^2$ corrections [149].

Hence, all the $B^{(*)} \to D^{(*)}$ form factors can be expressed in terms of ten IW functions. The same argument applies to the $B_s^{(*)} \to D_s^{(*)}$ form factors, which yields in total twenty IW functions. However, we give our results in the scenario where the ℓ_i functions are the same for the $B^{(*)} \to D^{(*)}$ and the $B_s^{(*)} \to D_s^{(*)}$ decays. This follows from the fact that the $SU(3)$ flavour breaking effects in these functions is of the order of ε^3, which we discard.

The dispersive bounds are then imposed to constrain these fourteen independent IW func-

	our results	
exp. likelihood	—	all exp.
$\mathcal{B}(\bar{B}^0 \to D^+\{e^-,\mu^-\}\bar{\nu})/\lvert V_{cb}\rvert^2$	13.48 ± 0.34	13.54 ± 0.32
$\mathcal{B}(\bar{B}^0 \to D^{*+}\{e^-,\mu^-\}\bar{\nu})/\lvert V_{cb}\rvert^2$	33.87 ± 1.82	32.69 ± 0.76
correlation	0.13	0.09
$\lvert V_{cb}\rvert \times 10^3$ from $\bar{B} \to D\{e^-,\mu^-\}\bar{\nu}$	40.7 ± 1.1	40.7 ± 1.1
$\lvert V_{cb}\rvert \times 10^3$ from $\bar{B} \to D^*\{e^-,\mu^-\}\bar{\nu}$	38.8 ± 1.4	39.5 ± 0.9
$\lvert V_{cb}\rvert \times 10^3$ combined incl. corr.	40.0 ± 0.9	40.0 ± 0.7
$\mathcal{B}(\bar{B}_s^0 \to D_s^+\{e^-,\mu^-\}\bar{\nu})/\lvert V_{cb}\rvert^2$	14.00 ± 0.40	13.99 ± 0.40
$\mathcal{B}(\bar{B}_s^0 \to D_s^{*+}\{e^-,\mu^-\}\bar{\nu})/\lvert V_{cb}\rvert^2$	33.04 ± 2.88	32.06 ± 2.54
correlation	-0.07	-0.10

Table 4.6: Branching ratios in units of $|V_{cb}|^2$ and $|V_{cb}|$ extracted using the HFLAV averages of the $\mathcal{B}(\bar{B}^0 \to D^+\{e^-,\mu^-\}\bar{\nu})$ and $\mathcal{B}(\bar{B}^0 \to D^{*+}\{e^-,\mu^-\}\bar{\nu})$ branching fractions [59].

tions. Considering simultaneously the $B^{(*)} \to D^{(*)}$ and the $B_s^{(*)} \to D_s^{(*)}$ form factors in the dispersive bounds has the advantage to increase the saturation of the bounds, which leads to stronger constraints.

All the details of our fits are given in ref. [2]. Here, we just show the $B \to D^*$ plots. As one can see in figure 4.5, the use of the dispersive bounds and HQET significantly reduces the uncertainties, especially for the $B \to D^*$ transition where only one lattice QCD point at q^2_{max} is available. This approach can be systematically improved including more transitions in the bounds in order to saturate them. One can also consider higher order α_s and HQET corrections in eq. (4.73).

4.3.2 Selected Phenomenological Applications

Now that we have extracted the form factors in the whole physically allowed region, we are able to predict several observables in B decays. Here, we are going to focus on the lepton flavour universality ratios, due to the tension between their SM predictions and experimental measurements.

It is instructive to compare results obtained only using LCSRs or LCSRs + lattice QCD (LQCD) with the ones using LCSRs + LQCD + dispersive bounds (DB) + HQET. For the lepton flavour universality ratios R_D and R_{D^*}, widely discussed in chapter 1, we obtain

$$\text{LCSR only [1]} \qquad R_D\Big|_{\text{SM}} = 0.269 \pm 0.100\,,$$

$$\text{LCSR only [1]} \qquad R_{D^*}\Big|_{\text{SM}} = 0.242 \pm 0.048\,,$$

$$\text{LCSR + LQCD [1]} \qquad R_D\Big|_{\text{SM}} = 0.296 \pm 0.006\,,$$

$$\text{LCSR + LQCD [1]} \qquad R_{D^*}\Big|_{\text{SM}} = 0.256 \pm 0.020\,,$$

$$\text{LCSR + LQCD + DB + HQET [2]} \qquad R_{D}\Big|_{\text{SM}} = 0.299 \pm 0.003\,,$$

$$\text{LCSR + LQCD + DB + HQET [2]} \qquad R_{D^*}\Big|_{\text{SM}} = 0.247 \pm 0.005\,.$$

Notice that in ref. [1] and ref. [2] we use the same theoretical constraints, and the use of dispersive bounds and HQET reduces the uncertainties in R_D and R_{D^*} of two and four times, respectively. The tension between our theoretical predictions and the HFLAV experimental averages [59] of R_D and R_{D^*} is 3.8σ. This tension is higher than the one between the HFLAV theoretical and experimental averages (see chapter 1).

We also predict the R_{D_s} and $R_{D_s^*}$ ratios

$$\text{LCSR + LQCD + DB + HQET [2]} \qquad R_{D_s}\Big|_{\text{SM}} = 0.297 \pm 0.003\,,$$

$$\text{LCSR + LQCD + DB + HQET [2]} \qquad R_{D_s^*}\Big|_{\text{SM}} = 0.245 \pm 0.008$$

with similar uncertainties to those of R_D and R_{D^*}. These ratios will be measured in the near future by the LHCb collaboration.

Another interesting phenomenological application is the extraction of $|V_{cb}|$. In table 4.6, we show our results for the branching fractions $\mathcal{B}(\bar{B}^0 \to D^{(*)+}\{e^-,\mu^-\}\bar{\nu})$ and $\mathcal{B}(\bar{B}_s^0 \to D_s^{*+}\{e^-,\mu^-\}\bar{\nu})$ in units of $|V_{cb}|^2$. To extract $|V_{cb}|$, we use the HFLAV averages of the $\mathcal{B}(\bar{B}^0 \to D^{+}\{e^-,\mu^-\}\bar{\nu})$ and $\mathcal{B}(\bar{B}^0 \to D^{*+}\{e^-,\mu^-\}\bar{\nu})$ branching fractions [59]. Our results for $|V_{cb}|$ are listed in table 4.6 as well. The extraction of $|V_{cb}|$ using B_s decays has been carried out for the first time in ref. [11] for the first time.

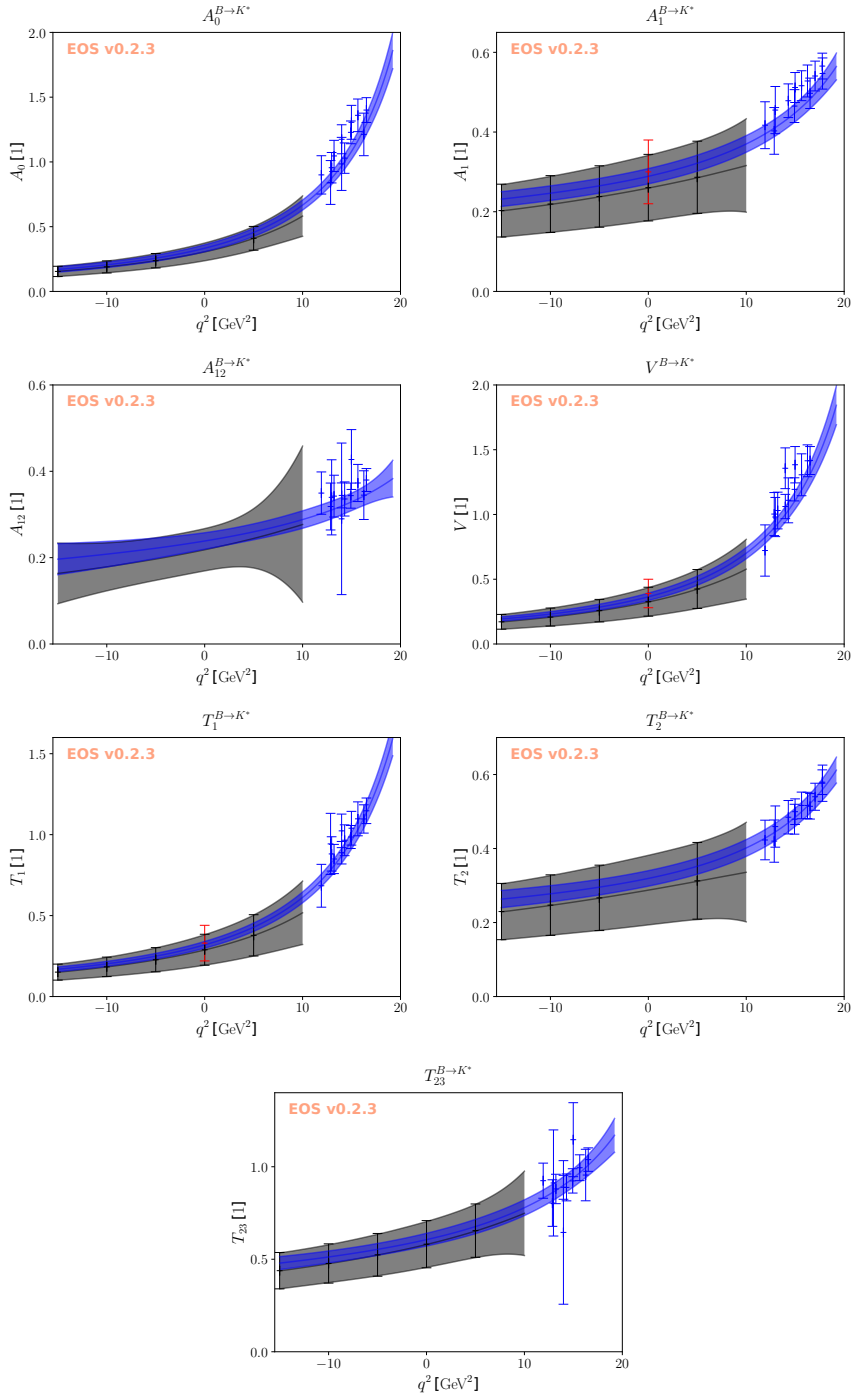

Figure 4.3: Plots of our results (grey points) and LQCD results from ref. [87, 88] (blue points) for the $B \to K^*$ form factors. Central values and 68% probability envelopes as functions of q^2 from fits to our results only (grey) and a combination of our results and LQCD results (blue) are shown as well. Previous results from LCSRs using B-LCDAs [112] at $q^2 = 0$ are not used in the fits and shown in red for illustrative purpose only. Solid lines represent the central values, and shaded areas illustrate the 68% probability envelope.

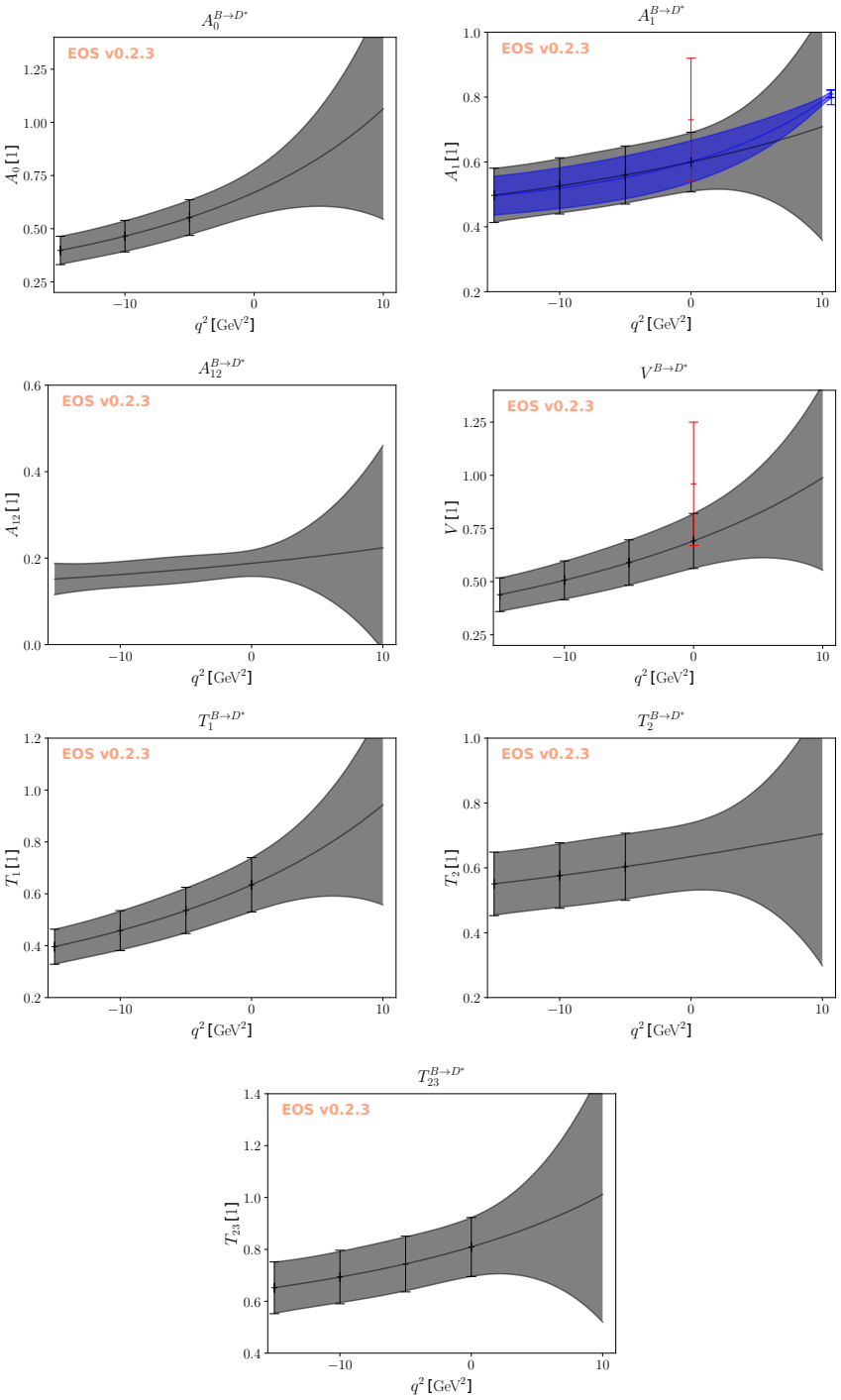

Figure 4.4: Plot of $B \to D^*$ form factors, LQCD results from refs. [89, 90]. For a description see figure 4.3.

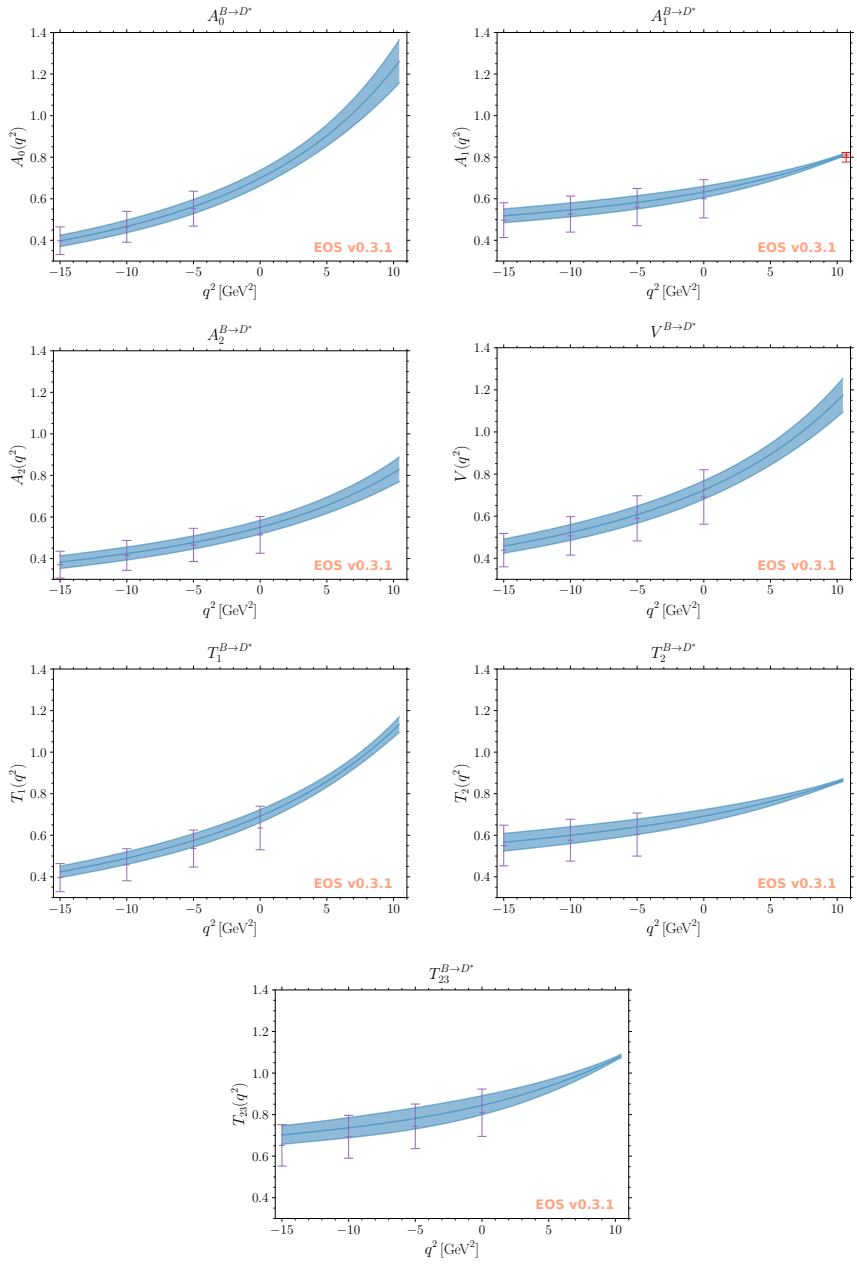

Figure 4.5: Plots of our LCSRs results (purple points) and our fits results (light-blue 68% probability envelopes) that combine LCSRs, LQCD, dispersive bounds and HQET relations for the form factors.

Conclusion

We calculated the $B \to \pi, \rho, K^{(*)}, D^{(*)}$ and $B_s \to D_s^{(*)}$ form factors using the light-cone sum rules (LCSRs) with B-meson light-cone distribution amplitudes (B-LCDAs). We improved upon the previous studies of refs. [112, 127] by including for the first time the two-particle next-to-next-to-leading twist (NNLT) contributions and the full set of three-particle B-LCDAs. Our numerical results show that the two-particle NNLT contributions are rather important, since they reduce the central values of the form factors by $\sim [20, 30]\%$, while our three-particle contributions are much smaller than in refs. [112, 127] for the reasons discussed below.

In rare B decays there are also important contributions that come from non-local hadronic matrix elements, besides the leading contributions proportional to local hadronic matrix elements, which are parametrized in terms of form factors. The soft-gluon contribution to the charm loop in $B \to K^{(*)}\ell\ell$ is one of the most important among these non-local contributions. As shown in ref. [14], this contribution can be calculated using a LCSR, in which only the three-particle B-LCDAs contribute. The set of three-particle B-LCDAs used in ref. [14] (and also in refs. [112, 127]) is incomplete. In fact, only four B-LCDAs were considered, while there are eight independent three-particle B-LCDAs [114]. Moreover, these eight B-LCDAs need to be recast in terms of B-LCDAs with definite twist, such that the twist expansion can be consistently truncated. Taking into account these differences in the treatment of the three-particle B-LCDAs, we obtain numerical results for the soft-gluon contribution to the charm loop one order of magnitude smaller than in ref. [14]. This is due to a partial cancellation between the original four B-LCDAs considered in refs. [14, 112, 127] and the ones introduced in ref. [114].

In addition, we use the most recent prediction of the parameters $\lambda_{B,H}^2$ and $\lambda_{B,E}^2$ [139], which is substantially different from the values used in [14, 112, 127]. This makes our results one further order of magnitude smaller. Hence, our numerical results for the three-particle contributions are two orders of magnitude smaller than the previous estimates, indicating that the soft-gluon contribution to the charm loop is essentially negligible.

Next, we extended the dispersive bounds to the case where non-negligible subthreshold branch cuts are present. This implies that in the z plane, instead of integrating over the whole unit circle, one has to integrate over an arc of it. The orthonormal polynomials on an arc of a circle are much more complicated than the monomials in z, which constitute an orthonormal set on the unit circle. One application of these generalised dispersive bounds are the non-local hadronic matrix elements in $B \to K^{(*)}\ell\ell$. We discussed this case in detail in section 4.2.

Finally, we used the form factors parametrization proposed in ref. [66] to obtain the form

factors in the whole kinematical range, exploiting both our LCSRs results and the available lattice QCD results. Imposing the dispersive bounds and employing heavy quark effective theory, we further constrained the form factors. We then predicted several observables in semileptonic B decays using the form factor values we obtained. The lepton flavour universality ratios R_D and R_{D^*} are among the most interesting observables due to the tension between the theoretical predictions and the experimental measurements. Our predictions increase this tension to 3.8σ. We also predict R_{D_s} and $R_{D_s^*}$ in view of the forthcoming measurements of the LHCb collaboration.

Appendices

Appendix A

Conventions

For the convenience of the reader, we collect here the notations and conventions used in this work.

A.1 Units

Throughout this work we use natural units where

$$\hbar = c = 1\,, \qquad \text{and} \qquad e = \sqrt{4\pi\alpha_e}\,. \tag{A.1}$$

Here $\hbar$ is the reduced Planck constant, c the speed of light, and $\alpha_e \simeq 1/137$ is the fine-structure constant. Equation (A.1) implies that in this system

$$[\text{length}] = [\text{time}] = [\text{mass}]^{-1} = [\text{energy}]^{-1}\,.$$

In words, the units of measurement of length, time, mass, and energy are related. In particle physics the eV (and its powers) is conventionally chosen as the unit of measurement of all physical quantities. To convert a physical quantity from natural units to SI units, one needs to multiply this quantity by powers of $\hbar$ and c to give the correct SI dimension.

A.2 Signs and Dirac Algebra

The Minkowski metric reads

$$g_{\mu\nu} = \begin{pmatrix} +1 & 0 & 0 & 0 \\ 0 & -1 & 0 & 0 \\ 0 & 0 & -1 & 0 \\ 0 & 0 & 0 & -1 \end{pmatrix}, \tag{A.2}$$

from which follows that

$$p_\mu p^\mu \equiv p \cdot p = m^2 > 0\,.$$

The Dirac matrices (or gamma matrices) γ^μ are defined by the anticommutation relation

$$\{\gamma_\mu, \gamma_\nu\} = 2g_{\mu\nu}\mathbb{1}_4\,, \tag{A.3}$$

where $\mathbb{1}_4$ is the 4×4 identity matrix, which are implied throughout this work.
Moreover, we define

$$\gamma_5 = -\frac{i}{4!}\varepsilon_{\mu\nu\alpha\beta}\gamma^\mu\gamma^\nu\gamma^\alpha\gamma^\beta\,, \tag{A.4}$$

$$\sigma_{\mu\nu} = \frac{i}{2}[\gamma_\mu, \gamma_\nu]\,, \tag{A.5}$$

where the convention for the Levi-Civita tensor adopted in this work is $\varepsilon_{0123} = +1$, which matches the convention of refs. [1, 14, 112] and the Bjorken-Drell textbook [151].
The chiral projection operators are

$$P_L = \frac{1-\gamma_5}{2}\,, \qquad\qquad P_R = \frac{1+\gamma_5}{2}\,, \tag{A.6}$$

which define the left- and right-chiral Dirac fields

$$\psi_L = P_L\psi\,, \qquad\qquad \psi_R = P_R\psi\,, \tag{A.7}$$

with $\psi_L + \psi_R = \psi$. It is important to do not confuse helicity with chirality, and hence left- and right-handed fields with left- and right-chiral fields (see ref. [152] for a review).

Appendix B

Parametrization of Meson-to-meson Matrix Elements

B.1 $B \to P$ and $B \to V$ Form Factors

The meson form factors (FFs) are functions of the momentum transfer q^2 that parametrize local hadron-to-hadron matrix elements. In this thesis, we use the following definition for the B to pseudoscalar (P) and B to vector (V) meson FFs:

$$\langle P(k)|\,\bar{q}_1\gamma^\mu b\,|B(p)\rangle = \left[(p+k)^\mu - \frac{m_B^2 - m_P^2}{q^2}q^\mu\right] f_+^{B\to P} + \frac{m_B^2 - m_P^2}{q^2}q^\mu\, f_0^{B\to P}\,, \tag{B.1}$$

$$\langle P(k)|\,\bar{q}_1\sigma^{\mu\nu}\,q_\nu b\,|B(p)\rangle = \frac{i f_T^{B\to P}}{m_B + m_P}\left[q^2\,(p+k)^\mu - (m_B^2 - m_P^2)\,q^\mu\right]\,, \tag{B.2}$$

$$\langle V(k,\eta)|\,\bar{q}_1\gamma^\mu b\,|B(p)\rangle = \epsilon^{\mu\nu\rho\sigma}\eta_\nu^* p_\rho k_\sigma \frac{2V^{B\to V}}{m_B + m_V}\,, \tag{B.3}$$

$$\langle V(k,\eta)|\,\bar{q}_1\gamma^\mu\gamma_5 b\,|B(p)\rangle = i\eta_\nu^*\left[g^{\mu\nu}(m_B + m_V)A_1^{B\to V} - \frac{(p+k)^\mu q^\nu}{m_B + m_V}\,A_2^{B\to V} - q^\mu q^\nu\frac{2m_V}{q^2}\left(A_3^{B\to V} - A_0^{B\to V}\right)\right], \tag{B.4}$$

$$\langle V(k,\eta)|\,\bar{q}_1 i\sigma^{\mu\nu}\,q_\nu b\,|B(p)\rangle = 2\epsilon^{\mu\nu\rho\sigma}\eta_\nu^* p_\rho k_\sigma T_1^{B\to V}\,, \tag{B.5}$$

$$\langle V(k,\eta)|\,\bar{q}_1 i\sigma^{\mu\nu}\,q_\nu\gamma_5 b\,|B(p)\rangle = i\eta_\nu^*\Bigg[\left(g^{\mu\nu}(m_B^2 - m_V^2) - (p+k)^\mu q^\nu\right)T_2^{B\to V} + q^\nu\left(q^\mu - \frac{q^2}{m_B^2 - m_V^2}(p+k)^\mu\right)T_3^{B\to V}\Bigg], \tag{B.6}$$

where q_1 denotes a light quark and $p = q + k$. Here and throughout this thesis we omit the explicit q^2 dependence of the FFs, writing simply $F \equiv F(q^2)$. We also define, for convenience,

the following combinations of FFs

$$f_0^{B\to P} \equiv f_+^{B\to P} + \frac{q^2}{m_B^2 - m_P^2} f_-^{B\to P}\,, \tag{B.7}$$

$$A_{12}^{B\to V} \equiv \frac{(m_B + m_V)^2(m_B^2 - m_V^2 - q^2)A_1^{B\to V} - \lambda(q^2)A_2^{B\to V}}{16 m_B m_V^2 (m_B + m_V)}\,, \tag{B.8}$$

$$T_{23}^{B\to V} \equiv \frac{(m_B^2 - m_V^2)(m_B^2 + 3m_V^2 - q^2)T_2^{B\to V} - \lambda(q^2)T_3^{B\to V}}{8 m_B m_V^2 (m_B - m_V)}\,, \tag{B.9}$$

$$T_{23A}^{B\to V} \equiv T_2^{B\to V} + \frac{q^2}{m_B^2 - m_V^2} T_3^{B\to V}\,, \tag{B.10}$$

$$T_{23B}^{B\to V} \equiv \frac{1}{2} T_2^{B\to V} + \frac{1}{2}\left(\frac{q^2}{m_B^2 - m_V^2} - 1\right) T_3^{B\to V}\,, \tag{B.11}$$

and use the notation

$$f_{+/-}^{B\to P} \equiv f_+^{B\to P} + f_-^{B\to P}\,, \tag{B.12}$$

$$A_{30}^{B\to V} \equiv A_3^{B\to V} - A_0^{B\to}\,, \tag{B.13}$$

where $\lambda(q^2) \equiv \lambda(m_B^2, m_V^2, q^2)$ is the Källèn function. Notice that there are only three independent $B \to V$ FFs for the matrix element of the current $\bar{q}_1 \gamma^\mu \gamma_5 b$ and hence there must be a relation between $V^{B\to V}$, $A_1^{B\to V}$, $A_2^{B\to V}$, and $A_3^{B\to V}$. Defining the $B \to V$ FF for a pseudoscalar current as

$$\langle V(k,\eta)|\, \bar{q}_1 \gamma_5 b\, |B(p)\rangle = \left(\frac{2 m_V (\eta^* \cdot q)}{i(m_b + m_{q_1})}\right) A_0^{B\to V}\,, \tag{B.14}$$

such a relation can be found contracting eq. (B.4) with q_μ and using the equation of motion for the quarks:

$$A_3^{B\to V} = \frac{m_B + m_V}{2 m_V} A_1^{B\to V} - \frac{m_B - m_V}{2 m_V} A_2^{B\to V}\,. \tag{B.15}$$

The relations

$$f_+^{B\to P}(q^2 = 0) = f_0^{B\to P}(q^2 = 0) \qquad \text{and} \qquad A_0^{B\to V}(q^2 = 0) = A_3^{B\to V} \tag{B.16}$$

at zero momentum transfer must hold to cancel the kinematical singularities of eq. (B.1) and eq. (B.4). In addition, the algebraic relations between $\sigma^{\mu\nu}$ and $\sigma^{\mu\nu}\gamma_5$ give rise to the identity

$$T_1^{B\to V}(q^2 = 0) = T_2^{B\to V}(q^2 = 0)\,. \tag{B.17}$$

The FFs definitions given above are clearly not unique. A consistent FFs definition has to fulfil all the criteria listed here below.

The FFs definitions must be Lorentz covariant, that is, the l.h.s. and r.h.s. transform under the same representation of the Lorentz group. For example, the l.h.s. of eq. (B.1) transforms as a vector ($J^P = 1^-$), because it is a matrix element of a vector current ($J^P = 1^-$) with a pseudoscalar meson ($J^P = 0^-$) in both the initial and the final state. To construct a

quantity that transforms like a vector on the r.h.s., the only possibility is to use the only two vectors that appear in the process, i.e. the four momenta q^μ and k^μ, each one multiplied by a scalar function. These scalar functions depend on scalar quantities. The only scalar available is q^2, since k^2 is fixed and $k \cdot q$ can be written as a function of q^2. Thus, a FFs definition in this case can be written in the form

$$\langle P(k)|\, \bar{q}_1 \gamma^\mu b\, |B(p)\rangle = a(q^2) q^\mu + b(q^2) k^\mu \,.$$

The definition (B.1), even though it looks more complicated, is more convenient for certain applications. For instance, as shown in section 3.3, taking the modulus squared of eq. (B.1) the dispersive bounds take a simpler form.

It is now easy to understand why the $B \to P$ matrix element of the axial vector current vanishes identically, namely

$$\langle P(k)|\, \bar{q}_1 \gamma^\mu \gamma_5 b\, |B(p)\rangle = 0 \,.$$

This matrix element transforms as an axial vector, but it is not possible to construct a quantity that transforms in the same way using only q^μ and k^μ. The situation is different for the $B \to V$ matrix element of the axial vector current. Here we have an additional independent vector, i.e. the polarisation vector of V, and it is possible to construct a quantity that transform as an axial vector as shown in eq. (B.3).

A matrix element has to be parametrized in the most general way, including all the independent Lorentz structures. The number of independent FFs might be smaller than the number of independent Lorentz structures. As we have seen in the case of eq. (B.4), definitions with redundant FFs are also possible. In such a case, there are relations that allow to get rid of the redundant FFs like eq. (B.15).

A way to find all the independent form factors is to write down all the independent Lorentz structures, using all the vectors available for the case considered (meson momenta and polarisation vectors), and to calculate the helicity amplitudes, whose definition is given below. Let us consider, for example, the matrix element $\langle P(k)|\, \bar{q}_1 \gamma^\mu b\, |B^*(p,\eta)\rangle$ and decompose it into all the available Lorentz structures:

$$\langle P(k)|\, \bar{q}_1 \gamma^\mu b\, |B^*(p,\eta)\rangle = \eta^\mu \bar{A}_1^{B\to V} + p^\mu (\eta\cdot k) \bar{A}_2^{B\to V} + k^\mu (\eta\cdot k) \bar{A}_2^{B\to V} \,. \tag{B.18}$$

We can compute the helicity amplitudes defined as

$$\mathcal{M}_{(i,j)} = (\varepsilon_i^\mu)^* \,\langle P(k)|\, \bar{q}_1 \gamma_\mu b\, |B^*(p,\eta_j)\rangle \,, \tag{B.19}$$

where $\varepsilon^*(i)$ is the polarisation vector of the virtual gauge boson. In the B-meson rest frame, we choose

$$\eta_0 = (0,0,0,1)\,, \qquad \eta_+ = (0,+1,-i,0)\,, \qquad \eta_- = (0,-1,-i,0)\,,$$

$$\varepsilon_0 = \frac{1}{\sqrt{q^2}}(|\vec{q}|,0,0,-q_0)\,, \quad \varepsilon_+ = (0,+1,i,0)\,, \quad \varepsilon_- = (0,-1,i,0)\,, \quad \varepsilon_t = \frac{1}{\sqrt{q^2}} q^\mu \,,$$

where

$$q_0 = m_B - E_P \,, \qquad \text{and} \qquad E_P = \frac{m_B^2 + m_P^2 - q^2}{2 m_B} \,.$$

The subscripts "±" and "0" denote the transverse and longitudinal polarisations, respectively. Since the meson in the final state is on-shell, we do not need to include its time-like polarisation "t". One can show that there are only three non-vanishing linearly independent helicity amplitudes, and hence three independent FFs as in eq. (B.18). In general, the number m of independent helicity amplitudes is always smaller than or equal to the number n of independent Lorentz structures. If it is smaller, there are $n-m$ relations between form the FFs.

Helicity amplitudes are also very useful to diagonalize the FFs definitions, which are more convenient for the calculation of the dispersive bounds.

FFs definitions must be free of singularities and fulfil eventual constraints. We have already mentioned that if a FFs definition contains kinematical singularities, those must be removed by imposing appropriate relations (e.g. see eq. (B.16)). In addition, one should also check that the definitions are consistent. For instance, the r.h.s. of eqs. (B.5)-(B.6) must vanish when contracted with q_μ, since $\sigma_{\mu\nu}$ is an antisymmetric tensor.

B.2 Non-local Matrix Elements in $B \to K^{(*)}\ell\ell$

The non-local matrix elements in $B \to K^{(*)}\ell\ell$ have been widely discussed in chapter 4. Here, we show two different parametrizations in terms of invariant amplitudes.

In subsection 4.1.4 we have defined the non-local matrix element

$$\mathcal{H}^\mu(q,k) = i\int \mathrm{d}^4x\, e^{iq\cdot x}\, \langle K^{(*)}(k)|\mathcal{K}^\mu(x,0)|B(q+k)\rangle\,, \tag{B.20}$$

with

$$\mathcal{K}^\mu(x,0) \equiv T\big\{J^\mu_{cc}(x), (C_1O_1^c + C_2O_2^c)\,(0)\big\}\,, \tag{B.21}$$

which in ref. [14] is parametrized as

$$\mathcal{H}^\mu_{BK}(q,k) = ((k\cdot q)q_\mu - q^2k_\mu)\mathcal{H}_{BK}(q^2)\,, \tag{B.22}$$

$$\begin{aligned}\mathcal{H}^\mu_{BK^*}(q,k) &= \epsilon_{\mu\alpha\beta\gamma}\eta^{*\alpha}q^\beta k^\gamma \mathcal{H}_1(q^2)\\ &\quad + i\left((m_B^2 - m_{K^*}^2)\eta^*_\mu - (\eta^*\cdot q)(2k+q)_\mu\right)\mathcal{H}_2(q^2)\\ &\quad + i(\eta^*\cdot q)\left(q_\mu - \frac{q^2}{m_B^2-m_{K^*}^2}(2k+q)_\mu\right)\mathcal{H}_3(q^2)\,,\end{aligned} \tag{B.23}$$

where

$$\mathcal{H}_i = (3C_1 + C_2)\,\mathcal{V}_i + 2C_2\tilde{\mathcal{V}}_i$$

are the invariant amplitudes. While the functions $\mathcal{V}_i$ can be expressed in terms of the traditional $B \to K^*$ form factors, the functions $\tilde{\mathcal{V}}_i$ parametrize non-local hadronic matrix elements and hence they are not related to the $B \to K^*$ form factors. The definition of the functions $\tilde{\mathcal{V}}_i$ has been given subsection 4.1.4, where we have also computed them using light-cone sum rules.

Alternatively, $\mathcal{H}^\mu$ can also be parametrized as

$$\begin{aligned}\mathcal{H}^\mu_{BK}(q,k) &= m_B^2\, S_0^\mu\, \mathcal{H}_{BK,0}(q^2)\,,\\ \mathcal{H}^\mu_{BK^*}(q,k) &= m_B^2\,\eta^*_\alpha\left(S_\perp^{\alpha\mu}\mathcal{H}_{BK^*,\perp}(q^2) - S_\parallel^{\alpha\mu}\mathcal{H}_{BK^*,\parallel}(q^2) - S_0^{\alpha\mu}\mathcal{H}_{BK^*,0}(q^2)\right)\,,\end{aligned} \tag{B.24}$$

where

$$\mathcal{S}^{\mu}_{(0)} = 2k^{\mu} - \frac{2(q\cdot k)}{q^2}q^{\mu}\,, \quad \mathcal{S}^{\alpha\mu}_{(\|)} = \frac{i\,m_B}{\sqrt{2}}\left[g^{\alpha\mu} - \frac{4(q\cdot k)}{\lambda}q^{\alpha}k^{\mu} + \frac{4m^2_{K^*}}{\lambda}q^{\alpha}q^{\mu}\right]\,,$$
$$\mathcal{S}^{\alpha\mu}_{(\perp)} = \frac{\sqrt{2}\,m_B}{\sqrt{\lambda}}\epsilon^{\alpha\mu kq}\,, \qquad \mathcal{S}^{\alpha\mu}_{(0)} = \frac{4i\,m_{K^*}m_B}{\sqrt{q^2}\,\lambda}\left[q^2q^{\alpha}k^{\mu} - (q\cdot k)\,q^{\alpha}q^{\mu}\right]\,. \tag{B.25}$$

Comparing these two different definitions, we obtain

$$\begin{aligned}
\mathcal{H}_{BK,0} &= -\frac{q^2}{2m_B^2}\,\mathcal{H}_{BK}\,,\\
\mathcal{H}_{BK^*,\perp} &= \frac{\sqrt{\lambda(q^2)}}{\sqrt{2}m_B^3}\,\mathcal{H}_1\,,\\
\mathcal{H}_{BK^*,\|} &= -\sqrt{2}\,\frac{m_B^2 - m_{K^*}^2}{m_B^3}\,\mathcal{H}_2\,,\\
\mathcal{H}_{BK^*,0} &= -\frac{\sqrt{q^2}}{2m_B^3m_{K^*}}\,\left((m_B^2 + 3m_{K^*}^2 - q^2)\mathcal{H}_2 - \frac{\lambda(q^2)}{m_B^2 - m_{K^*}^2}\mathcal{H}_3\right)\,.
\end{aligned} \tag{B.26}$$

Appendix C

LCSRs Input Parameters

In this appendix we list all the inputs used to evaluate numerically the light-cone sum rules (LCSRs) with B-meson light-cone distribution amplitudes (B-LCDAs) presented in this work. For the meson masses we use the Particle Data Group [27] averages, while for the quark masses we take their value in the $\overline{\text{MS}}$ scheme at the scale $\mu = 2\,\text{GeV}$. The values of decay constants of final state mesons, the effective thresholds and the Borel parameters are collected in table C.1. For the B-meson decay constants, we use the most precise lattice QCD predictions taken from ref. [153], which read

$$f_B = (189.4 \pm 1.4)\,\text{MeV}\,, \qquad f_{B_s} = (230.7 \pm 1.3)\,\text{MeV}\,. \tag{C.1}$$

The most critical inputs in our analyses are $\lambda_{B_{(s)},+}$, $\lambda^2_{B_{(s)},E}$ and $\lambda^2_{B_{(s)},H}$, given their substantial uncertainties. They appear in the explicit models of the B-LCDAs (see e.g. refs. [37, 112, 114]) and hence any LCSR strongly depends on these parameters. The first inverse moment $1/\lambda_{B,+}$ of the B-LCDA $\phi_+(\omega)$ is defined as

$$\frac{1}{\lambda_{B,+}(\mu)} \equiv \int_0^\infty \mathrm{d}\omega \frac{\phi_+(\omega,\mu)}{\omega}\,. \tag{C.2}$$

This is clearly a non-perturbative quantity and as such it can be computed with the methods discussed in chapter 3, namely lattice QCD and QCD sum rules. However, unlike the case of light-meson light-cone distribution amplitudes, where lattice QCD has been and is still of great help evaluating the moments of such distribution amplitudes, for the B-LCDAs the situation is different (see e.g. ref. [163]). In fact, the prediction of $\lambda_{B,+}$ involve the calculation of non-local matrix elements, which are extremely challenging to treat for lattice QCD. Therefore, there are no lattice QCD predictions of $\lambda_{B,+}$ and we use the value

$$\lambda_{B,+}(\mu = 1\,\text{GeV}) = (0.46 \pm 0.11)\,\text{GeV}\,, \tag{C.3}$$

obtained with SVZ sum rules in ref. [164].

An alternative method to obtain $\lambda_{B,+}$ was proposed in ref. [38] and further developed in ref. [37]. The idea is to extract $\lambda_{B,+}$ from the experimental data of the radiative decay $B \to \gamma\ell\nu$. Since this decay mode has not been observed so far and there are only bounds on its branching fraction from the BaBar and Belle collaborations [165–168], it is only possible to put a lower limit on the size of $\lambda_{B,+}$. Nevertheless, the Belle II experiment is expected to increase the precision in $B \to \gamma\ell\nu$ significantly, allowing a better estimate of $\lambda_{B,+}$ than the one of eq. (C.3). The same procedure can also be applied using the lattice predictions of the

process	decay constant $f_{P,V}$ [MeV]	s_0 [GeV^2]	M^2 [GeV^2]
$B \to \pi$	130.2 ± 1.4	$0.7 \pm 0.014^{\times}$	1.0 ± 0.5
$B \to K$	155.6 ± 0.4	$1.05 \pm 0.021^{\times}$	1.0 ± 0.5
$B \to D$	212.6 ± 0.5	$[5.8,\ 7.8]^{\dagger}$	4.5 ± 1.5
$B_s \to D_s$	249.9 ± 0.4	$[6.9,\ 11.0]^{\dagger}$	4.5 ± 1.5
$B \to \rho$	213 ± 5	$1.6 \pm 0.032^{\times}$	1.0 ± 0.5
$B \to K^*$	204 ± 7	$[1.4,\ 1.7]^{\dagger}$	1.0 ± 0.5
$B \to D^*$	249 ± 21	$[6.9,\ 8.0]^{\dagger}$	4.5 ± 1.5
$B_s \to D_s^*$	293 ± 19	$[7.9,\ 11.8]^{\dagger}$	4.5 ± 1.5

Table C.1: List of the processes considered with the respective decay constants, effective thresholds s_0 and Borel parameters M^2. We use values of the decay constants given in refs. [66, 153–161], while we use the same Borel windows as in refs. [112, 127]. The values of s_0 marked with $\times$ are taken from refs. [91, 95, 162], with the uncertainties estimated from the uncertainty of the corresponding decay constant. Intervals marked with † represent the union of intervals for the individual form factors obtained with the procedure described in subsection 4.1.2.

$B \to \gamma\ell\nu$ form factors instead of the experimental data, as suggested in ref. [169].

The three-particle local B-to-vacuum matrix elements are parametrized by the constants $\lambda^2_{B_{(s)},E}$ and $\lambda^2_{B_{(s)},H}$, as two-particle local B-to-vacuum matrix elements are parametrized by the mesons decay constants. These parameters were introduced in ref. [132] and are defined by

$$\begin{aligned} \langle 0|\, \bar{q}_2(0) g_s(\vec{\alpha}\cdot\vec{E})\gamma_5 h_v(0)\,|\bar{B}_{q_2}(v)\rangle &= f_B m_B \lambda^2_{B_{q_2},E}\,, \\ \langle 0|\, \bar{q}_2(0) g_s(\vec{\sigma}\cdot\vec{H})\gamma_5 h_v(0)\,|\bar{B}_{q_2}(v)\rangle &= i f_B m_B \lambda^2_{B_{q_2},H} \end{aligned} \tag{C.4}$$

in the B-meson rest frame, where $\alpha^i \equiv \gamma^0\gamma^i$, $E_i \equiv \mathbf{G}_{0i}$ and $H_i \equiv -\frac{1}{2}\varepsilon_{ijk}\mathbf{G}_{jk}$. Equations (C.4) imply that [114]

$$\begin{aligned} \langle 0|\, \bar{q}_2^{\alpha}(0) g_s \mathbf{G}_{\mu\nu}(0) h_v^{\beta}(0)\,|\bar{B}_{q_2}(v)\rangle = &-\frac{i}{12} f_B m_B \lambda^2_{B_{q_2},H}\,\mathrm{Tr}\left\{\gamma_5\Gamma(1+\not{v})\sigma_{\mu\nu}\right\} \\ &-\frac{1}{12} f_B m_B \left(\lambda^2_{B_{q_2},H} - \lambda^2_{B_{q_2},E}\right)\mathrm{Tr}\left\{\gamma_5\Gamma(1+\not{v})(v_\mu\gamma_\nu - v_\nu\gamma_\mu)\right\}\,, \end{aligned} \tag{C.5}$$

where Γ stands for an arbitrary Dirac structure. The parameters $\lambda^2_{B,E}$ and $\lambda^2_{B,H}$ have been calculated with SVZ sum rules as well, obtaining

$$\lambda^2_{B,E}(\mu = 1\,\mathrm{GeV}) = (0.11 \pm 0.06)\,\mathrm{GeV}^2\,, \quad \lambda^2_{B,H}(\mu = 1\,\mathrm{GeV}) = (0.18 \pm 0.07)\,\mathrm{GeV}^2 \tag{C.6}$$

in ref. [132] and

$$\lambda^2_{B,E}(\mu = 1\,\mathrm{GeV}) = (0.03 \pm 0.02)\,\mathrm{GeV}^2\,, \quad \lambda^2_{B,H}(\mu = 1\,\mathrm{GeV}) = (0.06 \pm 0.03)\,\mathrm{GeV}^2 \tag{C.7}$$

in ref. [139]. The result (C.7) includes further QCD corrections with respect to (C.6), which improve the stability of the sum rule and reduce the central values. Thus, we use the results of ref. [139] for our numerical analyses.

Notice that both results give the same ratio

$$\frac{\lambda_{B,H}^2}{\lambda_{B,E}^2} \simeq 0.5\,,$$

in contrast to refs. [14, 112, 127], where the numerical results are obtained for $\lambda_{B,H}^2 = \lambda_{B,E}^2$. Furthermore, the central value used in these references is

$$\lambda_{B,H}^2 = \lambda_{B,E}^2 = \frac{2}{3}\bar{\Lambda}\,,$$

where $\bar{\Lambda} \equiv m_B - m_b$, which is much higher than the one in eq. (C.7). This leads to an overestimate of the three-particle contributions in the LCSRs to calculate the form factors and the soft-gluon contribution to the charm loop, which are discussed in chapter 4.

Since we also consider B_s-meson decays and currently there are no calculations for $\lambda_{B_s,+}$, $\lambda_{B_s,E}^2$ and $\lambda_{B_s,H}^2$, we need to estimate these parameters. We follow the same procedure that we used in ref. [2]. As shown in ref. [132], the relation

$$\lambda_{B_{q_2},+} = \frac{2}{3}\bar{\Lambda}_{q_2} \tag{C.8}$$

holds at leading order in α_s. We therefore use this equation to assess the $SU(3)$ flavor symmetry breaking in the parameter $\lambda_{B_{q_2},+}$. We take the difference between eq. (C.8) with $q = s$ and eq. (C.8) with[1] $q = u/d$, which gives

$$\lambda_{B_s,+} = \lambda_{B,+} + \frac{2}{3}\left(\bar{\Lambda}_s - \bar{\Lambda}\right)\,. \tag{C.9}$$

The advantage of taking the difference is the cancellation of the UV-divergent corrections in fixed-order perturbation theory [170]. Using $\bar{\Lambda}_d = 0.500\,\text{GeV}$, $\bar{\Lambda}_s = 0.590\,\text{GeV}$ and eq. (C.3), we estimate

$$\lambda_{B_s,+}(\mu = 1\,\text{GeV}) = (0.52 \pm 0.11)\,\text{GeV}\,. \tag{C.10}$$

For the parameters $\lambda_{B_s,+}$ and $\lambda_{B_s,E}^2$, given their large uncertainties and their smaller impact on the numerical results, we neglect potential $SU(3)$ flavor symmetry breaking effects, setting $\lambda_{B_s,E}^2 = \lambda_{B,E}^2$ and $\lambda_{B_s,H}^2 = \lambda_{B,H}^2$.

[1] Here and throughout this thesis we work in the isospin limit.

Appendix D

Results for the Form Factors LCSR

In this appendix we give the coefficients of the sum rule (4.29). The normalisation factors are:

$$K^{(f_+^{B\to P})} = K^{(f_{+/-}^{B\to P})} = f_P, \qquad K^{(f_T^{B\to P})} = \frac{f_P(m_B^2 - m_P^2 - q^2)}{m_B(m_B + m_P)},$$

$$K^{(V^{B\to V})} = \frac{2f_V m_V}{m_B(m_B + m_V)}, \qquad K^{(A_1^{B\to V})} = \frac{2f_V m_V(m_B + m_V)}{m_B^2},$$

$$K^{(A_2^{B\to V})} = \frac{2f_V m_V}{m_B + m_V}, \qquad K^{(A_{30}^{B\to V})} = \frac{4f_V m_V^2}{q^2},$$

$$K^{(T_1^{B\to V})} = K^{(T_{23A}^{B\to V})} = K^{(T_{23B}^{B\to V})} = \frac{2f_V m_V}{m_B}.$$

In the next sections we give the $C_n^{(F,\psi)}$ coefficients of eqs. (4.30) and (4.31). For all the form factors, the following relations hold among the three-particle contributions:

$$C_n^{(F,\bar{\bar{\psi}}_4)} = -C_n^{(F,\bar{\bar{\phi}}_3)} - C_n^{(F,\bar{\bar{\phi}}_4)}, \qquad C_n^{(F,\bar{\bar{\chi}}_4)} = C_n^{(F,\bar{\bar{\phi}}_3)} - C_n^{(F,\bar{\bar{\phi}}_4)}.$$

D.1 $B \to P$

Two-particle Contributions

The coefficients of eq. (4.30), for the two-particle DAs, are listed in the following. For $f_+^{B\to P}$ we find the non-vanishing coefficients:

$$C_1^{(f_+^{B\to P},\phi_+)} = -\bar{\sigma}\,,$$

$$C_2^{(f_+^{B\to P},\bar{\phi})} = -m_B\bar{\sigma}^2\,,$$

$$C_2^{(f_+^{B\to P},g_+)} = -4\bar{\sigma}, \qquad C_3^{(f_+^{B\to P},g_+)} = 8m_1^2\bar{\sigma}\,,$$

$$C_3^{(f_+^{B\to P},\bar{g})} = -8m_B\bar{\sigma}^2\,, \qquad C_4^{(f_+^{B\to P},\bar{g})} = 24m_1^2 m_B\bar{\sigma}^2\,.$$

For $f_{+/-}^{B\to P}$ we find:

$$C_1^{(f_{+/-}^{B\to P},\phi_+)} = 2\sigma - 1\,,$$

$$C_2^{(f_{+/-}^{B\to P},\bar\phi)} = 2m_B\sigma\bar\sigma - m_1\,,$$

$$C_2^{(f_{+/-}^{B\to P},g_+)} = 4(2\sigma-1)\,, \qquad C_3^{(f_{+/-}^{B\to P},g_+)} = -8m_1^2(2\sigma-1)\,,$$

$$C_3^{(f_{+/-}^{B\to P},\bar g)} = 16m_B\sigma\bar\sigma\,, \qquad C_4^{(f_{+/-}^{B\to P},\bar g)} = 24m_1^2(m_1-2m_B\sigma\bar\sigma)\,.$$

For $f_T^{B\to P}$ we find:

$$C_1^{(f_T^{B\to P},\bar\phi)} = \frac{1}{m_B}, \qquad C_2^{(f_T^{B\to P},\bar\phi)} = \frac{-(m_B^2\bar\sigma^2 - m_1^2 + 2q^2\sigma - q^2)}{m_B},$$

$$C_2^{(f_T^{B\to P},\bar g)} = \frac{8}{m_B}, \qquad C_3^{(f_T^{B\to P},\bar g)} = \frac{-8(m_B^2\bar\sigma^2 + 2m_1^2 + 2q^2\sigma - q^2)}{m_B},$$

$$C_4^{(f_T^{B\to P},\bar g)} = \frac{24m_1^2(m_B^2\bar\sigma^2 - m_1^2 + 2q^2\sigma - q^2)}{m_B}.$$

Three-particle Contributions

The coefficients of eq. (4.31), for the three-particle DAs, for $f_+^{B\to P}$ follow. For ϕ_3:

$$C_2^{(f_+^{B\to P},\phi_3)} = -\frac{2m_1}{m_B} - u\bar\sigma\,,$$

$$C_2^{(f_+^{B\to P},\bar\phi_3)} = \frac{u}{m_B}\,, \qquad C_3^{(f_+^{B\to P},\bar\phi_3)} = -\frac{2}{m_B}(u(m_B^2\bar\sigma^2+q^2) + 4m_Bm_1\bar\sigma + um_1^2)\,,$$

$$C_4^{(f_+^{B\to P},\bar{\bar\phi}_3)} = -6m_1\bar\sigma(2m_B\bar\sigma + m_1(2u-1))\,.$$

For ϕ_4:

$$C_2^{(f_+^{B\to P},\phi_4)} = \bar\sigma(1-u)\,,$$

$$C_2^{(f_+^{B\to P},\bar\phi_4)} = \frac{u-1}{m_B}\,,$$

$$C_3^{(f_+^{B\to P},\bar\phi_4)} = 2um_B\bar\sigma^2 + 4m_1\bar\sigma + 2\frac{(1-u)(m_1^2+q^2)}{m_B}\,,$$

$$C_3^{(f_+^{B\to P},\bar{\bar\phi}_4)} = \frac{2}{m_B}(m_B\bar\sigma(2u-1) + 2m_1)\,,$$

$$C_4^{(f_+^{B\to P},\bar{\bar\phi}_4)} = \frac{6}{m_B}(m_B^2\bar\sigma^2 - q^2)(m_B\bar\sigma(2u-1) + 2m_1)\,.$$

For ψ_4:

$$C_2^{(f_+^{B\to P},\bar\psi_4)} = \frac{1-2u}{m_B}\,, \qquad C_3^{(f_+^{B\to P},\bar\psi_4)} = \frac{2}{m_B}(2u-1)(m_1^2 - m_B^2\bar\sigma^2 + q^2)\,.$$

For χ_4:

$$C_2^{(f_+^{B\to P},\bar\chi_4)} = \frac{1}{m_B}\,,$$

$$C_3^{(f_+^{B\to P},\bar{\chi}_4)} = -\frac{2}{m_B}(m_B^2\bar{\sigma}^2(2u-1) + 4m_B m_1\bar{\sigma} + m_1^2 + q^2)\,.$$

The coefficients of eq. (4.31), for the three-particle DAs, for $f_{+/-}^{B\to P}$ follow. For ϕ_3:

$$\begin{aligned}
C_2^{(f_{+/-}^{B\to P},\phi_3)} =& (3-2\bar{\sigma})u - \frac{4m_1}{m_B}\,,\\
C_2^{(f_{+/-}^{B\to P},\bar{\phi}_3)} =& 2u\frac{(\bar{\sigma}-1)}{m_B\bar{\sigma}}\,,\\
C_3^{(f_{+/-}^{B\to P},\bar{\phi}_3)} =& -\frac{2}{m_B\bar{\sigma}}(m_B^2\bar{\sigma}^2(2\bar{\sigma}-3)u\\
&+(2\bar{\sigma}-1)(4m_B m_1\bar{\sigma}+uq^2)+um_1^2(2\bar{\sigma}+1))\,,\\
C_4^{(f_{+/-}^{B\to P},\bar{\bar{\phi}}_3)} =& -6m_1(4m_B(\bar{\sigma}-1)\bar{\sigma}+m_1(2\bar{\sigma}+1)(2u-1))\,.
\end{aligned}$$

For ϕ_4:

$$\begin{aligned}
C_2^{(f_{+/-}^{B\to P},\phi_4)} =& (1-u)(2\bar{\sigma}+1)\,,\\
C_2^{(f_{+/-}^{B\to P},\bar{\phi}_4)} =& \frac{2}{m_B\bar{\sigma}}(\bar{\sigma}-1)(u-1)\,,\\
C_3^{(f_{+/-}^{B\to P},\bar{\phi}_4)} =& \frac{2}{m_B\bar{\sigma}}(m_B^2\bar{\sigma}^2(2\bar{\sigma}u-u-1)+m_B m_1\bar{\sigma}(4\bar{\sigma}-1)\\
&+m_1^2(2\bar{\sigma}+1)(1-u)+q^2(2\bar{\sigma}-2\bar{\sigma}u+u-1))\,,\\
C_3^{(f_{+/-}^{B\to P},\bar{\bar{\phi}}_4)} =& \frac{2}{m_B\bar{\sigma}}(2m_B(\bar{\sigma}-2)\bar{\sigma}(2u-1)+m_1(4\bar{\sigma}-3))\,,\\
C_4^{(f_{+/-}^{B\to P},\bar{\bar{\phi}}_4)} =& \frac{6}{m_B\bar{\sigma}}(m_1(4\bar{\sigma}-1)(m_B^2\bar{\sigma}^2-q^2)+2m_B(\bar{\sigma}-1)\bar{\sigma}(2u-1)(m_B^2\bar{\sigma}^2-q^2))\\
&+\frac{6}{m_B\bar{\sigma}}(m_B m_1^2\bar{\sigma}(2u-1)-m_1^3)\,.
\end{aligned}$$

For ψ_4:

$$\begin{aligned}
C_2^{(f_{+/-}^{B\to P},\bar{\psi}_4)} =& \frac{2}{m_B\bar{\sigma}}(\bar{\sigma}-1)(1-2u)\,,\\
C_3^{(f_{+/-}^{B\to P},\bar{\psi}_4)} =& \frac{2}{m_B\bar{\sigma}}((2\bar{\sigma}-1)(2u-1)(q^2-m_B^2\bar{\sigma}^2)-2m_B m_1\bar{\sigma}+m_1^2(2\bar{\sigma}+1)(2u-1))\,.
\end{aligned}$$

For χ_4:

$$\begin{aligned}
C_2^{(f_{+/-}^{B\to P},\bar{\chi}_4)} =& \frac{2}{m_B\bar{\sigma}}(\bar{\sigma}-1)\,,\\
C_3^{(f_{+/-}^{B\to P},\bar{\chi}_4)} =& -\frac{2}{m_B\bar{\sigma}}(m_B^2\bar{\sigma}^2(4u(\bar{\sigma}-1)-2\bar{\sigma}+1)\\
&+4m_B m_1\bar{\sigma}(2\bar{\sigma}-1)+m_1^2(2\bar{\sigma}+1)+q^2(2\bar{\sigma}-1))\,.
\end{aligned}$$

The coefficients of eq. (4.31), for the three-particle DAs, for $f_T^{B\to P}$ follow. For ϕ_3:

$$
\begin{aligned}
C_1^{(f_T^{B\to P},\phi_3)} &= \frac{2u}{m_B^2\bar\sigma}\,,\\
C_2^{(f_T^{B\to P},\phi_3)} &= -\frac{2u}{m_B^2\bar\sigma}(m_B^2\bar\sigma^2 - m_1^2 - 2q^2\bar\sigma + q^2)\,,\\
C_2^{(f_T^{B\to P},\bar\phi_3)} &= \frac{4}{m_B^2\bar\sigma}(m_B\bar\sigma u + m_1)\,,\\
C_3^{(f_T^{B\to P},\bar\phi_3)} &= -\frac{4}{m_B^2\bar\sigma}(m_B^2\bar\sigma^2 - m_1^2 - 2q^2\bar\sigma + q^2)(m_B\bar\sigma u + m_1)\,,\\
C_3^{(f_T^{B\to P},\bar{\bar\phi}_3)} &= 12\frac{m_1}{m_B}\,,\\
C_4^{(f_T^{B\to P},\bar{\bar\phi}_3)} &= -12\frac{m_1}{m_B}(m_B^2\bar\sigma^2 - m_1^2 - 2q^2\bar\sigma + q^2)\,.
\end{aligned}
$$

For ϕ_4:

$$
\begin{aligned}
C_2^{(f_T^{B\to P},\bar\phi_4)} &= -\frac{2}{m_B}\,,\\
C_3^{(f_T^{B\to P},\bar\phi_4)} &= \frac{2}{m_B}(m_B^2\bar\sigma^2 - m_1^2 - 2q^2\bar\sigma + q^2)\,,\\
C_2^{(f_T^{B\to P},\bar{\bar\phi}_4)} &= -\frac{4}{m_B^2\bar\sigma}(2u-1)\,,\\
C_3^{(f_T^{B\to P},\bar{\bar\phi}_4)} &= \frac{2}{m_B^2\bar\sigma}(2u-1)(m_1^2 - m_B^2\bar\sigma^2 + q^2(5-4\bar\sigma))\,,\\
C_4^{(f_T^{B\to P},\bar{\bar\phi}_4)} &= \frac{6}{m_B^2\bar\sigma}(2u-1)(m_1^2 - m_B^2\bar\sigma^2 + q^2)(m_1^2 - m_B^2\bar\sigma^2 + q^2(2\bar\sigma-1))\,.
\end{aligned}
$$

For ψ_4:

$$
\begin{aligned}
C_2^{(f_T^{B\to P},\bar\psi_4)} &= -\frac{4m_1}{m_B^2\bar\sigma}\,,\\
C_3^{(f_T^{B\to P},\bar\psi_4)} &= \frac{4m_1}{m_B^2\bar\sigma}(m_B^2\bar\sigma^2 - m_1^2 - 2q^2\bar\sigma + q^2)\,.
\end{aligned}
$$

For χ_4:

$$
\begin{aligned}
C_2^{(f_T^{B\to P},\bar\chi_4)} &= \frac{4}{m_B^2\bar\sigma}(m_B\bar\sigma u + m_1)\,,\\
C_3^{(f_T^{B\to P},\bar\chi_4)} &= -\frac{4}{m_B^2\bar\sigma}(m_B\bar\sigma u + m_1)(m_B^2\bar\sigma^2 - m_1^2 - 2q^2\bar\sigma + q^2)\,.
\end{aligned}
$$

D.2 $B \to V$

Two-particle Contributions

The coefficients of eq. (4.30), for the two-particle DAs, are listed in the following. For $V^{B\to V}$ we find:

$$C_1^{(V^{B\to V},\phi_+)} = -\frac{1}{m_B}\,,$$
$$C_2^{(V^{B\to V},\bar{\phi})} = -\frac{m_1}{m_B}\,,$$
$$C_2^{(V^{B\to V},g_+)} = -\frac{4}{m_B}, \qquad C_3^{(V^{B\to V},g_+)} = \frac{8m_1^2}{m_B}\,,$$
$$C_4^{(V^{B\to V},\bar{g})} = \frac{24m_1^3}{m_B}\,.$$

For $A_1^{B\to V}$ we find:

$$C_1^{(A_1^{B\to V},\phi_+)} = \frac{q^2-(m_B\bar{\sigma}+m_1)^2}{m_B^2\bar{\sigma}}\,,$$
$$C_1^{(A_1^{B\to V},\bar{\phi})} = -\frac{m_1}{m_B^2\bar{\sigma}}, \qquad C_2^{(A_1^{B\to V},\bar{\phi})} = \frac{m_1(q^2-(m_B\bar{\sigma}+m_1)^2)}{m_B^2\bar{\sigma}}\,,$$
$$C_1^{(A_1^{B\to V},g_+)} = -\frac{4}{m_B^2\bar{\sigma}}, \qquad C_2^{(A_1^{B\to V},g_+)} = \frac{4(q^2-m_B^2\bar{\sigma}^2+m_1^2)}{m_B^2\bar{\sigma}}\,,$$
$$C_3^{(A_1^{B\to V},g_+)} = \frac{8m_1^2((m_B\bar{\sigma}+m_1)^2-q^2)}{m_B^2\bar{\sigma}}\,,$$
$$C_2^{(A_1^{B\to V},\bar{g})} = -\frac{8}{m_B}\,, \qquad C_3^{(A_1^{B\to V},\bar{g})} = \frac{8m_1^2(2m_B\bar{\sigma}+3m_1)}{m_B^2\bar{\sigma}}\,,$$
$$C_4^{(A_1^{B\to V},\bar{g})} = \frac{24m_1^3((m_B\bar{\sigma}+m_1)^2-q^2)}{m_B^2\bar{\sigma}}\,.$$

For $A_2^{B\to V}$ we find:

$$C_1^{(A_2^{B\to V},\phi_+)} = 2\sigma-1\,,$$
$$C_2^{(A_2^{B\to V},\bar{\phi})} = 2m_B\sigma\bar{\sigma}-m_1\,,$$
$$C_2^{(A_2^{B\to V},g_+)} = 4(2\sigma-1)\,, \qquad C_3^{(A_2^{B\to V},g_+)} = -8m_1^2(2\sigma-1)\,,$$
$$C_3^{(A_2^{B\to V},\bar{g})} = 16m_B\sigma\bar{\sigma}\,, \qquad C_4^{(A_2^{B\to V},\bar{g})} = 24m_1^2(m_1-2m_B\sigma\bar{\sigma})\,.$$

For $A_{30}^{B\to V}$ we find:

$$C_1^{(A_{30}^{B\to V},\phi_+)} = 2\sigma+1\,,$$

$$C_2^{(A_{30}^{B\to V},\bar{\phi})} = m_1 - 2m_B\sigma(\sigma+1)\,,$$

$$C_2^{(A_{30}^{B\to V},g_+)} = 4(2\sigma+1)\,, \qquad C_3^{(A_{30}^{B\to V},g_+)} = -8m_1^2(2\sigma+1)\,,$$

$$C_3^{(A_{30}^{B\to V},\bar{g})} = -16m_B\sigma(\sigma+1)\,, \qquad C_4^{(A_{30}^{B\to V},\bar{g})} = 24m_1^2(2m_B\sigma(\sigma+1)-m_1)\,.$$

For $T_1^{B\to V}$ we find:

$$C_1^{(T_1^{B\to V},\phi_+)} = -\frac{(m_B\bar{\sigma}+m_1)}{m_B}\,,$$

$$C_2^{(T_1^{B\to V},\bar{\phi})} = -m_1\frac{(m_B\bar{\sigma}+m_1)}{m_B}\,,$$

$$C_2^{(T_1^{B\to V},g_+)} = -4\bar{\sigma}\,, \qquad C_3^{(T_1^{B\to V},g_+)} = 8m_1^2\frac{(m_B\bar{\sigma}+m_1)}{m_B}\,,$$

$$C_2^{(T_1^{B\to V},\bar{g})} = -\frac{4}{m_B}\,, \qquad C_3^{(T_1^{B\to V},\bar{g})} = \frac{8m_1^2}{m_B}\,,$$

$$C_4^{(T_1^{B\to V},\bar{g})} = 24m_1^3\frac{(m_B\bar{\sigma}+m_1)}{m_B}\,.$$

For $T_{23A}^{B\to V}$ we find:

$$C_1^{(T_{23A}^{B\to V},\phi_+)} = -\frac{(m_B\bar{\sigma}+m_1)}{m_B}\,,$$

$$C_2^{(T_{23A}^{B\to V},\bar{\phi})} = -\frac{(m_1(m_B\bar{\sigma}+m_1)-2q^2\sigma)}{m_B}\,,$$

$$C_2^{(T_{23A}^{B\to V},g_+)} = -4\bar{\sigma}\,, \qquad C_3^{(T_{23A}^{B\to V},g_+)} = 8m_1^2\frac{(m_B\bar{\sigma}+m_1)}{m_B}\,,$$

$$C_2^{(T_{23A}^{B\to V},\bar{g})} = -\frac{4}{m_B}\,, \qquad C_3^{(T_{23A}^{B\to V},\bar{g})} = \frac{8(m_1^2+2q^2\sigma)}{m_B}\,,$$

$$C_4^{(T_{23A}^{B\to V},\bar{g})} = 24m_1^2\frac{(m_1(m_B\bar{\sigma}+m_1)-2q^2\sigma)}{m_B}\,.$$

For $T_{23B}^{B\to V}$ we find:

$$C_1^{(T_{23B}^{B\to V},\phi_+)} = \frac{(m_B\sigma-m_1)}{m_B}\,,$$

$$C_1^{(T_{23B}^{B\to V},\bar{\phi})} = \frac{\sigma}{m_B\bar{\sigma}}\,, \qquad C_2^{(T_{23B}^{B\to V},\bar{\phi})} = \frac{m_Bm_1\sigma\bar{\sigma}-m_B^2\sigma\bar{\sigma}^2+(2\sigma-1)(m_1^2-q^2\sigma)}{m_B\bar{\sigma}}\,,$$

$$C_2^{(T_{23B}^{B\to V},g_+)} = 4\sigma\,, \qquad C_3^{(T_{23B}^{B\to V},g_+)} = 8m_1^2\frac{(m_1-m_B\sigma)}{m_B}\,,$$

$$C_2^{(T_{23B}^{B\to V},\bar{g})} = 4\frac{(3\sigma-1)}{m_B\bar{\sigma}}\,, \qquad C_3^{(T_{23B}^{B\to V},\bar{g})} = -8\frac{\sigma(m_B^2\bar{\sigma}^2+3m_1^2+q^2(2\sigma-1))-m_1^2}{m_B\bar{\sigma}}\,,$$

$$C_4^{(T_{23B}^{B\to V},\bar{g})} = \frac{24m_1^2}{m_B\bar{\sigma}}(m_B^2\sigma\bar{\sigma}^2 - m_Bm_1\sigma\bar{\sigma} + (2\sigma-1)(q^2\sigma - m_1^2))\,.$$

Where $T_{23A}^{B\to V}$ and $T_{23B}^{B\to V}$ are defined in eqs. (4.24) and (4.25).

Three-particle Contributions

The coefficients of eq. (4.31), for the three-particle DAs, for $V^{B\to V}$ follow. For ϕ_3:

$$\begin{aligned}
C_2^{(V^{B\to V},\phi_3)} &= \frac{u}{m_B}\,,\\
C_2^{(V^{B\to V},\bar{\phi}_3)} &= \frac{2u}{m_B^2\bar{\sigma}}\,,\\
C_3^{(V^{B\to V},\bar{\phi}_3)} &= \frac{2u}{m_B^2\bar{\sigma}}(m_B^2\bar{\sigma}^2 + m_1^2 - q^2)\,,\\
C_4^{(V^{B\to V},\bar{\bar{\phi}}_3)} &= \frac{6m_1^2}{m_B}(2u-1)\,.
\end{aligned}$$

For ϕ_4:

$$\begin{aligned}
C_2^{(V^{B\to V},\phi_4)} &= \frac{u-1}{m_B}\,,\\
C_2^{(V^{B\to V},\bar{\phi}_4)} &= 2\frac{(u-1)}{m_B^2\bar{\sigma}}\,,\\
C_3^{(V^{B\to V},\bar{\phi}_4)} &= \frac{2}{m_B^2\bar{\sigma}}(u-1)(m_1^2-q^2) - \frac{2m_1}{m_B} + 2\bar{\sigma}(u-1)\,,\\
C_3^{(V^{B\to V},\bar{\bar{\phi}}_4)} &= -\frac{6m_1}{m_B^2\bar{\sigma}}\,,\\
C_4^{(V^{B\to V},\bar{\bar{\phi}}_4)} &= -\frac{6m_1}{m_B^2\bar{\sigma}}(m_B^2\bar{\sigma}^2 + m_Bm_1\bar{\sigma}(1-2u) + m_1^2 - q^2)\,.
\end{aligned}$$

For ψ_4:

$$\begin{aligned}
C_2^{(V^{B\to V},\bar{\psi}_4)} &= \frac{2-4u}{m_B^2\bar{\sigma}}\,,\\
C_3^{(V^{B\to V},\bar{\psi}_4)} &= \frac{2}{m_B^2\bar{\sigma}}((2u-1)(q^2 - m_B^2\bar{\sigma}^2) + 2m_Bm_1\bar{\sigma} + m_1^2(1-2u))\,.
\end{aligned}$$

For χ_4:

$$\begin{aligned}
C_2^{(V^{B\to V},\bar{\chi}_4)} &= \frac{2}{m_B^2\bar{\sigma}}\,,\\
C_3^{(V^{B\to V},\bar{\chi}_4)} &= \frac{2}{m_B^2\bar{\sigma}}(m_1^2 - q^2) + 2\bar{\sigma}\,.
\end{aligned}$$

The coefficients of eq. (4.31), for the three-particle DAs, for $A_1^{B\to V}$ follow. For ϕ_3:

$$
\begin{aligned}
C_1^{(A_1^{B\to V},\phi_3)} &= \frac{u}{m_B^2\bar\sigma}\,,\\
C_2^{(A_1^{B\to V},\phi_3)} &= u\frac{(m_1^2-q^2)}{m_B^2\bar\sigma}+\frac{2m_1}{m_B}+u\bar\sigma\,,\\
C_1^{(A_1^{B\to V},\bar\phi_3)} &= \frac{2u}{m_B^3\bar\sigma^2}\,,\\
C_2^{(A_1^{B\to V},\bar\phi_3)} &= \frac{1}{m_B^3\bar\sigma^2}(4m_Bm_1\bar\sigma-2um_B^2\bar\sigma^2+4m_1^2u-4q^2u)\,,\\
C_3^{(A_1^{B\to V},\bar\phi_3)} &= \frac{2}{m_B^3\bar\sigma^2}(m_B^2\bar\sigma^2+m_1^2-q^2)(m_B^2\bar\sigma^2u+2m_Bm_1\bar\sigma+m_1^2u-q^2u)\,,\\
C_3^{(A_1^{B\to V},\bar{\bar\phi}_3)} &= \frac{6m_1}{m_B^2\bar\sigma}(2m_B\bar\sigma+m_1(2u-1))\,.\\
C_4^{(A_1^{B\to V},\bar{\bar\phi}_3)} &= \frac{6m_1^2}{m_B^2\bar\sigma}(m_B^2\bar\sigma^2(2u-1)+2m_Bm_1\bar\sigma+(2u-1)(m_1^2-q^2))\,.
\end{aligned}
$$

For ϕ_4:

$$
\begin{aligned}
C_1^{(A_1^{B\to V},\phi_4)} =&\frac{u-1}{m_B^2\bar\sigma}\,,\\
C_2^{(A_1^{B\to V},\phi_4)} =&\frac{u-1}{m_B^2\bar\sigma}(m_B^2\bar\sigma^2+m_1^2-q^2)\,,\\
C_1^{(A_1^{B\to V},\bar\phi_4)} =&2\frac{(u-1)}{m_B^3\bar\sigma^2}\,,\\
C_2^{(A_1^{B\to V},\bar\phi_4)} =&\frac{1}{m_B^3\bar\sigma^2}(2m_B^2\bar\sigma^2u-2m_Bm_1\bar\sigma+4(u-1)(m_1^2-q^2))\,,\\
C_3^{(A_1^{B\to V},\bar\phi_4)} =&\frac{2}{m_B^3\bar\sigma^2}((m_B\bar\sigma+m_1)^2-q^2)(m_B^2\bar\sigma^2(u-1)\\
&+m_Bm_1\bar\sigma(1-2u)+(u-1)(m_1^2-q^2))\,,\\
C_2^{(A_1^{B\to V},\bar{\bar\phi}_4)} =&\frac{2}{m_B^3\bar\sigma^2}(2m_B\bar\sigma(2u-1)-3m_1)\,,\\
C_3^{(A_1^{B\to V},\bar{\bar\phi}_4)} =&\frac{12m_1}{m_B^3\bar\sigma^2}(q^2-m_1^2)-\frac{2}{m_B^2\bar\sigma}(2u-1)(m_1^2+2q^2)-\frac{4m_1}{m_B}+4\bar\sigma(2u-1)\,,\\
C_4^{(A_1^{B\to V},\bar{\bar\phi}_4)} =&-\frac{6m_1}{m_B^3\bar\sigma^2}(m_Bm_1\bar\sigma(2u-1)(m_B^2\bar\sigma^2-q^2)+(q^2-m_B^2\bar\sigma^2)^2\\
&+m_1^3m_B\bar\sigma(2u-1)+m_1^4-2m_1^2q^2)\,.
\end{aligned}
$$

For ψ_4:

$$C_1^{(A_1^{B\to V},\bar{\psi}_4)} = -\frac{2}{m_B^3\bar{\sigma}^2}(2u-1)\,,$$

$$C_2^{(A_1^{B\to V},\bar{\psi}_4)} = -\frac{2}{m_B^3\bar{\sigma}^2}(2u-1)(m_B^2\bar{\sigma}^2+2m_1^2-2q^2)\,,$$

$$C_3^{(A_1^{B\to V},\bar{\psi}_4)} = -\frac{2}{m_B^3\bar{\sigma}^2}(2u-1)((q^2-m_B^2\bar{\sigma}^2)^2-2m_1^2(m_B^2\bar{\sigma}^2+q^2)+m_1^4)\,.$$

For χ_4:

$$C_1^{(A_1^{B\to V},\bar{\chi}_4)} = \frac{2}{m_B^3\bar{\sigma}^2}\,,$$

$$C_2^{(A_1^{B\to V},\bar{\chi}_4)} = \frac{2}{m_B^3\bar{\sigma}^2}(m_B^2\bar{\sigma}^2(1-2u)+2m_Bm_1\bar{\sigma}+2m_1^2-2q^2)\,,$$

$$\begin{aligned}C_3^{(A_1^{B\to V},\bar{\chi}_4)} =& \frac{2}{m_B^3\bar{\sigma}^2}(m_B^4\bar{\sigma}^4+2m_B^3m_1\bar{\sigma}^3-2m_B^2\bar{\sigma}^2(m_1^2(1-2u)+q^2)\\ &+2m_Bm_1\bar{\sigma}(m_1^2-q^2)+(m_1^2-q^2)^2)\,.\end{aligned}$$

The coefficients of eq. (4.31), for the three-particle DAs, for $A_2^{B\to V}$ follow. For ϕ_3:

$$C_2^{(A_2^{B\to V},\phi_3)} = \frac{4m_1}{m_B}-(2\bar{\sigma}+1)u\,,$$

$$C_2^{(A_2^{B\to V},\bar{\phi}_3)} = \frac{2u}{m_B\bar{\sigma}}(\bar{\sigma}-1)\,,$$

$$\begin{aligned}C_3^{(A_2^{B\to V},\bar{\phi}_3)} =& \frac{1}{m_B\bar{\sigma}}(2u(m_B^2(3-2\bar{\sigma})\bar{\sigma}^2-2q^2\bar{\sigma}+q^2)\\ &+8m_Bm_1\bar{\sigma}(2\bar{\sigma}-1)-2m_1^2(2\bar{\sigma}u+u))\,,\end{aligned}$$

$$C_4^{(A_2^{B\to V},\bar{\bar{\phi}}_3)} = 6m_1(4m_B(\bar{\sigma}-1)\bar{\sigma}+m_1(2\bar{\sigma}+(6-4\bar{\sigma})u-3))\,.$$

For ϕ_4:

$$C_2^{(A_2^{B\to V},\phi_4)} = (1-u)(2\bar{\sigma}-3)\,,$$

$$C_2^{(A_2^{B\to V},\bar{\phi}_4)} = \frac{2}{m_B\bar{\sigma}}(u-1)(\bar{\sigma}-1)\,,$$

$$\begin{aligned}C_3^{(A_2^{B\to V},\bar{\phi}_4)} =& \frac{2}{m_B\bar{\sigma}}(m_B^2\bar{\sigma}^2(2\bar{\sigma}u-u-1)+m_Bm_1(3-4\bar{\sigma})\bar{\sigma}+m_1^2(2\bar{\sigma}+1)(1-u)\\ &+q^2(2\bar{\sigma}-2\bar{\sigma}u+u-1))\,,\end{aligned}$$

$$C_3^{(A_2^{B\to V},\bar{\bar{\phi}}_4)} = \frac{2}{m_B\bar{\sigma}}(2m_B(\bar{\sigma}-2)\bar{\sigma}(2u-1)+m_1(9-4\bar{\sigma}))\,,$$

$$\begin{aligned}C_4^{(A_2^{B\to V},\bar{\bar{\phi}}_4)} =& \frac{6}{m_B\bar{\sigma}}(2m_B(\bar{\sigma}-1)\bar{\sigma}(2u-1)(m_B^2\bar{\sigma}^2-q^2)\\ &+3m_Bm_1^2\bar{\sigma}(1-2u)+3m_1^3+m_1(4\bar{\sigma}-3)(q^2-m_B^2\bar{\sigma}^2))\,.\end{aligned}$$

For ψ_4:

$$\begin{aligned}
C_2^{(A_2^{B\to V},\bar{\psi}_4)} =& \frac{2}{m_B\bar{\sigma}}(1-2u)(\bar{\sigma}-1)\,,\\
C_3^{(A_2^{B\to V},\bar{\psi}_4)} =& \frac{1}{m_B\bar{\sigma}}(2(2\bar{\sigma}-1)(2u-1)(q^2-m_B^2\bar{\sigma}^2)\\
&-4m_Bm_1\bar{\sigma}+2m_1^2(2\bar{\sigma}+1)(2u-1))\,.
\end{aligned}$$

For χ_4:

$$\begin{aligned}
C_2^{(A_2^{B\to V},\bar{\chi}_4)} =& \frac{2}{m_B\bar{\sigma}}(\bar{\sigma}-1)\,,\\
C_3^{(A_2^{B\to V},\bar{\chi}_4)} =& -\frac{2}{m_B\bar{\sigma}}(m_B^2\bar{\sigma}^2(-2\bar{\sigma}+4(\bar{\sigma}-1)u+1)\\
&+4m_Bm_1(1-2\bar{\sigma})\bar{\sigma}+m_1^2(2\bar{\sigma}+1)+q^2(2\bar{\sigma}-1))\,.
\end{aligned}$$

The coefficients of eq. (4.31), for the three-particle DAs, for $A_{30}^{B\to V}$ follow. For ϕ_3:

$$\begin{aligned}
C_2^{(A_{30}^{B\to V},\phi_3)} =& \frac{4m_1}{m_B}+(5-2\bar{\sigma})u\,,\\
C_2^{(A_{30}^{B\to V},\bar{\phi}_3)} =& \frac{2u}{m_B\bar{\sigma}}(\bar{\sigma}-3)\,,\\
C_3^{(A_{30}^{B\to V},\bar{\phi}_3)} =& -\frac{2}{m_B\bar{\sigma}}(u(m_B^2\bar{\sigma}(\bar{\sigma}(2\bar{\sigma}-9)+8)+q^2(2\bar{\sigma}-3))\\
&+4m_Bm_1(3-2\bar{\sigma})\bar{\sigma}+m_1^2(2\bar{\sigma}+3)u)\,,\\
C_4^{(A_{30}^{B\to V},\bar{\bar{\phi}}_3)} =& 6m_1(4m_B(\bar{\sigma}-2)(\bar{\sigma}-1)+m_1(2\bar{\sigma}+(2-4\bar{\sigma})u-1))\,.
\end{aligned}$$

For ϕ_4:

$$\begin{aligned}
C_2^{(A_{30}^{B\to V},\phi_4)} =& 2\bar{\sigma}-2\bar{\sigma}u+u-1\,,\\
C_2^{(A_{30}^{B\to V},\bar{\phi}_4)} =& \frac{2}{m_B\bar{\sigma}}(u-1)(\bar{\sigma}-3)\,,\\
C_3^{(A_{30}^{B\to V},\bar{\phi}_4)} =& \frac{1}{m_B\bar{\sigma}}(2m_B^2\bar{\sigma}(2\bar{\sigma}^2u-3\bar{\sigma}(u+1)+4)+2m_Bm_1(5-4\bar{\sigma})\bar{\sigma}\\
&-2m_1^2(2\bar{\sigma}+3)(u-1)-2q^2(2\bar{\sigma}-3)(u-1))\,,\\
C_3^{(A_{30}^{B\to V},\bar{\bar{\phi}}_4)} =& \frac{2}{m_B\bar{\sigma}}(2m_B((\bar{\sigma}-6)\bar{\sigma}+6)(2u-1)+m_1(15-4\bar{\sigma}))\,,\\
C_4^{(A_{30}^{B\to V},\bar{\bar{\phi}}_4)} =& \frac{6}{m_B\bar{\sigma}}(2m_B^3(\bar{\sigma}-2)(\bar{\sigma}-1)\bar{\sigma}^2(2u-1)+m_B^2m_1(5-4\bar{\sigma})\bar{\sigma}^2\\
&-m_B(2u-1)(m_1^2(\bar{\sigma}-4)+2q^2(\bar{\sigma}-2)(\bar{\sigma}-1))+m_1(5m_1^2+q^2(4\bar{\sigma}-5)))\,.
\end{aligned}$$

For ψ_4:

$$C_2^{(A_{30}^{B\to V},\bar{\psi}_4)} = \frac{2}{m_B\bar{\sigma}}(1-2u)(\bar{\sigma}-3)\,,$$

$$C_3^{(A_{30}^{B\to V},\bar{\psi}_4)} = \frac{2}{m_B\bar{\sigma}}((2\bar{\sigma}-3)(2u-1)(q^2-m_B^2\bar{\sigma}^2)+2m_Bm_1\bar{\sigma}+m_1^2(2\bar{\sigma}+3)(2u-1))\,.$$

For χ_4:

$$\begin{aligned}C_2^{(A_{30}^{B\to V},\bar{\chi}_4)} =& \frac{2}{m_B\bar{\sigma}}(\bar{\sigma}-3)\,,\\ C_3^{(A_{30}^{B\to V},\bar{\chi}_4)} =& -\frac{2}{m_B\bar{\sigma}}(m_B^2\bar{\sigma}((3-2\bar{\sigma})\bar{\sigma}+4(\bar{\sigma}-2)(\bar{\sigma}-1)u)\\ &+4m_Bm_1(3-2\bar{\sigma})\bar{\sigma}+m_1^2(2\bar{\sigma}+3)+q^2(2\bar{\sigma}-3))\,.\end{aligned}$$

The coefficients of eq. (4.31), for the three-particle DAs, for $T_1^{B\to V}$ follow. For ϕ_3:

$$\begin{aligned}C_2^{(T_1^{B\to V},\phi_3)} &= \frac{m_1}{m_B}+u\bar{\sigma}\,,\\ C_2^{(T_1^{B\to V},\bar{\phi}_3)} &= \frac{1}{m_B^2\bar{\sigma}}(2m_1-m_B\bar{\sigma}u)\,,\\ C_3^{(T_1^{B\to V},\bar{\phi}_3)} &= \frac{2}{m_B^2\bar{\sigma}}(m_B^2\bar{\sigma}^2+m_1^2-q^2)(m_B\bar{\sigma}u+m_1)\,,\\ C_3^{(T_1^{B\to V},\bar{\bar{\phi}}_3)} &= 6\frac{m_1}{m_B}\,.\\ C_4^{(T_1^{B\to V},\bar{\bar{\phi}}_3)} &= 6\frac{m_1^2}{m_B}(m_B\bar{\sigma}(2u-1)+m_1)\,.\end{aligned}$$

For ϕ_4:

$$\begin{aligned}C_2^{(T_1^{B\to V},\phi_4)} &= (u-1)\bar{\sigma}\,,\\ C_2^{(T_1^{B\to V},\bar{\phi}_4)} &= \frac{u}{m_B}\,,\\ C_3^{(T_1^{B\to V},\bar{\phi}_4)} &= \frac{2}{m_B}(-(m_B\bar{\sigma}+m_1)(m_1u-m_B\bar{\sigma}(u-1))-q^2u+q^2)\,,\\ C_2^{(T_1^{B\to V},\bar{\bar{\phi}}_4)} &= \frac{2}{m_B^2\bar{\sigma}}(2u-1)\,,\\ C_3^{(T_1^{B\to V},\bar{\bar{\phi}}_4)} &= \frac{1}{m_B^2\bar{\sigma}}(-2(2u-1)(q^2-m_B^2\bar{\sigma}^2)-2m_Bm_1\bar{\sigma}+m_1^2(4-8u))\,,\\ C_4^{(T_1^{B\to V},\bar{\bar{\phi}}_4)} &= \frac{6m_1}{m_B^2\bar{\sigma}}(-m_B^3\bar{\sigma}^3+m_Bq^2\bar{\sigma}-m_1(2u-1)(m_1^2-q^2))\,.\end{aligned}$$

For ψ_4:

$$C_2^{(T_1^{B\to V},\bar{\psi}_4)} = \frac{1}{m_B^2\bar{\sigma}}(m_B\bar{\sigma}(1-2u)-2m_1)\,,$$

$$C_3^{(T_1^{B\to V},\bar{\psi}_4)} = \frac{2}{m_B^2\bar{\sigma}}(m_B^3\bar{\sigma}^3(1-2u) + m_B^2 m_1\bar{\sigma}^2 + m_B\bar{\sigma}(2u-1)(m_1^2+q^2) - m_1^3 + m_1 q^2)\,.$$

For χ_4:

$$C_2^{(T_1^{B\to V},\bar{\chi}_4)} = \frac{1}{m_B^2\bar{\sigma}}(m_B\bar{\sigma}(1-2u) + 2m_1)\,,$$

$$C_3^{(T_1^{B\to V},\bar{\chi}_4)} = 2\left(\frac{m_1^3 - m_1 q^2}{m_B^2\bar{\sigma}} - \frac{-2m_1^2 u + m_1^2 + q^2}{m_B} + m_B\bar{\sigma}^2 + m_1\bar{\sigma}\right)\,.$$

The coefficients of eq. (4.31), for the three-particle DAs, for $T_{23A}^{B\to V}$ follow. For ϕ_3:

$$\begin{aligned}
C_2^{(T_{23A}^{B\to V},\phi_3)} =& \frac{m_B m_1 - 4q^2 u}{m_B^2} + \bar{\sigma}u\,,\\
C_2^{(T_{23A}^{B\to V},\bar{\phi}_3)} =& \frac{1}{m_B^2\bar{\sigma}}(2m_1 - m_B\bar{\sigma}u)\,,\\
C_3^{(T_{23A}^{B\to V},\bar{\phi}_3)} =& \frac{2}{m_B^2\bar{\sigma}}(m_B^3\bar{\sigma}^3 u + \bar{\sigma}(m_B u(m_1^2+3q^2) + 4m_1 q^2)\\
&+ m_B\bar{\sigma}^2(m_B m_1 - 4q^2 u) + m_1^3 - m_1 q^2)\,,\\
C_3^{(T_{23A}^{B\to V},\bar{\bar{\phi}}_3)} =& 6\frac{m_1}{m_B}\,.\\
C_4^{(T_{23A}^{B\to V},\bar{\bar{\phi}}_3)} =& 6\frac{m_1}{m_B}(m_B m_1\bar{\sigma}(2u-1) + m_1^2 + 4q^2(\bar{\sigma}-1))\,.
\end{aligned}$$

For ϕ_4:

$$\begin{aligned}
C_2^{(T_{23A}^{B\to V},\phi_4)} =& \bar{\sigma}(u-1)\,,\\
C_2^{(T_{23A}^{B\to V},\bar{\phi}_4)} =& \frac{u}{m_B}\,,\\
C_3^{(T_{23A}^{B\to V},\bar{\phi}_4)} =& -\frac{2}{m_B}((m_B\bar{\sigma}+m_1)(m_1 u - m_B\bar{\sigma}(u-1)) + q^2(-2\bar{\sigma}+u+1))\,,\\
C_2^{(T_{23A}^{B\to V},\bar{\bar{\phi}}_4)} =& \frac{2}{m_B^2\bar{\sigma}}(2u-1)\,,\\
C_3^{(T_{23A}^{B\to V},\bar{\bar{\phi}}_4)} =& \frac{2}{m_B^2\bar{\sigma}}((2u-1)(m_B^2\bar{\sigma}^2 + q^2(4\bar{\sigma}-7)) - m_B m_1\bar{\sigma} + m_1^2(2-4u))\,,\\
C_4^{(T_{23A}^{B\to V},\bar{\bar{\phi}}_4)} =& -\frac{6}{m_B^2\bar{\sigma}}(m_1(m_B^3\bar{\sigma}^3 - m_B q^2\bar{\sigma}) + 2q^2(\bar{\sigma}-1)(2u-1)(q^2 - m_B^2\bar{\sigma}^2)\\
&+ m_1^4(2u-1) + m_1^2 q^2(2\bar{\sigma}+1)(2u-1))\,.
\end{aligned}$$

For ψ_4:

$$C_2^{(T_{23A}^{B\to V},\bar{\psi}_4)} = \frac{1}{m_B^2\bar{\sigma}}(m_B\bar{\sigma}(1-2u) - 2m_1)\,,$$

$$C_3^{(T_{23A}^{B\to V},\bar{\psi}_4)} = \frac{2}{m_B^2\bar{\sigma}}(m_B^3\bar{\sigma}^3(1-2u) + m_B^2 m_1\bar{\sigma}^2 + \bar{\sigma}(m_B(2u-1)(m_1^2+q^2) - 4m_1q^2) - m_1^3 + m_1q^2)\,.$$

For χ_4:

$$C_2^{(T_{23A}^{B\to V},\bar{\chi}_4)} = \frac{1}{m_B^2\bar{\sigma}}(m_B\bar{\sigma} - 2m_B\bar{\sigma}u + 2m_1)\,,$$

$$C_3^{(T_{23A}^{B\to V},\bar{\chi}_4)} = \frac{2}{m_B^2\bar{\sigma}}(m_B^3\bar{\sigma}^3 + \bar{\sigma}(2m_Bu(m_1^2+2q^2) - m_B(m_1^2+q^2) + 4m_1q^2) + m_B\bar{\sigma}^2(m_Bm_1 - 4q^2u) + m_1^3 - m_1q^2)\,.$$

The coefficients of eq. (4.31), for the three-particle DAs, for $T_{23B}^{B\to V}$ follow. For ϕ_3:

$$C_1^{(T_{23B}^{B\to V},\phi_3)} = -2\frac{u}{m_B^2\bar{\sigma}}\,,$$

$$C_2^{(T_{23B}^{B\to V},\phi_3)} = \frac{1}{m_B^2\bar{\sigma}}(u(m_B^2\bar{\sigma}(3\bar{\sigma}-1) + q^2(2-4\bar{\sigma})) + m_Bm_1\bar{\sigma} - 2m_1^2u)\,,$$

$$C_2^{(T_{23B}^{B\to V},\bar{\phi}_3)} = \frac{1}{m_B^2\bar{\sigma}}(m_B(2-5\bar{\sigma})u + 6m_1)\,,$$

$$C_3^{(T_{23B}^{B\to V},\bar{\phi}_3)} = \frac{2}{m_B^2\bar{\sigma}}(m_1(q^2(4\bar{\sigma}-3) - m_B^2\bar{\sigma}^2) + m_B(\bar{\sigma}-1)u(3m_B^2\bar{\sigma}^2 - 4q^2\bar{\sigma} + q^2) - m_Bm_1^2(\bar{\sigma}-1)u + 3m_1^3)\,,$$

$$C_3^{(T_{23B}^{B\to V},\bar{\bar{\phi}}_3)} = 6\frac{m_1}{m_B\bar{\sigma}}(3\bar{\sigma}-2)\,.$$

$$C_4^{(T_{23B}^{B\to V},\bar{\bar{\phi}}_3)} = 6\frac{m_1}{m_B\bar{\sigma}}((3\bar{\sigma}-2)m_1^2 + m_B(2u-1)(\bar{\sigma}-1)\bar{\sigma}m_1 - 2(\bar{\sigma}-1)(m_B^2\bar{\sigma}^2 - 2q^2\bar{\sigma} + q^2))\,.$$

For ϕ_4:

$$C_2^{(T_{23B}^{B\to V},\phi_4)} = (\bar{\sigma}-1)(u-1)\,,$$

$$C_2^{(T_{23B}^{B\to V},\bar{\phi}_4)} = \frac{1}{m_B\bar{\sigma}}(2\bar{\sigma} + (\bar{\sigma}-2)u)\,,$$

$$C_3^{(T_{23B}^{B\to V},\bar{\phi}_4)} = \frac{2}{m_B\bar{\sigma}}((\bar{\sigma}-1)(m_B^2\bar{\sigma}^2(u-2) + 2q^2\bar{\sigma} - q^2u) - m_Bm_1(\bar{\sigma}-1)\bar{\sigma} - m_1^2(\bar{\sigma}(u-1)+u))\,,$$

$$C_2^{(T_{23B}^{B\to V},\bar{\bar{\phi}}_4)} = \frac{6}{m_B^2\bar{\sigma}^2}(\bar{\sigma}-1)(2u-1)\,,$$

$$C_3^{(T_{23B}^{B\to V},\bar{\bar{\phi}}_4)} = \frac{1}{m_B^2\bar{\sigma}^2}(4(2u-1)(m_B^2\bar{\sigma}^3 + q^2(2(\bar{\sigma}-3)\bar{\sigma}+3))$$
$$- 2m_B m_1(\bar{\sigma}-3)\bar{\sigma} - 6m_1^2(\bar{\sigma}+2)(2u-1))\,,$$
$$C_4^{(T_{23B}^{B\to V},\bar{\bar{\phi}}_4)} = -\frac{6}{m_B^2\bar{\sigma}^2}((2u-1)(2\bar{\sigma}+1)m_1^4 - m_B\bar{\sigma}m_1^3 + (2u-1)(m_B^2(1-2\bar{\sigma})\bar{\sigma}^2$$
$$+ q^2(2\bar{\sigma}^2+\bar{\sigma}-2))m_1^2 + m_B(\bar{\sigma}-1)\bar{\sigma}(m_B^2\bar{\sigma}^2 - q^2)m_1$$
$$+ (2u-1)(\bar{\sigma}-1)(m_B^2\bar{\sigma}^2 - q^2)(m_B^2\bar{\sigma}^2 - 2q^2\bar{\sigma} + q^2))\,.$$

For ψ_4:

$$C_2^{(T_{23B}^{B\to V},\bar{\psi}_4)} = \frac{1}{m_B^2\bar{\sigma}}(m_B(\bar{\sigma} - 2(\bar{\sigma}-2)u - 2) - 6m_1)\,,$$
$$C_3^{(T_{23B}^{B\to V},\bar{\psi}_4)} = \frac{2}{m_B^2\bar{\sigma}}(m_B^3\bar{\sigma}^2(\bar{\sigma} - 2(\bar{\sigma}-1)u - 1) + m_B^2 m_1\bar{\sigma}(3\bar{\sigma}-2)$$
$$+ m_B(2u-1)(m_1^2(\bar{\sigma}+1) + q^2(\bar{\sigma}-1)) - 3m_1^3 + m_1q^2(3-4\bar{\sigma}))\,.$$

For χ_4:

$$C_2^{(T_{23B}^{B\to V},\bar{\chi}_4)} = \frac{1}{m_B^2\bar{\sigma}}(m_B(\bar{\sigma} + (4-6\bar{\sigma})u - 2) + 6m_1)\,,$$
$$C_3^{(T_{23B}^{B\to V},\bar{\chi}_4)} = \frac{2}{m_B^2\bar{\sigma}}(m_B^3(\bar{\sigma}-1)\bar{\sigma}^2(2u+1) - m_B^2 m_1\bar{\sigma}^2 + m_B(m_1^2(-\bar{\sigma}+2u-1)$$
$$- q^2(\bar{\sigma}-1)((4\bar{\sigma}-2)u+1)) + 3m_1^3 + m_1q^2(4\bar{\sigma}-3))\,.$$

Bibliography

[1] N. Gubernari, A. Kokulu and D. van Dyk, *$B \to P$ and $B \to V$ Form Factors from B-Meson Light-Cone Sum Rules beyond Leading Twist*, *JHEP* **01** (2019) 150 [1811.00983].

[2] M. Bordone, N. Gubernari, D. van Dyk and M. Jung, *Heavy-Quark expansion for $\bar{B}_s \to D_s^{(*)}$ form factors and unitarity bounds beyond the $SU(3)_F$ limit*, *Eur. Phys. J. C* **80** (2020) 347 [1912.09335].

[3] N. Gubernari, D. van Dyk and J. Virto, *Non-local matrix elements in $B \to K^{(*)}\ell^+\ell^-$ from light-cone sum rules and dispersive bounds, In preparation.*

[4] E. Aslanides et al., *Charting the European Course to the High-Energy Frontier*, 1912.13466.

[5] W. Altmannshofer, C. Niehoff, P. Stangl and D. M. Straub, *Status of the $B \to K^*\mu^+\mu^-$ anomaly after Moriond 2017*, *Eur. Phys. J.* **C77** (2017) 377 [1703.09189].

[6] ATLAS, CMS, LHCb collaboration, E. Graverini, *Flavour anomalies: a review*, *J. Phys. Conf. Ser.* **1137** (2019) 012025 [1807.11373].

[7] J. Albrecht, S. Reichert and D. van Dyk, *Status of rare exclusive B meson decays in 2018*, *Int. J. Mod. Phys. A* **33** (2018) 1830016 [1806.05010].

[8] E. McLean, C. Davies, J. Koponen and A. Lytle, *$B_s \to D_s\ell\nu$ Form Factors for the full q^2 range from Lattice QCD with non-perturbatively normalized currents*, *Phys. Rev. D* **101** (2020) 074513 [1906.00701].

[9] E. McLean, C. Davies, A. Lytle and J. Koponen, *Lattice QCD form factor for $B_s \to D_s^* l\nu$ at zero recoil with non-perturbative current renormalisation*, *Phys. Rev. D* **99** (2019) 114512 [1904.02046].

[10] I. Caprini, L. Lellouch and M. Neubert, *Dispersive bounds on the shape of $\bar{B} \to D^{(*)}$ lepton anti-neutrino form-factors*, *Nucl. Phys. B* **530** (1998) 153 [hep-ph/9712417].

[11] LHCb collaboration, R. Aaij et al., *Measurement of $|V_{cb}|$ with $B_s^0 \to D_s^{(*)-}\mu^+\nu_\mu$ decays*, *Phys. Rev. D* **101** (2020) 072004 [2001.03225].

[12] LHCb collaboration, R. Aaij et al., *Measurement of the shape of the $B_s^0 \to D_s^{*-}\mu^+\nu_\mu$ differential decay rate*, 2003.08453.

[13] LHCb collaboration, R. Aaij et al., *Angular analysis of the $B^0 \to K^{*0}\mu^+\mu^-$ decay using 3 fb^{-1} of integrated luminosity*, *JHEP* **02** (2016) 104 [1512.04442].

[14] A. Khodjamirian, T. Mannel, A. A. Pivovarov and Y. M. Wang, *Charm-loop effect in $B \to K^{(*)}\ell^+\ell^-$ and $B \to K^*\gamma$*, *JHEP* **09** (2010) 089 [1006.4945].

[15] D. R. Green, *High p_T physics at hadron colliders*, vol. 22. 2005.

[16] M. E. Peskin and D. V. Schroeder, *An Introduction to quantum field theory*. Addison-Wesley, Reading, USA, 1995.

[17] M. D. Schwartz, *Quantum Field Theory and the Standard Model*. Cambridge University Press, 2014.

[18] https://favpng.com/png_view/field-particle-physics-standard-model-elementary-particle-higgs-boson-png/JwgQnwMF.

[19] W. Buchmuller and D. Wyler, *Effective Lagrangian Analysis of New Interactions and Flavor Conservation*, *Nucl. Phys. B* **268** (1986) 621.

[20] B. Grzadkowski, M. Iskrzynski, M. Misiak and J. Rosiek, *Dimension-Six Terms in the Standard Model Lagrangian*, *JHEP* **10** (2010) 085 [1008.4884].

[21] CKMfitter Group collaboration, J. Charles, A. Hocker, H. Lacker, S. Laplace, F. R. Le Diberder, J. Malcles et al., *CP violation and the CKM matrix: Assessing the impact of the asymmetric B factories*, *Eur. Phys. J.* **C41** (2005) 1 [hep-ph/0406184].

[22] G. F. Giudice and M. McCullough, *A Clockwork Theory*, *JHEP* **02** (2017) 036 [1610.07962].

[23] C. Froggatt and H. Nielsen, *Trying to understand the standard model parameters*, *Surveys High Energ. Phys.* **18** (2003) 55 [hep-ph/0308144].

[24] W. Taylor and B. Zwiebach, *D-branes, tachyons, and string field theory*, in *Theoretical Advanced Study Institute in Elementary Particle Physics (TASI 2001): Strings, Branes and EXTRA Dimensions*, pp. 641–759, 10, 2003, hep-th/0311017, DOI.

[25] D. J. Gross and F. Wilczek, *Ultraviolet Behavior of Nonabelian Gauge Theories*, *Phys. Rev. Lett.* **30** (1973) 1343.

[26] H. Politzer, *Reliable Perturbative Results for Strong Interactions?*, *Phys. Rev. Lett.* **30** (1973) 1346.

[27] Particle Data Group collaboration, M. Tanabashi et al., *Review of Particle Physics*, *Phys. Rev.* **D98** (2018) 030001.

[28] S. L. Glashow, J. Iliopoulos and L. Maiani, *Weak Interactions with Lepton-Hadron Symmetry*, *Phys. Rev.* **D2** (1970) 1285.

[29] A. J. Buras, *Weak Hamiltonian, CP violation and rare decays*, in *Probing the standard model of particle interactions. Proceedings, Summer School in Theoretical Physics, NATO Advanced Study Institute, 68th session, Les Houches, France, July 28-September 5, 1997. Pt. 1, 2*, pp. 281–539, 1998, hep-ph/9806471.

[30] I. Doršner, S. Fajfer, A. Greljo, J. F. Kamenik and N. Košnik, *Physics of leptoquarks in precision experiments and at particle colliders*, *Phys. Rept.* **641** (2016) 1 [1603.04993].

[31] ATLAS collaboration, G. Aad et al., *Observation of a new particle in the search for the Standard Model Higgs boson with the ATLAS detector at the LHC*, *Phys. Lett. B* **716** (2012) 1 [1207.7214].

[32] T. Blake, G. Lanfranchi and D. M. Straub, *Rare B Decays as Tests of the Standard Model*, *Prog. Part. Nucl. Phys.* **92** (2017) 50 [1606.00916].

[33] M. Beneke, T. Feldmann and D. Seidel, *Systematic approach to exclusive $B \to V l^+ l^-$, $V\gamma$ decays*, *Nucl. Phys.* **B612** (2001) 25 [hep-ph/0106067].

[34] M. Beneke, G. Buchalla, M. Neubert and C. T. Sachrajda, *QCD factorization for $B \to \pi\pi$ decays: Strong phases and CP violation in the heavy quark limit*, *Phys. Rev. Lett.* **83** (1999) 1914 [hep-ph/9905312].

[35] M. Beneke, G. Buchalla, M. Neubert and C. T. Sachrajda, *QCD factorization for exclusive, nonleptonic B meson decays: General arguments and the case of heavy light final states*, *Nucl. Phys.* **B591** (2000) 313 [hep-ph/0006124].

[36] Y.-Y. Keum and H.-n. Li, *Nonleptonic charmless B decays: Factorization versus perturbative QCD*, *Phys. Rev.* **D63** (2001) 074006 [hep-ph/0006001].

[37] M. Beneke, V. M. Braun, Y. Ji and Y.-B. Wei, *Radiative leptonic decay $B \to \gamma\ell\nu_\ell$ with subleading power corrections*, *JHEP* **07** (2018) 154 [1804.04962].

[38] M. Beneke and J. Rohrwild, *B meson distribution amplitude from $B \to \gamma\ell\nu$*, *Eur. Phys. J.* **C71** (2011) 1818 [1110.3228].

[39] BaBar collaboration, J. P. Lees et al., *Measurement of an Excess of $\bar{B} \to D^{(*)}\tau^-\bar{\nu}_\tau$ Decays and Implications for Charged Higgs Bosons*, *Phys. Rev.* **D88** (2013) 072012 [1303.0571].

[40] Belle collaboration, M. Huschle et al., *Measurement of the branching ratio of $\bar{B} \to D^{(*)}\tau^-\bar{\nu}_\tau$ relative to $\bar{B} \to D^{(*)}\ell^-\bar{\nu}_\ell$ decays with hadronic tagging at Belle*, *Phys. Rev.* **D92** (2015) 072014 [1507.03233].

[41] LHCb collaboration, R. Aaij et al., *Measurement of the ratio of branching fractions $\mathcal{B}(\bar{B}^0 \to D^{*+}\tau^-\bar{\nu}_\tau)/\mathcal{B}(\bar{B}^0 \to D^{*+}\mu^-\bar{\nu}_\mu)$*, [Erratum: Phys. Rev. Lett.115,no.15,159901(2015)]*Phys. Rev. Lett.* **115** (2015) 111803 [1506.08614].

[42] Belle collaboration, S. Hirose et al., *Measurement of the τ lepton polarization and $R(D^*)$ in the decay $\bar{B} \to D^*\tau^-\bar{\nu}_\tau$ with one-prong hadronic τ decays at Belle*, *Phys. Rev.* **D97** (2018) 012004 [1709.00129].

[43] LHCb collaboration, R. Aaij et al., *Test of Lepton Flavor Universality by the measurement of the $B^0 \to D^{*-}\tau^+\nu_\tau$ branching fraction using three-prong τ decays*, *Phys. Rev.* **D97** (2018) 072013 [1711.02505].

[44] Belle collaboration, A. Abdesselam et al., *Measurement of $\mathcal{R}(D)$ and $\mathcal{R}(D^*)$ with a semileptonic tagging method*, 1904.08794.

[45] Belle collaboration, Y. Sato et al., *Measurement of the branching ratio of $\bar{B}^0 \to D^{*+}\tau^-\bar{\nu}_\tau$ relative to $\bar{B}^0 \to D^{*+}\ell^-\bar{\nu}_\ell$ decays with a semileptonic tagging method*, *Phys. Rev.* **D94** (2016) 072007 [1607.07923].

[46] LHCb collaboration, R. Aaij et al., *Test of lepton universality using $B^+ \to K^+\ell^+\ell^-$ decays*, *Phys. Rev. Lett.* **113** (2014) 151601 [1406.6482].

[47] Belle collaboration, J. T. Wei et al., *Measurement of the Differential Branching Fraction and Forward-Backword Asymmetry for $B \to K^{(*)}\ell^+\ell^-$*, *Phys. Rev. Lett.* **103** (2009) 171801 [0904.0770].

[48] BaBar collaboration, J. P. Lees et al., *Measurement of Branching Fractions and Rate Asymmetries in the Rare Decays $B \to K^{(*)}l^+l^-$*, *Phys. Rev.* **D86** (2012) 032012 [1204.3933].

[49] LHCb collaboration, R. Aaij et al., *Test of lepton universality with $B^0 \to K^{*0}\ell^+\ell^-$ decays*, *JHEP* **08** (2017) 055 [1705.05802].

[50] LHCb collaboration, R. Aaij et al., *Search for lepton-universality violation in $B^+ \to K^+\ell^+\ell^-$ decays*, *Phys. Rev. Lett.* **122** (2019) 191801 [1903.09252].

[51] F. U. Bernlochner, Z. Ligeti, M. Papucci and D. J. Robinson, *Combined analysis of semileptonic B decays to D and D^*: $R(D^{(*)})$, $|V_{cb}|$, and new physics*, [erratum: Phys. Rev.D97,no.5,059902(2018)]*Phys. Rev.* **D95** (2017) 115008 [1703.05330].

[52] D. Bigi and P. Gambino, *Revisiting $B \to D\ell\nu$*, *Phys. Rev.* **D94** (2016) 094008 [1606.08030].

[53] D. Bigi, P. Gambino and S. Schacht, *$R(D^*)$, $|V_{cb}|$, and the Heavy Quark Symmetry relations between form factors*, *JHEP* **11** (2017) 061 [1707.09509].

[54] M. Bordone, G. Isidori and A. Pattori, *On the Standard Model predictions for R_K and R_{K^*}*, *Eur. Phys. J.* **C76** (2016) 440 [1605.07633].

[55] N. Serra, R. Silva Coutinho and D. van Dyk, *Measuring the breaking of lepton flavor universality in $B \to K^*\ell^+\ell^-$*, *Phys. Rev.* **D95** (2017) 035029 [1610.08761].

[56] S. Jäger and J. Martin Camalich, *Reassessing the discovery potential of the $B \to K^*\ell^+\ell^-$*

decays in the large-recoil region: SM challenges and BSM opportunities, *Phys. Rev.* **D93** (2016) 014028 [1412.3183].

[57] B. Capdevila, S. Descotes-Genon, J. Matias and J. Virto, *Assessing lepton-flavour non-universality from $B \to K^* \ell\ell$ angular analyses*, *JHEP* **10** (2016) 075 [1605.03156].

[58] HPQCD collaboration, C. Bouchard, G. P. Lepage, C. Monahan, H. Na and J. Shigemitsu, *Standard Model Predictions for $B \to K \ell^+ \ell^-$ with Form Factors from Lattice QCD*, [Erratum: Phys. Rev. Lett.112,no.14,149902(2014)]*Phys. Rev. Lett.* **111** (2013) 162002 [1306.0434].

[59] HFLAV collaboration, Y. S. Amhis et al., *Averages of b-hadron, c-hadron, and τ-lepton properties as of 2018*, updated results and plots available at https://hflav.web.cern.ch/, 1909.12524.

[60] LHCb collaboration, R. Aaij et al., *Measurement of the ratio of branching fractions $\mathcal{B}(B_c^+ \to J/\psi\tau^+\nu_\tau)/\mathcal{B}(B_c^+ \to J/\psi\mu^+\nu_\mu)$*, *Phys. Rev. Lett.* **120** (2018) 121801 [1711.05623].

[61] LHCb collaboration, R. Aaij et al., *Differential branching fraction and angular analysis of the decay $B^0 \to K^{*0}\mu^+\mu^-$*, *JHEP* **08** (2013) 131 [1304.6325].

[62] W. Altmannshofer, P. Ball, A. Bharucha, A. J. Buras, D. M. Straub and M. Wick, *Symmetries and Asymmetries of $B \to K^*\mu^+\mu^-$ Decays in the Standard Model and Beyond*, *JHEP* **01** (2009) 019 [0811.1214].

[63] S. Descotes-Genon, J. Matias and J. Virto, *Understanding the $B \to K^*\mu^+\mu^-$ Anomaly*, *Phys. Rev.* **D88** (2013) 074002 [1307.5683].

[64] Belle collaboration, S. Wehle et al., *Lepton-Flavor-Dependent Angular Analysis of $B \to K^*\ell^+\ell^-$*, *Phys. Rev. Lett.* **118** (2017) 111801 [1612.05014].

[65] ATLAS collaboration, M. Aaboud et al., *Angular analysis of $B_d^0 \to K^*\mu^+\mu^-$ decays in pp collisions at $\sqrt{s} = 8$ TeV with the ATLAS detector*, *JHEP* **10** (2018) 047 [1805.04000].

[66] A. Bharucha, D. M. Straub and R. Zwicky, *$B \to V\ell^+\ell^-$ in the Standard Model from light-cone sum rules*, *JHEP* **08** (2016) 098 [1503.05534].

[67] CMS collaboration, A. M. Sirunyan et al., *Measurement of angular parameters from the decay $\mathrm{B}^0 \to \mathrm{K}^{*0}\mu^+\mu^-$ in proton-proton collisions at $\sqrt{s} = 8$ TeV*, *Phys. Lett.* **B781** (2018) 517 [1710.02846].

[68] C. Bobeth, M. Chrzaszcz, D. van Dyk and J. Virto, *Long-distance effects in $B \to K^*\ell\ell$ from analyticity*, *Eur. Phys. J.* **C78** (2018) 451 [1707.07305].

[69] D. Buttazzo, A. Greljo, G. Isidori and D. Marzocca, *B-physics anomalies: a guide to combined explanations*, *JHEP* **11** (2017) 044 [1706.07808].

[70] L. Di Luzio, A. Greljo and M. Nardecchia, *Gauge leptoquark as the origin of b-physics anomalies*, *Phys.Rev.D* **96** (2017) 115011 [1708.08450].

[71] M. Bordone, C. Cornella, J. Fuentes-Martín and G. Isidori, *Low-energy signatures of the PS^3 model: from B-physics anomalies to LFV*, *JHEP* **10** (2018) 148 [1805.09328].

[72] A. Datta, D. Sachdeva and J. Waite, *Unified explanation of $b \to s\mu^+\mu^-$ anomalies, neutrino masses, and $B \to \pi K$ puzzle*, *Phys. Rev.* **D100** (2019) 055015 [1905.04046].

[73] C. Cornella, J. Fuentes-Martin and G. Isidori, *Revisiting the vector leptoquark explanation of the B-physics anomalies*, *JHEP* **07** (2019) 168 [1903.11517].

[74] P. Gambino, M. Jung and S. Schacht, *The V_{cb} puzzle: An update*, *Phys. Lett.* **B795** (2019) 386 [1905.08209].

[75] A. Crivellin and S. Pokorski, *Can the differences in the determinations of V_{ub} and V_{cb} be explained by New Physics?*, *Phys. Rev. Lett.* **114** (2015) 011802 [1407.1320].

[76] K. G. Wilson, *Nonlagrangian models of current algebra*, *Phys. Rev.* **179** (1969) 1499.

[77] G. Buchalla, A. J. Buras and M. E. Lautenbacher, *Weak decays beyond leading logarithms*, *Rev. Mod. Phys.* **68** (1996) 1125 [hep-ph/9512380].

[78] K. G. Chetyrkin, M. Misiak and M. Munz, *Weak radiative B meson decay beyond leading logarithms*, [Erratum: Phys. Lett.B425,414(1998)]*Phys. Lett.* **B400** (1997) 206 [hep-ph/9612313].

[79] W. D. Goldberger, *Semileptonic B decays as a probe of new physics*, hep-ph/9902311.

[80] M. Jung and D. M. Straub, *Constraining new physics in $b \to c\ell\nu$ transitions*, *JHEP* **01** (2019) 009 [1801.01112].

[81] M. Bruno, M. Dalla Brida, P. Fritzsch, T. Korzec, A. Ramos, S. Schaefer et al., *The Λ-parameter in 3-flavour QCD and $\alpha_s(m_Z)$ by the ALPHA collaboration*, *PoS* **LATTICE2016** (2016) 197 [1701.03075].

[82] N. Isgur and M. B. Wise, *Heavy quark symmetry*, *Adv. Ser. Direct. High Energy Phys.* **10** (1992) 234.

[83] M. Neubert, *Heavy quark symmetry*, *Phys. Rept.* **245** (1994) 259 [hep-ph/9306320].

[84] A. V. Manohar and M. B. Wise, *Heavy quark physics*, *Camb. Monogr. Part. Phys. Nucl. Phys. Cosmol.* **10** (2000) 1.

[85] HPQCD collaboration, C. Bouchard, G. Lepage, C. Monahan, H. Na and J. Shigemitsu, *Rare decay $B \to K\ell^+\ell^-$ form factors from lattice QCD*, [Erratum: Phys.Rev.D 88, 079901 (2013)]*Phys. Rev. D* **88** (2013) 054509 [1306.2384].

[86] HPQCD collaboration, H. Na, C. M. Bouchard, G. P. Lepage, C. Monahan and J. Shigemitsu, *$B \to Dl\nu$ form factors at nonzero recoil and extraction of $|V_{cb}|$*, [Erratum: Phys.Rev.D 93, 119906 (2016)]*Phys. Rev. D* **92** (2015) 054510 [1505.03925].

[87] R. R. Horgan, Z. Liu, S. Meinel and M. Wingate, *Lattice QCD calculation of form factors describing the rare decays $B \to K^*\ell^+\ell^-$ and $B_s \to \phi\ell^+\ell^-$*, *Phys. Rev. D* **89** (2014) 094501 [1310.3722].

[88] R. Horgan, Z. Liu, S. Meinel and M. Wingate, *Rare B decays using lattice QCD form factors*, *PoS* **LATTICE2014** (2015) 372 [1501.00367].

[89] Fermilab Lattice, MILC collaboration, J. A. Bailey et al., *Update of $|V_{cb}|$ from the $\bar{B} \to D^*\ell\bar{\nu}$ form factor at zero recoil with three-flavor lattice QCD*, *Phys. Rev. D* **89** (2014) 114504 [1403.0635].

[90] HPQCD collaboration, J. Harrison, C. Davies and M. Wingate, *Lattice QCD calculation of the $B_{(s)} \to D^*_{(s)}\ell\nu$ form factors at zero recoil and implications for $|V_{cb}|$*, *Phys. Rev. D* **97** (2018) 054502 [1711.11013].

[91] P. Colangelo and A. Khodjamirian, *QCD sum rules, a modern perspective*, hep-ph/0010175.

[92] E. J. Eichten and C. Quigg, *Mesons with Beauty and Charm: New Horizons in Spectroscopy*, *Phys. Rev.* **D99** (2019) 054025 [1902.09735].

[93] L. V. Ahlfors, *Complex Analysis*. McGraw-Hill, New York, USA, 1979.

[94] C. Rossetti, *Metodi Matematici della Fisica*. Levrotto e Bella, Torino, Italy, 2000.

[95] M. A. Shifman, A. I. Vainshtein and V. I. Zakharov, *QCD and Resonance Physics. Theoretical Foundations*, *Nucl. Phys.* **B147** (1979) 385.

[96] E. Poggio, H. R. Quinn and S. Weinberg, *Smearing the Quark Model*, *Phys. Rev. D* **13** (1976) 1958.

[97] M. A. Shifman, *Quark hadron duality*, in *Proceedings, 8th International Symposium on Heavy Flavor Physics (Heavy Flavors 8)*, vol. 3, (Singapore), pp. 1447–1494, World Scientific, 7, 2000, hep-ph/0009131, DOI.

[98] D. Boito, I. Caprini, M. Golterman, K. Maltman and S. Peris, *Hyperasymptotics and quark-hadron duality violations in QCD*, *Phys. Rev.* **D97** (2018) 054007 [1711.10316].

[99] L. J. Reinders, H. Rubinstein and S. Yazaki, *Hadron Properties from QCD Sum Rules*, *Phys. Rept.* **127** (1985) 1.

[100] V. M. Braun and I. E. Filyanov, *QCD Sum Rules in Exclusive Kinematics and Pion Wave Function*, [Sov. J. Nucl. Phys.50,511(1989); Yad. Fiz.50,818(1989)]*Z. Phys.* **C44** (1989) 157.

[101] I. I. Balitsky, V. M. Braun and A. V. Kolesnichenko, *Radiative Decay Sigma$^+ \to p\gamma$ in Quantum Chromodynamics*, *Nucl. Phys.* **B312** (1989) 509.

[102] V. Belyaev and B. Ioffe, *Determination of Baryon and Baryonic Resonance Masses from QCD Sum Rules. 1. Nonstrange Baryons*, *Sov. Phys. JETP* **56** (1982) 493.

[103] B. L. Ioffe, *Condensates in quantum chromodynamics*, [Yad. Fiz.66,32(2003)]*Phys. Atom. Nucl.* **66** (2003) 30 [hep-ph/0207191].

[104] Flavour Lattice Averaging Group collaboration, S. Aoki et al., *FLAG Review 2019*, *Eur. Phys. J.* **C80** (2020) 113 [1902.08191].

[105] HPQCD collaboration, C. T. H. Davies, K. Hornbostel, J. Komijani, J. Koponen, G. P. Lepage, A. T. Lytle et al., *Determination of the quark condensate from heavy-light current-current correlators in full lattice QCD*, *Phys. Rev.* **D100** (2019) 034506 [1811.04305].

[106] S. Cheng, A. Khodjamirian and J. Virto, *$B \to \pi\pi$ Form Factors from Light-Cone Sum Rules with B-meson Distribution Amplitudes*, *JHEP* **05** (2017) 157 [1701.01633].

[107] C. McNeile, A. Bazavov, C. Davies, R. Dowdall, K. Hornbostel, G. Lepage et al., *Direct determination of the strange and light quark condensates from full lattice QCD*, *Phys. Rev. D* **87** (2013) 034503 [1211.6577].

[108] M. A. Shifman, A. Vainshtein and V. I. Zakharov, *QCD and Resonance Physics: Applications*, *Nucl. Phys. B* **147** (1979) 448.

[109] R. Horsley, G. Hotzel, E. Ilgenfritz, R. Millo, H. Perlt, P. Rakow et al., *Wilson loops to 20th order numerical stochastic perturbation theory*, *Phys. Rev. D* **86** (2012) 054502 [1205.1659].

[110] G. S. Bali, C. Bauer and A. Pineda, *Model-independent determination of the gluon condensate in four-dimensional SU(3) gauge theory*, *Phys. Rev. Lett.* **113** (2014) 092001 [1403.6477].

[111] A. Khodjamirian, T. Mannel and N. Offen, *B-meson distribution amplitude from the $B \to \pi$ form-factor*, *Phys. Lett. B* **620** (2005) 52 [hep-ph/0504091].

[112] A. Khodjamirian, T. Mannel and N. Offen, *Form-factors from light-cone sum rules with B-meson distribution amplitudes*, *Phys. Rev.* **D75** (2007) 054013 [hep-ph/0611193].

[113] I. I. Balitsky and V. M. Braun, *Evolution Equations for QCD String Operators*, *Nucl. Phys.* **B311** (1989) 541.

[114] V. Braun, Y. Ji and A. Manashov, *Higher-twist B-meson Distribution Amplitudes in HQET*, *JHEP* **05** (2017) 022 [1703.02446].

[115] P. Ball and R. Zwicky, *New results on $B \to \pi, K, \eta$ decay formfactors from light-cone sum rules*, *Phys. Rev. D* **71** (2005) 014015 [hep-ph/0406232].

[116] P. Ball and R. Zwicky, *$B_{d,s} \to \rho, \omega, K^*, \phi$ decay form-factors from light-cone sum rules revisited*, *Phys. Rev. D* **71** (2005) 014029 [hep-ph/0412079].

[117] N. N. Meiman, *Analytic expressions for upper limits of coupling constants in quantum field theory*, *Sov. Phys. JETP* **17** (1963) 830.

[118] S. Okubo, *Exact bounds for k-l-3 decay parameters*, *Phys. Rev. D* **3** (1971) 2807.

[119] S. Okubo and I.-F. Shih, *Exact inequality and test of chiral sw(3) theory in k-l-3 decay problem*, *Phys. Rev. D* **4** (1971) 2020.

[120] C. Bourrely, B. Machet and E. de Rafael, *Semileptonic Decays of Pseudoscalar Particles ($M \to M' \ell \nu_\ell$) and Short Distance Behavior of Quantum Chromodynamics*, *Nucl. Phys. B* **189** (1981) 157.

[121] E. de Rafael and J. Taron, *Constraints on heavy meson form-factors*, *Phys. Lett. B* **282** (1992) 215.

[122] E. de Rafael and J. Taron, *Analyticity properties and unitarity constraints of heavy meson form-factors*, *Phys. Rev. D* **50** (1994) 373 [hep-ph/9306214].

[123] C. Boyd, B. Grinstein and R. F. Lebed, *Constraints on form-factors for exclusive semileptonic heavy to light meson decays*, *Phys. Rev. Lett.* **74** (1995) 4603 [hep-ph/9412324].

[124] C. Boyd, B. Grinstein and R. F. Lebed, *Model independent extraction of |V(cb)| using dispersion relations*, *Phys. Lett. B* **353** (1995) 306 [hep-ph/9504235].

[125] C. Boyd, B. Grinstein and R. F. Lebed, *Precision corrections to dispersive bounds on form-factors*, *Phys. Rev. D* **56** (1997) 6895 [hep-ph/9705252].

[126] A. Bharucha, T. Feldmann and M. Wick, *Theoretical and Phenomenological Constraints on Form Factors for Radiative and Semi-Leptonic B-Meson Decays*, *JHEP* **09** (2010) 090 [1004.3249].

[127] S. Faller, A. Khodjamirian, C. Klein and T. Mannel, *$B \to D^{(*)}$ Form Factors from QCD Light-Cone Sum Rules*, *Eur. Phys. J. C* **60** (2009) 603 [0809.0222].

[128] F. De Fazio, T. Feldmann and T. Hurth, *Light-cone sum rules in soft-collinear effective theory*, [Erratum: Nucl.Phys.B 800, 405 (2008)]*Nucl. Phys. B* **733** (2006) 1 [hep-ph/0504088].

[129] F. De Fazio, T. Feldmann and T. Hurth, *SCET sum rules for $B \to P$ and $B \to V$ transition form factors*, *JHEP* **02** (2008) 031 [0711.3999].

[130] Y.-M. Wang and Y.-L. Shen, *QCD corrections to $B \to \pi$ form factors from light-cone sum rules*, *Nucl. Phys. B* **898** (2015) 563 [1506.00667].

[131] Y.-M. Wang, Y.-B. Wei, Y.-L. Shen and C.-D. Lü, *Perturbative corrections to $B \to D$ form factors in QCD*, *JHEP* **06** (2017) 062 [1701.06810].

[132] A. Grozin and M. Neubert, *Asymptotics of heavy meson form-factors*, *Phys. Rev. D* **55** (1997) 272 [hep-ph/9607366].

[133] B. O. Lange and M. Neubert, *Renormalization group evolution of the B meson light cone distribution amplitude*, *Phys. Rev. Lett.* **91** (2003) 102001 [hep-ph/0303082].

[134] H. Kawamura, J. Kodaira, C.-F. Qiao and K. Tanaka, *B-meson light cone distribution amplitudes in the heavy quark limit*, [Erratum: Phys.Lett.B 536, 344–344 (2002)]*Phys. Lett. B* **523** (2001) 111 [hep-ph/0109181].

[135] S. Descotes-Genon, A. Khodjamirian and J. Virto, *Light-cone sum rules for $B \to K\pi$ form factors and applications to rare decays*, *JHEP* **12** (2019) 083 [1908.02267].

[136] I. Sentitemsu Imsong, A. Khodjamirian, T. Mannel and D. van Dyk, *Extrapolation and unitarity bounds for the $B \to \pi$ form factor*, *JHEP* **02** (2015) 126 [1409.7816].

[137] D. van Dyk et al., *EOS release v0.3.2*, https://github.com/eos/eos/releases/tag/v0.3.2.

[138] A. V. Rusov, *Higher-twist effects in light-cone sum rule for the $B \to \pi$ form factor*, *Eur. Phys. J. C* **77** (2017) 442 [1705.01929].

[139] T. Nishikawa and K. Tanaka, *QCD Sum Rules for Quark-Gluon Three-Body Components in the B Meson*, *Nucl. Phys. B* **879** (2014) 110 [1109.6786].

[140] A. Khodjamirian, T. Mannel, N. Offen and Y.-M. Wang, *$B \to \pi \ell \nu_l$ Width and $|V_{ub}|$ from QCD Light-Cone Sum Rules*, *Phys. Rev. D* **83** (2011) 094031 [1103.2655].

[141] A. Khodjamirian and A. V. Rusov, *$B_s \to K \ell \nu_\ell$ and $B_{(s)} \to \pi(K) \ell^+ \ell^-$ decays at large recoil and CKM matrix elements*, *JHEP* **08** (2017) 112 [1703.04765].

[142] C.-D. Lü, Y.-L. Shen, Y.-M. Wang and Y.-B. Wei, *QCD calculations of $B \to \pi, K$ form factors with higher-twist corrections*, *JHEP* **01** (2019) 024 [1810.00819].

[143] M. Beylich, G. Buchalla and T. Feldmann, *Theory of $B \to K^{(*)} \ell^+ \ell^-$ decays at high q^2: OPE and quark-hadron duality*, *Eur. Phys. J. C* **71** (2011) 1635 [1101.5118].

[144] B. Grinstein and D. Pirjol, *Exclusive rare $B \to K^* \ell^+ \ell^-$ decays at low recoil: Controlling the long-distance effects*, *Phys. Rev. D* **70** (2004) 114005 [hep-ph/0404250].

[145] H. M. Asatrian, C. Greub and J. Virto, *Exact NLO matching and analyticity in $b \to s \ell \ell$*, *JHEP* **04** (2020) 012 [1912.09099].

[146] S. de Boer, *Two loop virtual corrections to $b \to (d, s) \ell^+ \ell^-$ and $c \to u \ell^+ \ell^-$ for arbitrary momentum transfer*, *Eur. Phys. J. C* **77** (2017) 801 [1707.00988].

[147] E. Eberhard, *Extending Dispersive Bounds to Include Sub-threshold Branch Cuts, Bachelor's thesis*.

[148] W. Detmold, C. Lehner and S. Meinel, *$\Lambda_b \to p \ell^- \bar{\nu}_\ell$ and $\Lambda_b \to \Lambda_c \ell^- \bar{\nu}_\ell$ form factors from lattice QCD with relativistic heavy quarks*, *Phys. Rev. D* **92** (2015) 034503 [1503.01421].

[149] M. Bordone, M. Jung and D. van Dyk, *Theory determination of $\bar{B} \to D^{(*)} \ell^- \bar{\nu}$ form factors at $\mathcal{O}(1/m_c^2)$*, *Eur. Phys. J. C* **80** (2020) 74 [1908.09398].

[150] A. F. Falk and M. Neubert, *Second order power corrections in the heavy quark effective theory. 1. Formalism and meson form-factors*, *Phys. Rev. D* **47** (1993) 2965 [hep-ph/9209268].

[151] J. D. Bjorken and S. D. Drell, *Relativistic quantum fields*. McGraw-Hill, 1965.

[152] P. B. Pal, *Dirac, Majorana and Weyl fermions*, *Am. J. Phys.* **79** (2011) 485 [1006.1718].

[153] A. Bazavov et al., *B- and D-meson leptonic decay constants from four-flavor lattice QCD*, *Phys. Rev. D* **98** (2018) 074512 [1712.09262].

[154] S. Aoki et al., *Review of lattice results concerning low-energy particle physics*, *Eur. Phys. J. C* **77** (2017) 112 [1607.00299].

[155] HPQCD, UKQCD collaboration, E. Follana, C. Davies, G. Lepage and J. Shigemitsu, *High Precision determination of the pi, K, D and D(s) decay constants from lattice QCD*, *Phys. Rev. Lett.* **100** (2008) 062002 [0706.1726].

[156] MILC collaboration, A. Bazavov et al., *Results for light pseudoscalar mesons*, *PoS* **LATTICE2010** (2010) 074 [1012.0868].

[157] RBC, UKQCD collaboration, R. Arthur et al., *Domain Wall QCD with Near-Physical Pions*, *Phys. Rev.* **D87** (2013) 094514 [1208.4412].

[158] R. Dowdall, C. Davies, G. Lepage and C. McNeile, *Vus from pi and K decay constants in full lattice QCD with physical u, d, s and c quarks*, *Phys. Rev. D* **88** (2013) 074504 [1303.1670].

[159] N. Carrasco et al., *Leptonic decay constants f_K, f_D, and f_{D_s} with $N_f = 2 + 1 + 1$ twisted-mass lattice QCD*, *Phys. Rev. D* **91** (2015) 054507 [1411.7908].

[160] Fermilab Lattice, MILC collaboration, A. Bazavov et al., *Charmed and Light Pseudoscalar Meson Decay Constants from Four-Flavor Lattice QCD with Physical Light Quarks*, *Phys. Rev. D* **90** (2014) 074509 [1407.3772].

[161] P. Gelhausen, A. Khodjamirian, A. A. Pivovarov and D. Rosenthal, *Decay constants of*

heavy-light vector mesons from QCD sum rules, [Erratum: Phys.Rev.D 89, 099901 (2014), Erratum: Phys.Rev.D 91, 099901 (2015)]*Phys. Rev. D* **88** (2013) 014015 [1305.5432].

[162] A. Khodjamirian, T. Mannel and M. Melcher, *Flavor SU(3) symmetry in charmless B decays*, *Phys. Rev. D* **68** (2003) 114007 [hep-ph/0308297].

[163] S. Descotes-Genon and C. Sachrajda, *Factorization, the light cone distribution amplitude of the B meson and the radiative decay $B \to \gamma \ell \nu_\ell$*, *Nucl. Phys. B* **650** (2003) 356 [hep-ph/0209216].

[164] V. Braun, D. Ivanov and G. Korchemsky, *The B meson distribution amplitude in QCD*, *Phys. Rev. D* **69** (2004) 034014 [hep-ph/0309330].

[165] BaBar collaboration, B. Aubert et al., *Search for the radiative leptonic decay $B^+ \to \gamma \ell^+ \nu_l$*, 0704.1478.

[166] BaBar collaboration, B. Aubert et al., *A Model-independent search for the decay $B^+ \to \ell^+ \nu_\ell \gamma$*, *Phys. Rev. D* **80** (2009) 111105 [0907.1681].

[167] Belle collaboration, A. Heller et al., *Search for $B^+ \to \gamma \ell^+ \nu$ decays with hadronic tagging using the full Belle data sample*, *Phys. Rev. D* **91** (2015) 112009 [1504.05831].

[168] Belle collaboration, M. Gelb et al., *Search for the rare decay of $B^+ \to \ell^+ \nu_\ell \gamma$ with improved hadronic tagging*, *Phys. Rev. D* **98** (2018) 112016 [1810.12976].

[169] C. Kane, C. Lehner, S. Meinel and A. Soni, *Radiative leptonic decays on the lattice*, in *37th International Symposium on Lattice Field Theory*, 6, 2019, 1907.00279.

[170] S. J. Lee and M. Neubert, *Model-independent properties of the B-meson distribution amplitude*, *Phys. Rev. D* **72** (2005) 094028 [hep-ph/0509350].

Acknowledgments

I would like to thank all the people who, directly or indirectly, supported me during my Ph.D. degree. First of all, I wish to thank my advisor Dr. Danny van Dyk, who guided me into flavour physics and the sum rules calculations. I am also grateful to him for introducing me to the international research community and giving me the possibility to present our works around the world.
Next, I would like to thank all my collaborators, which played a crucial role in my personal development and career:

- *Prof. Martin Jung, with his precious insights and his exceptional wisdom,*
- *Dr. Marzia Bordone, who has also been (and is) both an amazing colleague and a good friend,*
- *Dr. Christoph Bobeth, with his extraordinary understanding of particle physics,*
- *Dr. Javier Virto, with his unique way to look at things and his incredible ability to find solutions,*

I am also grateful to Prof. Alexander Khodjamirian for insightful discussions. He is, without any doubt, one of the most brilliant and experienced physicist I ever met.
I cannot forget to thank my family for all the love they constantly give me, and my friends for reminding me that there are plenty of pleasant things in life besides physics.
Last but not least, I would like to thank my girlfriend Alice for an incredible amount of things, which are just too many to be listed here.